



U.S. DEPARTMENT OF
ENERGY

Assessment of Strike of Adult Killer Whales by an OpenHydro Tidal Turbine Blade

Final Report

TJ Carlson
M Grear
AE Copping
M Halvorsen

R Jepsen
K Metzinger

January 2014



Pacific Northwest
NATIONAL LABORATORY

*Proudly Operated by **Battelle** Since 1965*

DISCLAIMER

This report was prepared as an account of work sponsored by an agency of the United States Government. Neither the United States Government nor any agency thereof, nor Battelle Memorial Institute, nor any of their employees, makes **any warranty, express or implied, or assumes any legal liability or responsibility for the accuracy, completeness, or usefulness of any information, apparatus, product, or process disclosed, or represents that its use would not infringe privately owned rights.** Reference herein to any specific commercial product, process, or service by trade name, trademark, manufacturer, or otherwise does not necessarily constitute or imply its endorsement, recommendation, or favoring by the United States Government or any agency thereof, or Battelle Memorial Institute. The views and opinions of authors expressed herein do not necessarily state or reflect those of the United States Government or any agency thereof.

PACIFIC NORTHWEST NATIONAL LABORATORY
operated by
BATTELLE
for the
UNITED STATES DEPARTMENT OF ENERGY
under Contract DE-AC05-76RL01830

Printed in the United States of America

Available to DOE and DOE contractors from the
Office of Scientific and Technical Information,
P.O. Box 62, Oak Ridge, TN 37831-0062;
ph: (865) 576-8401
fax: (865) 576-5728
email: reports@adonis.osti.gov

Available to the public from the National Technical Information Service
5301 Shawnee Rd., Alexandria, VA 22312
ph: (800) 553-NTIS (6847)
email: orders@ntis.gov <<http://www.ntis.gov/about/form.aspx>>
Online ordering: <http://www.ntis.gov>



This document was printed on recycled paper.

(8/2010)

Assessment of Strike of Adult Killer Whales by an OpenHydro Tidal Turbine Blade

Final Report

TJ Carlson
M Grear
AE Copping
M Halvorsen

R Jepsen¹
K Metzinger¹

January 2014

Prepared for
the U.S. Department of Energy
under Contract DE-AC05-76RL01830

Pacific Northwest National Laboratory
Richland, Washington 99352

¹ Sandia National Laboratories, Albuquerque, New Mexico.

Summary

Snohomish County Public Utility District No. 1 (SnoPUD) proposes to deploy two OpenHydro tidal turbines in Admiralty Inlet, Puget Sound. The fisheries service of the National Oceanic and Atmospheric Administration (NOAA Fisheries) has expressed concerns that the turbines may cause a risk for the highly endangered Southern Resident killer whale (SRKW) population if a whale is struck by an operating turbine. Because there are fewer than 90 SRKWs, significant injury of a single animal could place the population in jeopardy.

The potential risk to a SRKW can be parsed into the probability that a whale would encounter a turbine, the probability that the encounter would injure the whale, and the severity of any injury. The focus of this analysis is an estimate of the level of injury that might occur from an encounter between a turbine blade and a SRKW. Results of this analysis are intended to support NOAA Fisheries' determination of the permitting requirements for the tidal project.

Pacific Northwest National Laboratory (PNNL) and Sandia National Laboratories (SNL) were tasked by the U.S. Department of Energy to analyze the engineering and biological consequences of strike to a SRKW by an OpenHydro turbine blade. The approach taken by the two laboratories was to 1) develop a scenario for the most severe strike of a SRKW, 2) determine the morphological and biomechanical properties of SRKW tissues that might be affected by a strike, 3) model the forces associated with a SRKW strike by a turbine blade, and 4) estimate the potential effects on SRKW tissues of a strike.

In fiscal year 2012 (FY12), PNNL and SNL developed a worst-case exposure scenario for a SRKW being struck by a turbine blade, which entails the head of a large male SRKW, weighing approximately 4000 kg., placing its head in the path of the turbine blade. SNL modeled a blunt-edge turbine blade (based on proprietary design data obtained from OpenHydro) and calculated the force of blade impact on the animal. SNL built models of the turbine blades and their motion using specifications and data supplied by OpenHydro and developed a finite element model of the SRKW, based on dimensions and biomechanical properties provided by PNNL. PNNL initially estimated the biomechanical properties from literature values and surrogate materials, including synthetic rubber. In fiscal year 2013 (FY13), two SRKW carcasses were retrieved, allowing PNNL, in cooperation with investigators at the University of Washington's Friday Harbor Laboratory (FHL) to estimate the biomechanical properties of killer whale skin and blubber.

PNNL examined the available literature on blunt-force head trauma in marine mammals and consulted with marine veterinarians with experience in caring for injured animals and performing necropsies on animals found dead. The results of these investigations provided little additional insight into the likely fate of a SRKW struck by a turbine blade.

Comparison of the maximum force acting on soft tissue and bone, estimated by SNL using the finite element models of the turbine blade and whale with the tissue biomechanics data developed by PNNL, provided the basis for assessment of probable injury to a SRKW. The paucity of data available in the literature and very high variability in the SRKW tissue analysis does not allow for a precise estimate of the damage likely to be done to a SRKW by a turbine blade.

The results of the FY12 analyses provide the following insights into the potential risk of encounter to a SRKW with an OpenHydro tidal turbine in Admiralty Inlet: PNNL/SNL analyses determined that a SRKW is not likely to experience significant tissue injury likely to result in death or debilitating injury from impact by an OpenHydro turbine blade. The resulting blade impact forces calculated appear to be sufficient to cause some subcutaneous damage to the SRKW, while laceration of the skin is thought to be somewhat unlikely. Estimated impact force was insufficient to damage the orca's jawbone.

The FY12 and FY13 analyses differed primarily in the data used as input into the engineering model, along with some improvements to the engineering model itself. In FY12, marine mammal biomechanical data from a different species than SRKW was used as the input, as it was the best available in the literature. The testing to produce the data was completed in the lower end of the elastic range; these data were extrapolated to estimate biomechanics properties in the upper portion of the elastic range and at stresses that might lead to tissue failure. Additionally, no skin layer was used in the engineering model. In FY13, the two (juvenile and neonate) SRKW carcasses provided additional data to that available in the FY12 analysis. FHL assisted in testing the tissue (both skin and blubber) using a range of strain rates and carrying out the tests to tissue failure.

Based on the FY13 findings, the calculated blade impact forces with the degraded tissue-testing results appear to be sufficient to cause damage to the SRKW in the worst case scenario setting as described; however, the lack of fresh tissue in sufficient quantity does not allow for confidence in this result. The damage described in the FY13 results would be akin to understanding a dead whale, that was frozen then thawed, encountering the turbine. The damage must be interpreted to be possible subcutaneous injury (i.e. bruising) and the potential for stretching or laceration of the skin at high blade speeds which occur approximately 6% of the time; none of the injuries are expected to be lethal at the point of contact nor are they expected to lead to the death of the whale after the encounter. The goal of the FY13 tissue analyses was to refine the FY12 data; however, there is significant uncertainty concerning the behavior of the tissue. The engineering analysis performed in FY13 included a more robust model of the whale tissues, allowing for more confidence in the worst case outcome of an encounter between the whale and a turbine blade. However, based on the degraded quality of the test tissues, and the lack of comparable literature data to gauge the accuracy of the variability and quality of orca tissue, it is necessary to limit the interpretation of the FY13 analysis to that of the least reliable component, which is the tissue tested from the dead SRKWs. Due to the lack of confidence in the tissue samples tested, the results of the FY13 analysis should be viewed with caution.

Data available for the FY13 analyses were not optimum because the tissue available for testing was not from adult SKRW and was in poor condition. These factors make it likely that the analyses conducted produced results that were conservative in nature. The degree to which that the analyses may have been conservative (biased) is unknown. The error observed in the biomechanics data was not propagated through the analyses so it is not possible to bound the reported estimates for tissue response. Progress in assessment of the interaction of whales with underwater structures (moving or static) will require better and more tissue biomechanics data. Future analyses could better inform the interaction of marine mammals and tidal turbines with a more complete and sophisticated tissue analysis to provide more definitive tissue and bone biomechanical property data, and a more detailed modeling framework.

Acknowledgments

This study was conceived through the joint efforts of the U.S. Department of Energy, the National Oceanic and Atmospheric Administration, Snohomish County Public Utility District, OpenHydro, the University of Washington Northwest National Marine Renewable Energy Center (UW–NNMREC), Pacific Northwest National Laboratory (PNNL), and Sandia National Laboratories (SNL). Understanding the potential severity of strike from an OpenHydro turbine blade on a Southern Resident killer whale (SRKW) in Admiralty Inlet, Puget Sound, is a necessary step in the responsible deployment of tidal turbines in these waters.

Rich Jepsen and Kurt Metzinger at SNL undertook the engineering analysis, based on turbine specifications supplied by OpenHydro, and tidal velocities supplied by UW–NNMREC. Sandia analyses were passed on to the biomechanical analysis team at PNNL.

Tom Carlson, Mike Watkins, and their teams at PNNL examined the physiological and biomechanical properties of SRKWs and analyzed the likely effect of impacts, drawing from the engineering analysis.

Dr. Ted Cranfield at the University of California–Santa Cruz kindly supplied the team with computerized tomography scans of the head of a SRKW.

Dr. William McLellan of University of North Carolina–Wilmington, Dr. Steven Raverty of the province of British Columbia and University of British Columbia, Dr. Regina Campbell-Malone of Johns Hopkins University, Dr. James McBain of SeaWorld, and Dr. Joe Gaydos of the SeaDoc Society shared their expertise and experience in marine mammal injury and mortality. Brad Hanson of the National Marine Fisheries Service Northwest Fisheries Science Center reviewed the plan of study and provided helpful comments for tissue testing.

Acronyms and Abbreviations

CT	computerized tomography
cm	centimeter(s)
DOE	U.S. Department of Energy
FHL	Friday Harbor Laboratory
GPa	gigapascal(s)
HIC	head injury criteria
in.	inch(es)
kg	kilogram(s)
kPa	kilopascal(s)
lbf	pound-force
m	meter(s)
mm	millimeter(s)
m/s	meter(s) per second
MPa	megapascal(s)
N	Newtons
NARW	North Atlantic right whale
NOAA	National Oceanic and Atmospheric Administration
PNNL	Pacific Northwest National Laboratory
SNL	Sandia National Laboratories
SnoPUD	Snohomish County Public Utility District No. 1
SRKW	Southern Resident killer whale
UW–NNMREC	University of Washington–Northwest National Marine Renewable Energy Center

Contents

Summary	iii
Acknowledgments.....	v
Acronyms and Abbreviations	vi
1.0 Introduction	1
1.1 Project Purpose and Approach	1
1.2 Report Contents and Organization	2
2.0 Southern Resident Killer Whales.....	3
2.1 SRKW Habitat Use	3
2.2 Behavioral Ecology	3
3.0 SRKW Encounters with Tidal Turbine Blades	5
3.1 Scenario for an Encounter between a SRKW and an OpenHydro Turbine	5
3.2 Potential Consequences of Blade Strike to a SRKW	6
3.2.1 Whale Head Morphology	6
3.2.2 Biomechanics of Tissue	7
3.2.3 Tissue Analysis	8
3.2.4 Synthetic Tissue Estimates.....	11
3.2.5 Blunt Force Trauma Research.....	12
3.2.6 Assessments from Marine Veterinarians.....	12
4.0 Engineering Analysis of Impact	13
4.1 Geometry and Operational Characteristics of OpenHydro Turbines	13
4.2 Rotor Rotation Rates and Blade Speed	15
4.3 Blade Impact Scenarios and SRKW Characteristics.....	15
4.4 Analysis with a Finite Element Model	18
4.4.1 Model Setup	18
4.4.2 Impact Analysis Results	21
5.0 Discussion, Conclusions, and Lessons Learned	23
5.1 Interpretation of Engineering and Biomechanical Analyses	23
5.2 Uncertainty of Analyses Outcomes.....	25
5.3 Additional Information to Inform Analyses.....	26
5.4 Next Steps	26
5.5 Conclusion.....	27
6.0 References	28

Figures

1. This figure taken from NMFS (2008) shows the distribution of Southern Resident killer whale sightings from 1990 through 2005 (The Whale Museum 2005) in the Salish Sea.	4
2. Front and isometric view of OpenHydro schematic with spacing dimensions of blade edges.....	6
3. CT scan-based images of the head of an adult female SRKW from the side and from top view.....	7
4. Photographs from necropsy of L112 on February 12, 2012	11
5. Left: Front view of blade with spacing dimensions of blade edges. Right: Isometric view with spacing between blade faces.	13
6. Left: Angles between inner blade edges. Right: Angles between outer blade edges.....	14
7. Probability distribution of velocity at blade tip	15
8. Basic dimensions measured for SRKW	16
9. Maximum dimensions reported for an adult male SRKW.....	16
10. Plot of probability distribution for velocity at a location of 0.4 m from the tip of the blade.....	17
11. “Maximum velocity” SRKW and blade impact scenario schematic.	18
12. Finite element model, color coded for blade, skin, blubber and bone	19
13. Skin and bone models	20
14. Blubber strain, 3 m/s.....	22
15. Skin strain, 3 m/s.	22

Tables

1. Description of the condition of each Southern Resident killer whale from which tissue was recovered for biomechanical analysis.....	8
2. Juvenile tissue peak stress values at three crosshead speeds.	9
3. Juvenile tissue elastic modulus values at three crosshead speeds.....	9
4. Neonate tissue peak stress values at three crosshead speeds.	9
5. Neonate tissue elastic modulus values at three crosshead speeds.....	10
6. Material properties.	20
7. Level of certainty associated with each input to the FY13 engineering and biomechanical analyses.	25

1.0 Introduction

Snohomish County Public Utility District No. 1 (SnoPUD) has proposed to deploy two OpenHydro tidal turbines in Admiralty Inlet, Puget Sound. Due to the presence of the Southern Resident killer whale (SRKW) population (listed as an endangered species under the Endangered Species Act) in Puget Sound and Admiralty Inlet, the National Oceanic and Atmospheric Administration (NOAA Fisheries) has expressed concern that the turbines may cause a risk to the SRKW population. The SRKW population is often found in the inland waters of Washington, usually moving into the Puget Sound in the early autumn (NMFS 2008). Because the SRKW numbers are so small, significant injury of a single animal could place the population in jeopardy (Williams and Lusseau 2006). SRKW experts at the Center for Whale Research list 81 remaining individuals as of September 2013. SRKW spend more than 97% of their time within the top 30 m of the water column and dive to the turbine depth (approximately 55 m) only to feed (Baird 2003). Thus, the chance of a SRKW encountering a tidal turbine is negligibly small, but a SRKW might approach a turbine out of curiosity. Due to their endangered status, there are concerns regarding the potential severity of a strike on a SRKW, if it occurs. It is important to note that the velocity of a turbine blade will be highest and the potential for injury to a SRKW greatest during peak tidal flows; observations of SRKWs in Admiralty Inlet indicate that the animals are less likely to be in the channel during these times (Sea Mammal Research Unit unpublished data).

1.1 Project Purpose and Approach

To resolve this issue, Pacific Northwest National Laboratory (PNNL) and Sandia National Laboratories (SNL) were tasked by the U.S. Department of Energy (DOE) to carry out an analysis of the mechanics and biological consequences of a tidal turbine blade strike on a SRKW in FY12. Further refinement of the FY12 analysis began in FY13 by testing SRKW biomechanical properties and using those data as input for the engineering analyses. In doing so, the potential level of injury from such an interaction can be estimated and used to inform NOAA Fisheries about how to proceed with the permitting process for the tidal energy project.

The approach taken was as follows:

1. PNNL and SNL developed a scenario for the most severe strike of a SRKW, consisting of a large male SRKW inspecting the tidal turbine out of curiosity, by placing its rostrum between the blades.
2. SNL analyzed the geometry, mass, material properties, and speed characteristics of the tidal turbines and calculated the amount of force a tidal turbine blade is capable of creating. This force calculation was coupled with the dimensions and material properties of an adult SRKW weighing approximately 4000 kg in a computer simulation of a blade impact on the head of an adult SRKW.
3. PNNL used a computerized tomography (CT) scan of an adult SRKW head, similar in size to the hypothetical SRKW used in the engineering analysis, to understand the morphology and anatomy of a SRKW head.
4. To understand the biomechanical properties of SRKW skin and soft tissues, PNNL reviewed the scientific literature; because no tissue values were readily available, surrogate synthetic rubber materials were used to support estimates of the biomechanical properties. Determinations of how these tissues might resist mechanical damage by spreading force across the region affected by impact were made.

5. Two SRKWs were stranded and tissues were recovered from the carcasses for analysis. The SRKW tissue was tested to failure. Analyses of the SRKW tissue, and those of the surrogate materials, were used to estimate the level of injury that might occur from an encounter between a turbine blade and a SRKW.
6. By combining the maximum force calculations of the tidal turbine blade acting on the SRKW soft tissue and bone with SRKW tissue biomechanics and head anatomy data, PNNL and SNL estimated the potential effects of an encounter between a SRKW and a tidal turbine blade.
7. PNNL examined the scientific literature on blunt-force head trauma to determine whether there are appropriate analogues to effects of a tidal turbine blade on the head region of a SRKW.
8. PNNL sought real-world examples of strike on the head region of SRKW or other marine mammals through discussions with marine veterinarians who routinely treat or research injured marine mammals. The purpose of the real-world examples was to provide a semi-quantitative validation of the modeling results.

The purpose of this research is to demonstrate how these analyses could be used to provide information that may assist NOAA Fisheries in their permitting decisions for the tidal energy project in Admiralty Inlet, Washington.

1.2 Report Contents and Organization

The ensuing sections of this report briefly describe the engineering studies, tissue testing, biomechanical analyses, blunt-force head trauma literature review, and model validation efforts undertaken. The detailed analyses and findings of each step are contained in the appendices to this report. The findings are discussed and synthesized in the discussion/conclusion section of this report, with an emphasis on the lessons learned from this research. This strike analysis relies heavily on modeling the forces exerted by a moving turbine blade and estimating tissue response based on the estimated biomechanical properties of SRKW tissues; each step in the analysis process introduces a level of uncertainty into the result, stemming largely from the uncertainty surrounding the available input data and the scenario for interaction between the whale and turbine. A brief analysis of the level of accuracy associated with each portion of the analysis is provided in the discussion/conclusion section of this report.

2.0 Southern Resident Killer Whales

SRKWs are a population of approximately 81 individuals, as of September 2013. They are an endangered group of orca whales that live in three distinct pods (J, K, and L), which are family-based matriline. The SRKWs forage primarily on fish, particularly Chinook salmon (Baird 2003).

2.1 SRKW Habitat Use

SRKWs are typically present in the inland waters of Washington and British Columbia in the summer and fall, typically returning to the Salish Sea each year in May or June (NMFS 2008). SRKW habitat use is best known through sightings kept by several local organizations, including the Whale Museum and the Center for Whale Research, both headquartered in the San Juan Islands. Because these sightings are often land-based or from whale-watching boats, and because of the nature of such reports there is an unquantified and unknown whale location bias inherent in the sightings database. Each of the three SRKW pods has its own typical range, but the population generally spends some part of the fall in Puget Sound presumably to follow migrating adult Chinook salmon (NMFS 2008). Admiralty Inlet is the only ingress and egress to Puget Sound, and the whales are seen there much less frequently than in other Puget Sound locales, because they appear to quickly pass through the inlet upon entering and exiting the sound, then remain in the sound for a few days between passages through Admiralty Inlet (Figure 1). The number of SRKW individuals passing through Admiralty Inlet is estimated to be 42 per year, with a total of 1,442 transits through the area per year (Admiralty Inlet Pilot Tidal Project 2012).

2.2 Pilot Tidal Behavioral Ecology

Understanding SRKW behavior at the depths that tidal turbines will be deployed in Admiralty Inlet is an important step to understanding the potential risk of interaction between SRKWs and tidal turbines. A study with field locations at Juan de Fuca Strait, Haro Strait, and Boundary Pass, found that SRKWs present in the San Juan Islands in late summer spend only 2.4% of their time at depths of 30 m or greater (Baird 2003). The whales dive deeper while foraging for salmon and do not remain at depth for an extended amount of time. Tidal turbines planned for deployment in Admiralty Inlet will be placed on the sea floor at approximately the 55-m depth, thereby limiting the interaction of the SRKWs with the turbines. During a small study (land-based and boat-based) in the project area, SRKW spent 74% of their time travelling, with 80% of their recorded vocalizations originating above 30 m; the whales had several periods of resting with little vocal activity, often when they were traveling slowly. (Admiralty Inlet Pilot Tidal Project 2012). SRKWs are known to have a well-developed ability to avoid rocks and other stationary objects in the ocean (NMFS 2008).

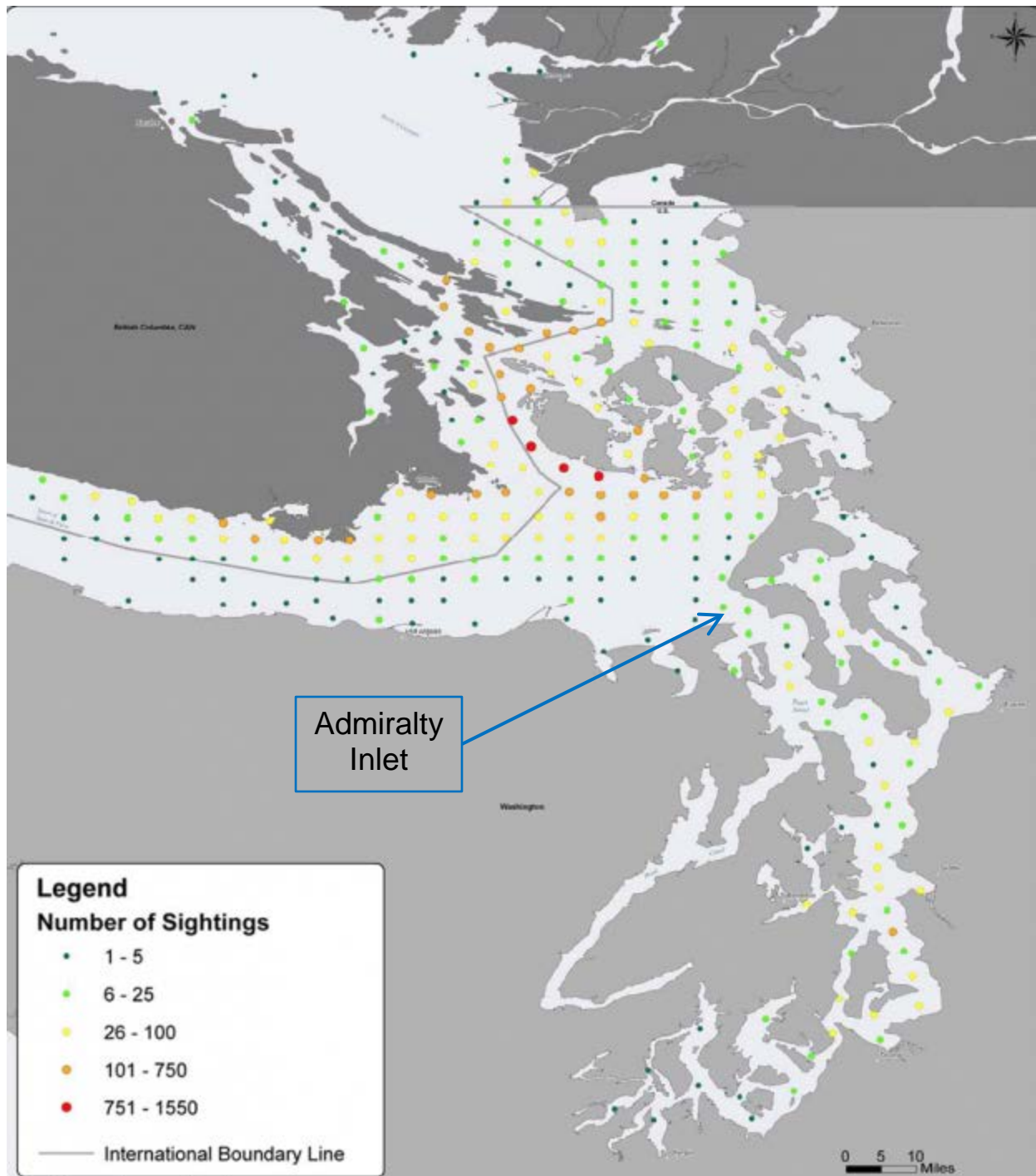


Figure 1. This figure taken from NMFS (2008) shows the distribution of SRKW sightings from 1990 through 2005 in the Salish Sea. Multiple sightings of whales in the same location on the same day were eliminated to reduce frequency of occurrence bias and resulted in 15,540 unique sightings.

3.0 SRKW Encounters with Tidal Turbine Blades

The potential risk to a SRKW can be parsed into the probability that a whale will encounter a turbine, the probability that the encounter will injure the whale, the severity of the injury, and the ability of the whale to survive and recover from such an injury. SRKWs are found in Admiralty Inlet only as they transit between the Straits of Juan de Fuca and Puget Sound. Available information indicates that the probability of encounter is likely to be small, as SRKWs spend 97% of their time in near the San Juan islands at depths less than 30 m (Baird 2003), while the tidal turbines will be placed at a depth of 55m, extending approximately 10m into the water column. When diving deeply, the whales are typically foraging SRKWs have highly evolved sensory systems including a remarkable acoustic echolocation capability that is likely to assist them in avoiding an object as large as a tidal turbine.

It is possible, however, that a SRKW might approach a turbine out of curiosity. In order for a SRKW to penetrate the plane of the turbine blade with its rostrum, the animal would have to approach at a very specific angle and with careful timing relative to the moving blades. The geometry of the turbine ensures that the likelihood of such an encounter is small (Figure 2). Because of the OpenHydro twelve-bladed horizontal axis turbine geometry, it is more likely that the whale would be hit with less force than has been calculated by the accompanying engineering analysis. For example, attempting to place a hand in a ceiling fan blade might result in a nick to one or more fingers but is unlikely to cause extensive damage to the whole hand, as one could not place the entire hand in the fan before the rotation of the blades would strike a portion (the fingers) of the hand. Calculations that characterize an encounter with a turbine could represent a range of risk to the SRKW influenced by many variables including the speed of the turbine blades, which vary with the speed of the tidal currents. The analysis presented here describes the worst-case scenario for potential injury to a SRKW from an encounter with a tidal turbine. The combination of SRKWs natural ability to avoid stationary objects; the difficulty of a SRKW positioning its rostrum fully into the slow moving turbine; and the SRKW's tendency to reside in the upper portion of the water column, all reduce the likelihood that such an event will occur.

3.1 Scenario for an Encounter between a SRKW and an OpenHydro Turbine

PNNL and SNL scientists and engineers developed a scenario designed to estimate the most risky conditions under which a strike could occur (turbine blade strike on the head of an adult whale at the highest tidal flows and, consequently, the highest turbine blade rotation speeds). SNL carried out blade impact modeling, using turbine specifications provided directly by OpenHydro, to determine the force with which a blade might strike the animal (Figure 2). PNNL examined available data on the biomechanical properties of the SRKW tissues derived from SRKW tissue testing and surrogate materials including synthetic rubber, natural rubber, other composite materials, and human skin.

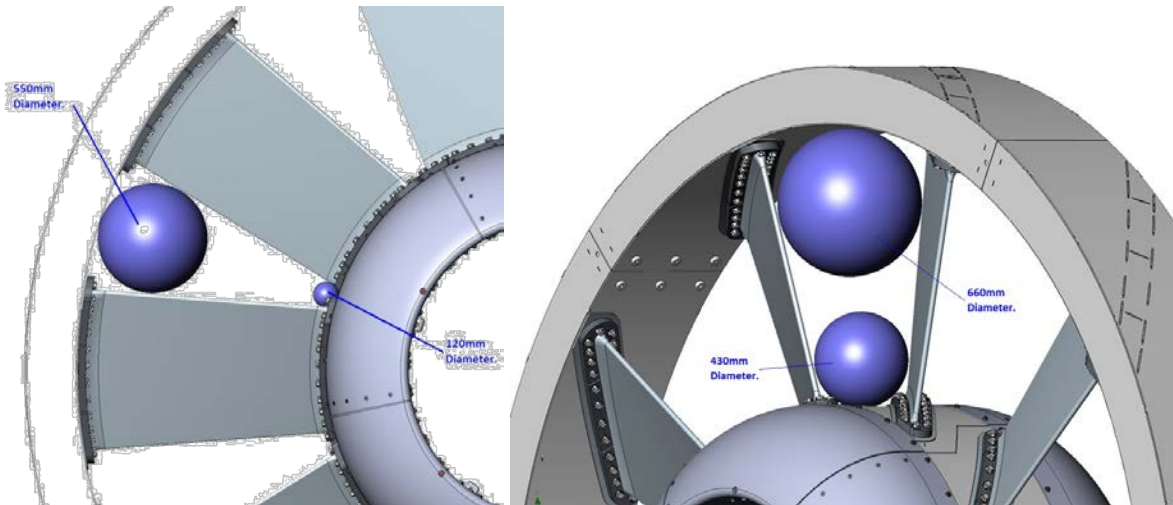


Figure 2. Front and isometric view of OpenHydro schematic with spacing dimensions of blade edges.

It was assumed that the greatest momentum transfer from the turbine blade to the animal will occur with the largest mass of animal and would constitute the worst-case risk, with the greatest potential for tissue damage. The scenario that met these conditions included a large male SRKW approaching the turbine out of curiosity and placing its rostrum between the turbine blades. From a population point of view, losing an adult male SRKW would not constitute the greatest risk, however this analysis was aimed at understanding the greatest risk to the individual, not the population. Based on the geometry of the turbine, including the turbine duct, the maximum penetration of the nose of a large adult SRKW into the turbine would be approximately 0.4 m from the tip of the nose. The geometry of the open-centered ducted turbine is such that, in order to be struck by the blade, the animal would need to approach the turbine at a very specific angle and with exact timing to achieve this penetration with its rostrum, further reducing the likelihood of blade strike. The open-centered ducted turbine has no exposed blade tip, so any potential strike must involve the edge of a blade.

3.2 Potential Consequences of Blade Strike to a SRKW

An estimate of the injury that might be done to the head of a SRKW from an encounter with a tidal turbine blade requires three elements: 1) understanding the structure of the SRKW head with the underlying tissues, 2) an estimate of the biomechanical properties of the skin and other tissues of the SRKW head, and 3) an estimate of the forces that could be imparted to the SRKW from the turbine blade.

3.2.1 Whale Head Morphology

PNNL obtained data for whale head morphology and anatomy from CT scans of the head of an adult SRKW that died in 2002 (Figure 3). Information about the biomechanical properties of whale tissues was found in the scientific literature (Appendix A).

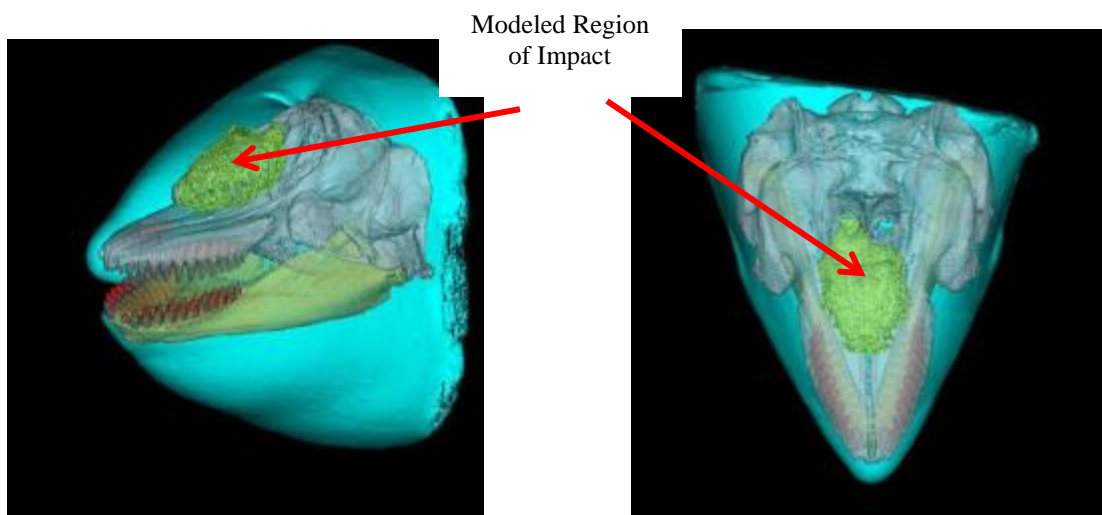


Figure 3. CT scan-based images of the head of an adult female SRKW from the side (left) and from top view (right). The teeth are shown in red, bone in light color, and the various soft tissues in other colors. The region of impact used for modeling purposes is indicated.

The adult killer whale for which CT scan data were available and the adult killer whale modeled were similar enough in size so that the available morphology and anatomy data from CT scans could be used in assessment of the probable injury to an adult killer whale caused by turbine blade strike. The tissues of concern included the skin of the whale, other soft tissue, and mandibular bone. Details of the head morphology analysis can be found in Appendix A.

3.2.2 Biomechanics of Tissue

Very little is known about the biomechanical properties of whale tissue under compression, particularly the skin, which functions to resist mechanical and other damage and to spread the force of an impact across a region that minimizes the stresses acting on underlying tissues; data that describe the biomechanical properties of the dorsal fin of a harbor porpoise under extension forces are provided by Hanson (2001). The lack of biomechanical data creates a challenge for estimating the potential biological effects of a turbine blade strike.

Review of the published and gray literature, augmented by contact with known marine mammal researchers, determined that there are limited data for the biomechanical properties of whale tissue in general and for killer whales in particular. The majority of biomechanical data available have been taken primarily to investigate the production and reception of sound by species that use echolocation to communicate and find food. For this reason, there is limited information about stress at which tissue mechanically fails. Hanson studied the failure of harbor porpoise dorsal fin tissue from the stress due to attachment of radio tags (Hanson 2001). There is some biomechanical information over a range of stresses for blubber (Soldevilla et al. 2005) and some information for whale bone (Campbell-Malone 2007), but there are almost no biomechanical data for whale skin and higher-density fibroelastic tissue. More details of the biomechanical analyses can be found in Appendix B. Available tissue biomechanical data from other species of whales was considered during analysis of the biomechanical data we acquired for SRKWs.

3.2.3 Tissue Analysis

Tissue from a stranded SRKW became available after the initial turbine blade strike analyses were completed with the death of L112—a three-year-old female (juvenile) that washed up at Long Beach, Washington in February 2012. PNNL tested SRKW tissue from the stranded SRKW in partnership with investigators at Friday Harbor Laboratory (FHL) at the University of Washington in January 2013. By the time testing was planned, a second SRKW was stranded—a neonate (calf) was found on Dungeness Spit, Washington, in January 2013. The testing related to both animals yielded some additional biomechanical information to inform a second round of modeling (Table 1). However, the tissue test results required considerable interpretation because the quality of tissue was noticeably degraded and there were few data for comparison. For example, trends seen in relationships between blubber and skin biomechanical properties were not consistent between the neonate and juvenile. Additional data from other SRKWs, particularly tissues that are in good condition from animals over a range of ages, will be necessary to resolve the observed ambiguities.

Table 1. Description of the condition of each Southern Resident killer whale from which tissue was recovered for biomechanical analysis.

SRKW	Age	Sex	Condition	Tissue Acquired	Model Application
L112	~3 years	Female	Washed up in Long Beach, WA in February 2012. Was frozen at Friday Harbor Labs for approximately a year before testing. The skin tissue was degraded and abraded; L112 had likely been dead a few days before washing ashore.	Received a 20-cm x 15-cm sample that contained all the skin and some of the blubber layer.	Biomechanical data used for both skin and blubber modeling.
J pod neonate	newborn	Male	Found on Dungeness Spit in January 2013. The time of death before discovery was shorter than that of L112. This whale was frozen whole for only a few weeks before testing and the tissues were in better condition than those of L112.	Received the entire head section of the neonate, including parts of the melon, but removed from the bone.	Biomechanical data used only for modeling skin.

3.2.3.1 Summary of Tissue Data Results

Tissue was tested in three different directions, 0° (dorsal to ventral), 90° (anterior to posterior), and 45°, as well as at different crosshead speeds. A complete summary of methods and results can be found in Appendix C. Table 2 through Table 5 summarize the tissue-testing results, as well as the variability of the data.

In the opinion of the FHL experts and PNNL biologists, the combination of the degradation of the L112 samples and the effects of the testing setup led to less resistant values for the resiliency of the tissue than would be expect from a living whole animal. The biomechanical data for neonatal tissue are expected to be more representative of living tissue, although the very young age of the animal contributes considerable uncertainty to using the biomechanical data for these tissues to model an adult SRKW.

Table 2. Juvenile tissue peak stress values at a crosshead speed of 1 mm/s.

Peak Stress (MPa)	
Skin	1.0 mm/s
0°	1.30 ±0.95 (6)
90°	2.23 ±0.86 (8)
Blubber	
0°	0.53 ±0.38 (8)
45°	0.58 ±0.33 (8)
90°	1.19 ±0.67 (8)
Mean ± SD (n)	

Table 3. Juvenile tissue elastic modulus values at three crosshead speeds.

Elastic Modulus (MPa)			
Skin	0.1 mm/s	1.0 mm/s	10.0 mm/s
0°		1.75 ±0.34 (4)	
90°		6.60 ±1.81 (8)	
Blubber			
0°	3.05±1.28 (8)	3.70 ±3.26 (8)	
90°	4.75 ±2.21 (8)	11.80 ±9.96 (8)	10.96 ±6.64 (8)
Mean ± SD (n)			

Table 4. Neonate tissue peak stress values at five crosshead speeds.

Peak Stress (MPa)					
Skin	0.01 mm/s	0.1 mm/s	1.0 mm/s	10.0 mm/s	15.0 mm/s
0°	0.71 ±0.07 (5)	0.75 ±0.07 (5)	1.21 ±0.50 (8)	1.71 ±0.95 (5)	1.45 ±0.34 (5)
45°			1.04±0.21 (8)		
90°			1.72 ±0.60 (10)		
Blubber					
0°	0.34 ±0.33 (5)	0.42 ±0.50 (5)	0.41 ±0.14 (10)	0.44 ±0.15 (5)	0.73 ±0.51 (3)
45°			0.37 ±0.17 (9)		
90°	0.20 ±0.00 (4)	0.32 ±0.04 (6)	0.49 ±0.16 (9)	0.70 ±0.22 (7)	0.88 ±0.33 (5)
Mean ± SD (n)					

Table 5. Neonate tissue elastic modulus values at five crosshead speeds.

Skin	Elastic Modulus (MPa)				
	0.01 mm/s	0.1 mm/s	1.0 mm/s	10.0 mm/s	15.0 mm/s
0°	0.66 ±0.17 (5)	6.22 ±5.64 (5)	2.96 ±0.51 (11)	1.35 ±1.15 (5)	1.48 ±0.26 (5)
45°			6.20 ±2.28 (9)		
90°			8.02 ±3.95 (11)		
Blubber					
0°	0.70 ±0.79 (5)	0.90 ±0.75 (5)	1.48 ±0.51 (8)	1.49±0.96 (5)	4.11 ±3.22 (5)
45°			2.59 ±0.86 (8)		
90°	0.39 ±0.13 (5)	0.52 ±0.14(5)	1.13 ±0.56 (9)	1.40 ±0.22 (5)	1.45 ±0.35 (5)
Mean ± SD (n)					

3.2.3.2 Tissue Degradation and Variability

The effect of tissue degradation on the variability of the results from Table 2 through Table 5 is a major concern in the interpretation of the tissue analysis results. Biomechanical attributes of biological tissue are expected to be highly variable; it is questionable, however, whether we can attribute much of the variability to natural causes or the degraded state of the tissue available for testing. According to Cascadia Research’s necropsy report on the juvenile, “...the whale was moderately decomposed...” (Figure 4) (Huggins et al. 2012). An important measurable indicator of the unreliability of the tissue was the fact that trends seen in the neonate did not match those seen in the juvenile: the neonatal blubber had a lower elastic modulus than the skin, while the juvenile blubber had a higher elastic modulus than the animal’s skin. However, the relationship between the neonatal and juvenile skin remains uncertain.



Figure 4. Photographs from necropsy of L112 on February 12, 2012. Photos A and B show the skin sample used for tissue testing, at the time of the necropsy. The tissue was frozen shortly thereafter. Photo C shows L112 prior to necropsy; the skin tissue was clearly already degraded at the time of the necropsy.

Tissue testing was limited, in addition to the state of available tissue, by the small amount of tissue available for testing. Particularly important was the small sample size available at each of the crosshead speeds over the range at which testing was needed to adequately characterize tissue response to impulsive impact. Small sample sizes, in addition to the variability in the strain response of degraded biological tissues to stress, resulted in estimates of the mean biomechanical properties of SRKW tissue with large standard errors.

3.2.4 Synthetic Tissue Estimates

The scarcity of biomechanical data led the PNNL researchers to seek surrogates to estimate the likely response of whale tissue to a turbine blade strike. Natural and synthetic rubbers materials were deemed to be most similar to SRKW skin. The lack of reliable biomechanical measurements of whale tissues at the

time of this element of the study did not allow for calculations with which to modify the engineering analysis; rather these assessments of surrogate tissues further reinforced the concept that the assessment of potential harm to the SRKW from a tidal turbine strike described in the FY12 is a conservative estimate. The details of the synthetic tissue literature review and analysis can be found in Appendix B.

3.2.5 Blunt Force Trauma Research

Additional information about the potential effects of a turbine blade strike on a SRKW can be gleaned from research and monitoring results of animal head trauma. PNNL researchers searched peer-reviewed and gray literature on blunt-force traumas of marine and terrestrial mammals. Peer-reviewed literature was accessed using the Web of Science and gray literature was accessed via Google searches and cited references in papers identified from the Web of Science searches. A key index for evaluating the severity of head trauma in humans and other animals has been developed, known as head injury criteria (HIC). Although such an index is not available for marine mammals, the process of developing a HIC might be instructive. While searching for pertinent literature about blunt-force trauma, PNNL researchers looked for papers that might support the development of a marine mammal HIC or other types of risk assessment tools for marine mammal interactions with objects. Literature on large and small terrestrial mammals was also reviewed. This literature review supported some insights into blunt-force head trauma in a variety of mammal species and also shed light on tools and methods that may be useful in assessing and modeling head trauma on SRKWs and other marine mammals. More details of the literature review and a complete list of papers reviewed can be found in Appendix E.

3.2.6 Assessments from Marine Veterinarians

In the absence of field observations to validate the outcome of the strike analysis, PNNL researchers sought input from marine veterinarians familiar with the effects of head trauma and other injuries in cetaceans and other marine mammals. The veterinarians provided professional insights into effects on marine mammals recovered from strandings and from observations of animals in captivity. In almost all cases, the insight gained from the veterinarians consisted of their best professional judgment and was described through anecdotes rather than through the presentation of data and drawing of conclusions. Details of the assessments from the marine veterinarians can be found in Appendix F.

4.0 Engineering Analysis of Impact

This section outlines the engineering analysis performed by SNL to determine the stresses in a SRKW from a potential impact with a tidal turbine blade. The analysis entailed determining the relevant geometry, mass, material, and speed characteristics of the OpenHydro turbine, rotor, and blade. SRKW dimensions and material properties were determined along with possible impact scenarios for the study.

The FY13 engineering analysis refined the FY12 work by creating a more complex and more accurate model for the SRKW. However, due to uncertainty associated with the condition of SRKW tissue tested for biomechanical analysis, the outcome of the FY13 analyses should be viewed with caution. Additional details of the engineering analysis can be found in Appendix D.

4.1 Geometry and Operational Characteristics of OpenHydro Turbines

The OpenHydro tidal turbine characteristics, including the material properties, dimensions, and blade speeds, remained unchanged from FY12 (Figure 5).

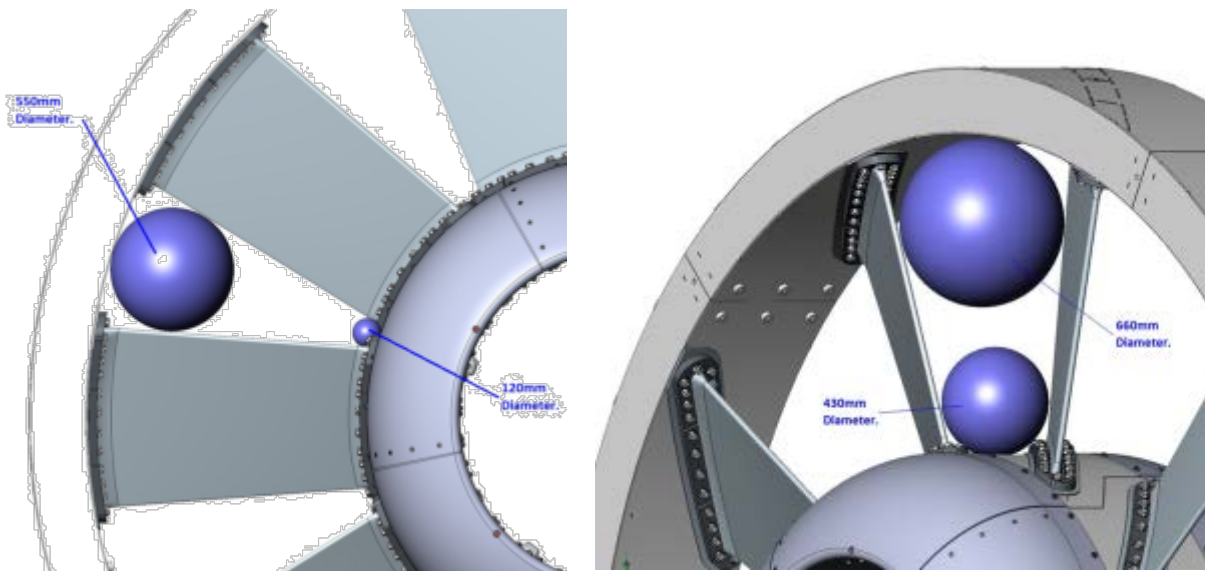


Figure 5. Left: Front view of blade with spacing dimensions of blade edges. Right: Isometric view with spacing between blade faces.

Relevant information was gathered on the geometry and operation of the OpenHydro turbines to be deployed in Puget Sound from the turbine company, under a non-disclosure agreement with SNL. The following information was obtained:

- design drawings with the necessary details of the blade assembly and rotor for the OpenHydro turbine. Key details included the number, location, shape, and angle of the blades, with dimensions of the leading edge of the blades.
- information about the materials and construction detail of the turbine blade assembly and rotor to compute blade mass and other physical properties

- information about the operating characteristics of the turbine, including revolutions per minute/blade speed at the range of tidal flows expected in Admiralty Inlet.

These data were provided by OpenHydro and interpreted with assistance from the University of Washington – Northwest National Marine Renewable Energy Center (UW–NNMREC). The data are summarized below. It should be noted that the design for the specific turbines to be deployed in Puget Sound is not finalized, and some parameters such as materials and moment of inertia are proprietary. For these parameters, estimates were based on consultation with OpenHydro. Overall, the dimensions and material properties supplied by OpenHydro were sufficient for the analysis.

The proposed device for deployment in Admiralty Inlet is an open-center OpenHydro tidal turbine with a nominal diameter of 6 m; the diameter of the rotor blades within the duct is 4.8 m. The rotor blades are about 1.25 m long with a central ducted open area with a nominal diameter of about 2.25 m. The rotor has a mass of 6200 kg. Figure 5 shows the spacing between the blade faces. Figure 6 shows the angles between the outer and inner blade edges.

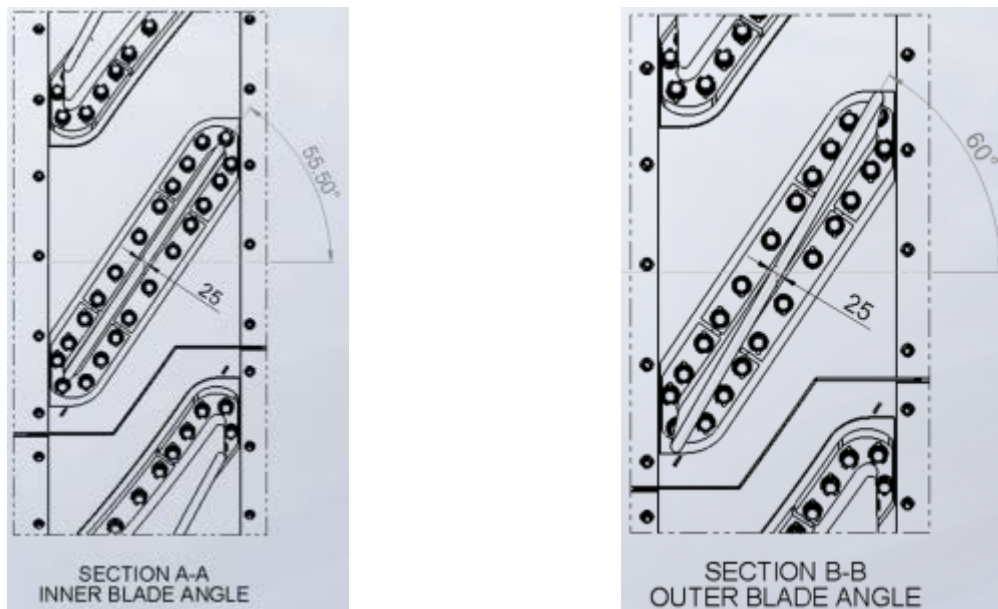


Figure 6. Left: Angles between inner blade edges. Right: Angles between outer blade edges.

Based on communications with OpenHydro, the blade material properties could be adequately modeled using a stiff plastic or composite material. Using either fiberglass composite or plastic resin such as Delrin is appropriate because both materials are stiffer than the SRKW material properties. An elastic modulus (material property defined as stress over strain for elastic deformation under an applied force) of 7 GPa was chosen for the blade based on information provided by OpenHydro.

The moment of inertia for the turbine could be adequately estimated assuming the rotor is a solid disc with a mass of 6200 kg and diameter of 4.8 m.

4.2 Rotor Rotation Rates and Blade Speed

From the information supplied by OpenHydro, and the expected tidal velocities within the Admiralty Inlet deployment site supplied by UW–NNMREC, the blade velocities can be calculated anywhere along the radius of the blade edge. Figure 7 shows the probabilities for the maximum possible velocity at the blade tip. The OpenHydro rotor or blade assembly is the only moving part on the turbine. The tips of the rotor blades are contained within a stationary outer duct and the center of the rotor is open. The design of the duct and its location relative to the rotor blade tips would make it extremely difficult for all but the smallest marine mammals to come into contact with the blade tip. The velocity of the blade at a radial location relative to the center of the rotor increases with radial distance at any rotor speed; this equates to the maximum blade velocity occurring at the tips of the blades. Based on the design of the rotor and duct assembly, it is not possible for an object the size of the rostral portion of the head of an adult SRKW to come into contact with the rotor blades at their tips. Contact with the rotor blades, if possible at all, must be at a location where the blade velocity is lower than the maximum velocity. The maximum expected impact scenario is discussed in the following section.

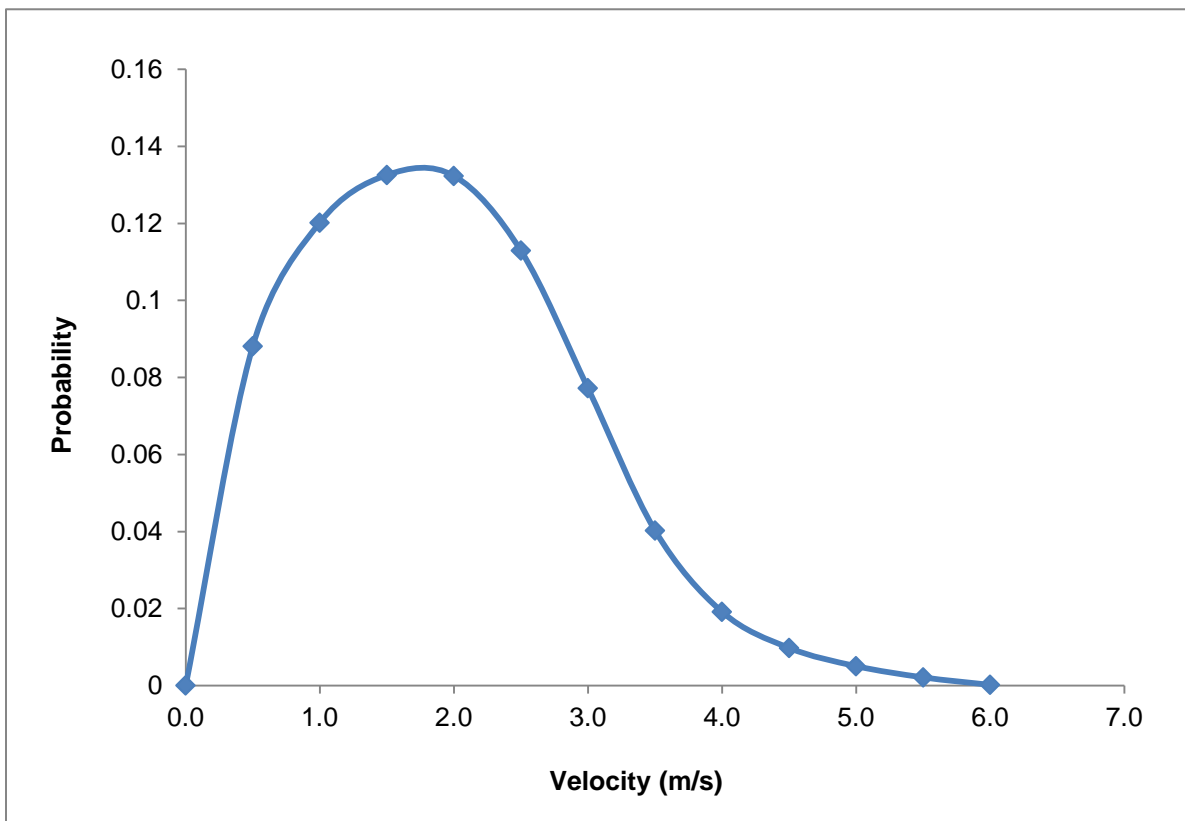


Figure 7. Probability distribution of velocity at blade tip. At low tidal velocity (26% of the time), the blade is stationary (not shown here).

4.3 Blade Impact Scenarios and SRKW Characteristics

The SRKW geometry and mass were based on Durban et al. (2009), as well as Fearnbach et al. 2011. An adult male was chosen because it has the greatest mass, forcing the affected tissue to absorb a maximum amount of the energy. The largest adult male reported by Durban et al. was used (Figure 8);

the peduncle and tail were not simulated in the model. The mass associated with the large adult male SRKW was approximately 4000 kg.

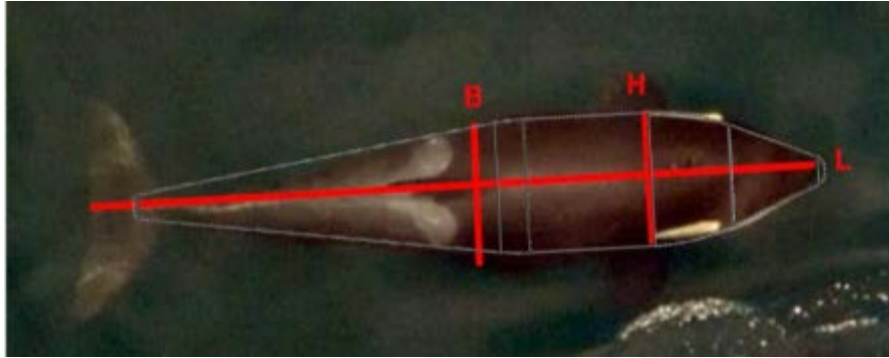


Figure 8. Basic dimensions measured for SRKW (Durban et al. 2009).

It will be difficult, if not impossible, for an adult SRKW to impact the blade at the radius farthest from the center of rotation due to the cowling around the turbine, and there is a similar restriction due to a cowling around the open area in the center of the rotor. Therefore, the blade velocity was applied to the location where the head of the whale could be inserted farthest into the turbine rotor, still an unlikely scenario but one that would have the most adverse effect on the whale. This causes the most absorption by the tissue due to impact and is the most conservative impact location scenario (Figure 5 [left] and Figure 9). The most severe impact with respect to tissue damage (i.e., skin and subcutaneous injury) would be for a large mass (i.e., adult male) to be hit as close to its center of mass as possible. This forces the tissue to absorb more of the impact rather than simply moving the mass (the whale) out of the way. The maximum penetration of the nose of the large adult SRKW would extend approximately 0.4 m from the tip of the nose, at a 2.0-m radius on the rotor. The probability distribution as a function of blade velocity is demonstrated in Figure 10. The probability distribution has a shape similar to the blade tip velocity (Figure 7), but has higher probabilities at lower velocities and the terminal velocity is lower because the radial distance for the modeled location of contact is closer to the center of rotation. The engineering analysis was performed at 1, 2, 3, 4, and 5 m/s, informed by the velocity distribution seen in Figure 10.

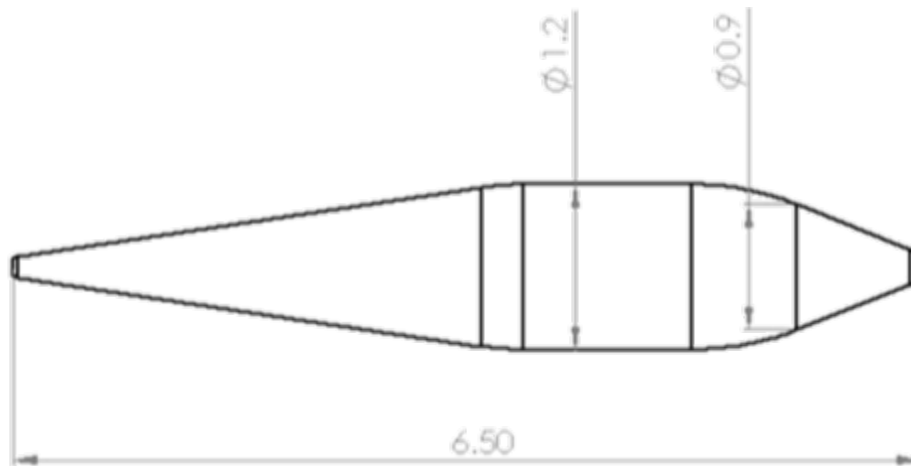


Figure 9. Maximum dimensions reported for an adult male SRKW.

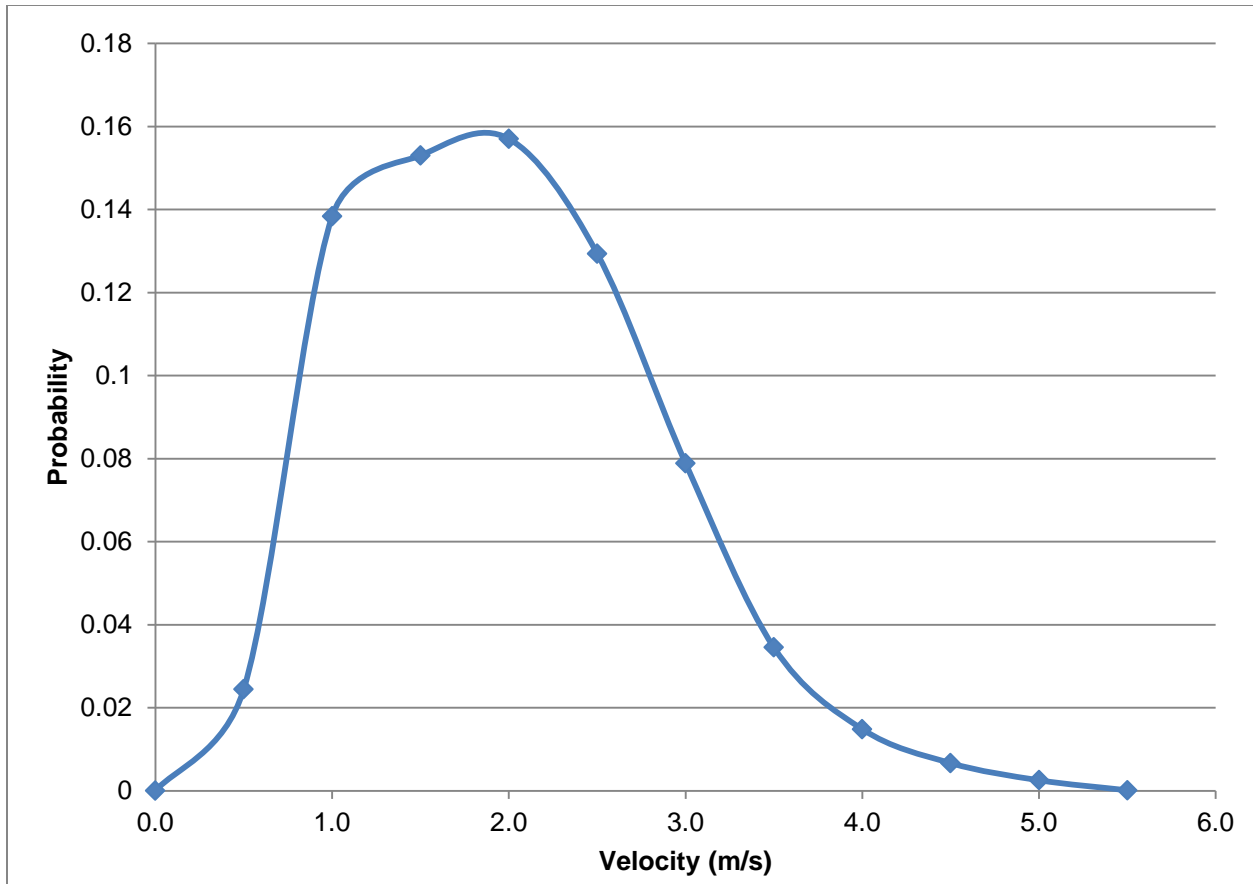


Figure 10. Plot of probability distribution for velocity at a location of 0.4 m from the tip of the blade.

A much smaller juvenile SRKW was also examined with regard to comparative geometry and momentum transfer. In this case, the smaller head of the juvenile SRKW allows for a longer radius of the blade to make impact and impart velocities about 10% higher than what an adult would experience. However, there are more significant issues to address with regard to the momentum transfer and impact force each body experiences. A juvenile can be approximated by scaling the dimensions of an adult by one-half. If this juvenile is struck by a half-scale turbine, its tissue stresses would match those of an adult struck by a full-scale turbine. (Both whales are assumed to have the same biomechanical properties.) Now consider a juvenile struck by a full-scale turbine blade. Because the inertia of the half-scale turbine is already large relative to the whale, the effect of the increased mass of the full-scale blade is expected to be more than offset by the increased impact area. This would lead to lower tissue stresses in the juvenile.

Other scenarios were also considered but have been discounted as being too implausible, including:

- a generalized and conservative closed-form solution, featuring a fixed “whale” mass upon impact, described by a single elastic modulus for the whale tissue (blubber)
- a finite element analysis model using blade and whale models from Figure 11 and a variable elastic modulus for whale tissue (blubber). In this situation, the whale model will be fixed and thus force the tissue to absorb all the impact.

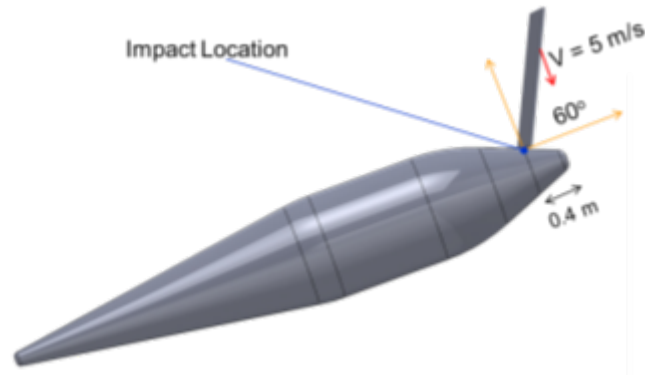


Figure 11. “Maximum velocity” SRKW and blade impact scenario schematic.

The primary problem with these scenarios is the overly simplistic “fixing” of the SRKW mass. The “fixed” scenario forces the SRKW tissue to absorb all the impact, which is grossly incorrect because the body is, in reality, free to both translate and rotate away from the impact point. The fact that the impact location on the SRKW is a great distance from the center of gravity of the body (~2–3 m) also means that momentum transfer into rotation is significant in this case and should not be excluded from the analysis.

As the forward velocity starts to significantly affect the resultant velocity above the maximum blade velocity of 5 m/s, the result approaches a ramming scenario, where the whale swims into the turbine at a velocity greater than 3 m/s. Previous meetings and discussions with regulators have discounted the ramming scenario. The curiosity or “inspection” scenario has the SRKW moving at a forward velocity of 3 m/s or less (Williams and Noren 2009; Noren 2011). While this study uses “blade velocity only” simulations, further work could explore the effect of both blade and whale masses moving. The blade velocity was modeled with a range of 1-5 m/s.

4.4 Analysis with a Finite Element Model

The specifications for the turbines, blades, and rotational forces were determined using input from the turbine manufacturer (OpenHydro) and specifications for the SRKW inferred from information about the animals from published literature and reports. Tissue biomechanical properties were provided to SNL by PNNL, based on synthetic tissue characteristics and informed by SRKW tissue testing carried out in FY13. A detailed explanation of the material properties provided to SNL can be found in Appendix D, as well as the full tissue-testing results in Appendix C. SNL created a modeling system to accommodate the turbine blades, SRKW body shape and mass, and the SRKW tissue properties, using a finite element model.

4.4.1 Model Setup

The modeling could have taken advantage of closed-form solutions that are available for certain impact scenarios. However, the large deformations and the evolving nature of the contact interface for a blade striking a large mammal suggest the need for a finite element analysis. Figure 12 and Figure 13 show the model domain created for this study. The dimensions are based on a 4128-kg adult SRKW, as shown in Figure 8. The turbine rotor is represented by a single blade (shown in light blue) that is constrained to move in one direction. The ballast elements on the end of the blade (shown in darker blue)

are modeled to be of very large density so that the linear momentum of the massive (4460-kg) blade corresponds to the angular momentum of the rotor (as defined by the manufacturer). The SRKW skin, blubber, and bone are shown in black, red, and gray, respectively. The model domain does not include the surrounding water that is expected to have a modest effect on the peak loads; this simplification reduces the model size and complexity. The use of a symmetry plane also helps reduce the model size (1.6 million elements). Including the surrounding water in the domain necessitates significantly more computational resources than are currently available with the funding and schedule restraints of the project. The average magnitude of the velocity for the moving portion of the whale body upon impact is quite slow and the drag forces in water are $F = \frac{1}{2} A C_d \rho v^2$, with C_D (drag coefficient) being approximately 1 for a cylindrical shape. At peak load for the 3-m/s impact scenario, the only portion of the whale that begins to move is the forward region of the head from the point of impact to the tip of the nose (about 0.4 m in length). The velocity of this region is about 2 m/s and the area perpendicular to the velocity of the moving portion is about 0.2 m². This means the restraining forces by the water on the body during peak loading is about 400 N or 100 lbf, which is quite small in comparison to the average 4000 kg of an adult SRKW. Therefore, the surrounding water is thought not to have a large confining effect at these impact speeds.

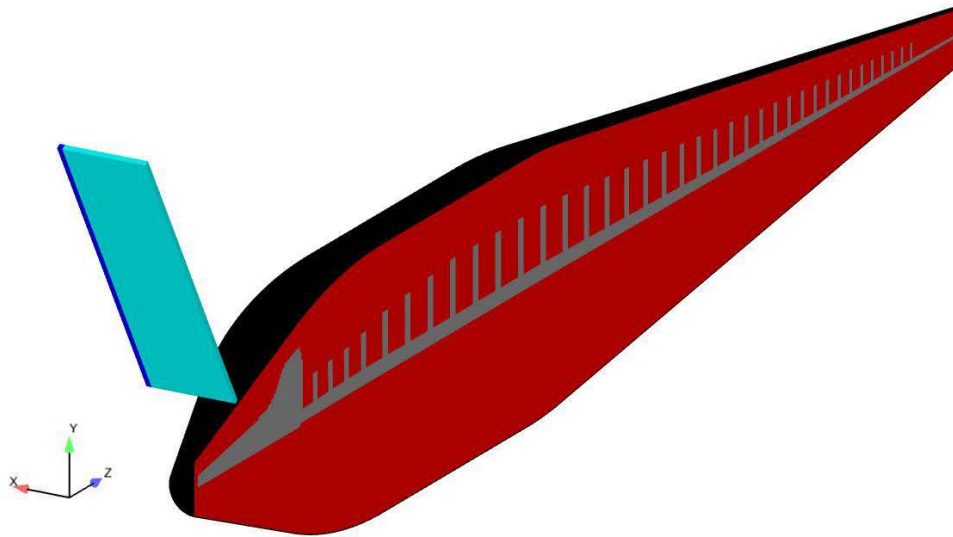


Figure 12. Finite element model, color coded for blade, skin, blubber and bone (with symmetry plane).

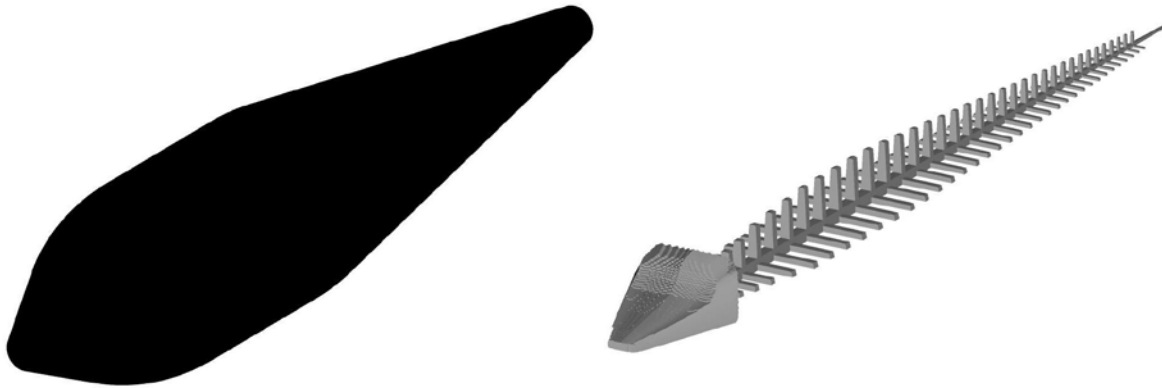


Figure 13. Skin and bone models (full geometry).

Table 6 lists the material properties used for the engineering study. Initially, the engineering analysis was performed using the biomechanical data for juvenile skin and blubber. Because the juvenile tissue was significantly degraded, the neonatal skin biomechanical data was used in an exploratory analysis to consider how the presence of skin might affect the distribution of force in underlying whale tissue at blade strike. The predicted tissues strains are similar for the neonatal and the juvenile skin properties. The Poisson's ratio for the nearly incompressible blubber and bone were chosen to match the measured sound speeds, and verified by testing at FHL. The skin, blubber, and bone materials use a Neo-Hookean constitutive model that is valid for large deformations.

Table 6. Material properties.

Material	Elastic Modulus (MPa)	Density (kg/m ³)	Poisson's Ratio	Estimated Engineering Strain Thresholds for Tissue Failure
Juvenile Skin*	6.6	1000	0.4994	NA
Juvenile Blubber*	11.8	1000	0.4990	0.5
Neonatal Skin*	8.02	1000	0.4993	0.6
Bone	300	1000	0.4745	NA
Blade	7000	1200	0.3	NA
Ballast	7000	2325100	0.3	NA

* The Neo-Hookean constitutive model used for these materials is valid for large deformations.

More complex material models could be used. Highly deformable materials such as skin, blubber, and rubber represent a group of materials that respond differently when stressed in compression versus tension; the load-deflection behavior can be very nonlinear. These materials can be represented with a hyperelastic constitutive model such as the Mooney–Rivlin model available in the SNL code, Presto (Koterak et al. 2006). These models have parameters that must be determined by testing specimens under different loading conditions (tension, compression, and shear). The tests are then analyzed with the chosen parameters to ensure the fit adequately represents the measured behavior. Some finite element codes automate the process, accept various types of test data, and determine the parameters for the selected constitutive model. However, the simplest hyperelastic model (Neo-Hookean) was selected because almost all of the tissue was tested in tension.

4.4.2 Impact Analysis Results

The transient dynamics code Presto was used to consider impact speeds of 1 to 5 m/s. This range is based on the shapes of the marine and hydrokinetic device and a SRKW, as well as the expected range of the rotor's angular speeds. In these simulations, the heavy blade is given an initial velocity, and its edges are allowed to translate but not rotate. The blade slows a small amount as it pushes the whale out of the way. Figure 14 and Figure 15 show the maximum principal logarithmic strain in the blubber and skin, respectively, for an impact speed of 3 m/s. This baseline simulation uses blubber properties from the juvenile and skin properties from the neonate. This approach was taken because the juvenile skin sample was significantly degraded.

Although the images in Figure 14 and Figure 15 show what appears to be fairly deep depression of the tissue, and the maximum principal (logarithmic) strains might cause tearing in many structural materials (e.g., steel, glass composites), these levels are quite acceptable for materials like human skin, other animal tissues, or natural rubber. For comparison, one could produce similarly proportional depression and strain (with little discomfort) by simply pressing one's index finger into one's thigh. Based on the estimated strain thresholds listed in Table 6, some significant tissue damage, such as bruising or tearing, might occur at high blade speeds (3 m/s or higher) in the worst case scenario described for a blade strike. A cumulative probability distribution reveals that the turbine blade speed at the radial location of impact is lower than 3 m/s 94.1% of the time. There is however no indication that the forces involved would result in a lethal outcome of the SRKW encountering the turbine blade, nor that the damage is likely to result in the whale's death after the encounter, as one might expect if the jawbone (mandible) of the animal were fractured. It should be noted however that this reported damage is based on degraded tissue data, and thus is not an accurate representation of the likely outcome. Additional data are available in Appendix D.

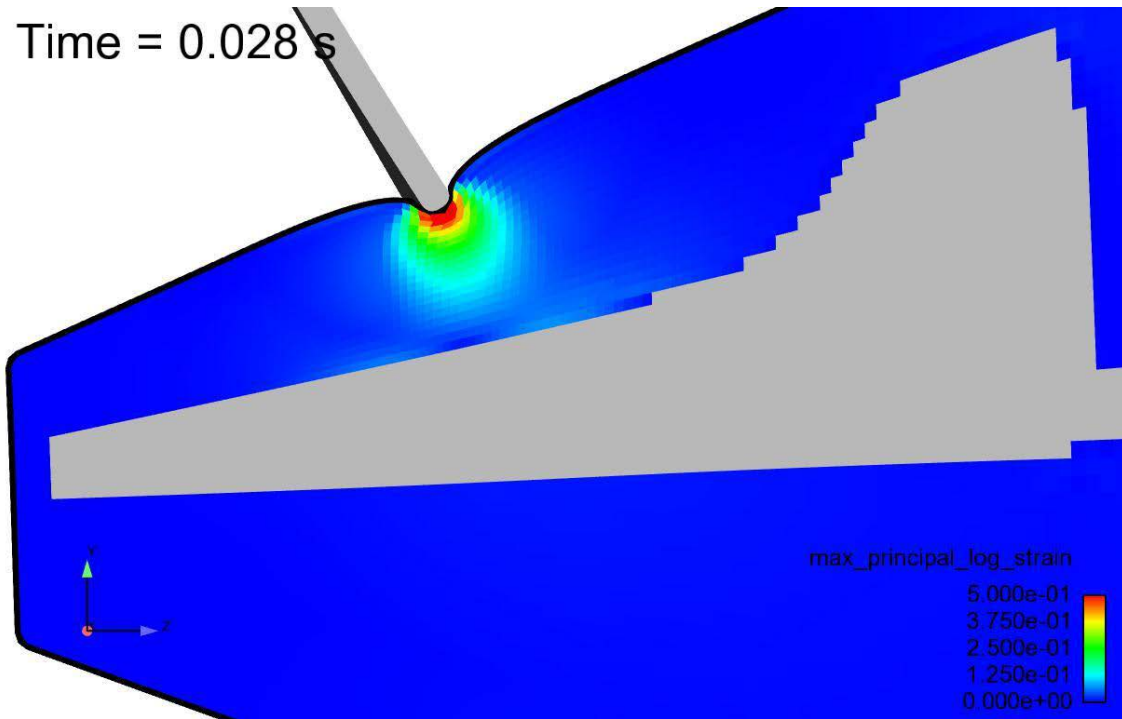


Figure 14. Blubber strain, 3 m/s.

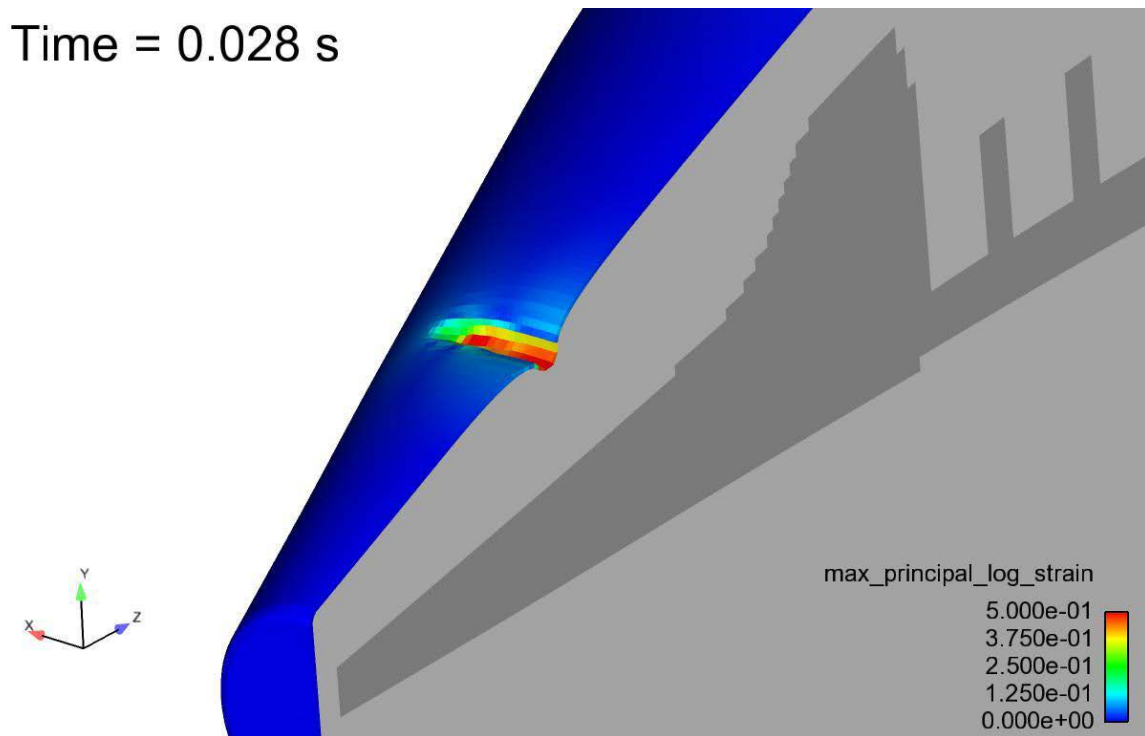


Figure 15. Skin strain, 3 m/s.

5.0 Discussion, Conclusions, and Lessons Learned

Under the worst case encounter scenario analyzed for this report, the turbine blade would hit the whale on the top of its skull and melon. The blubber and skin are expected to absorb the majority of the impact force; force sufficient to break the mandible is unlikely to be transferred deep into the animal's body, based on knowledge of forces required to break the jaw of larger whales. Some of the force from the turbine blade will be transferred to the whole SRKW body, in effect "pushing" the whale out of the way of the blade; this occurs because the whale's center of mass is far away from the point of impact. The tissue overlying the whale's skull acts as a "bumper" that absorbs and redistributes stresses from the blade strike.

Little published data on the biomechanical properties of marine mammal tissues exists, and none on animals similar to SRKWs. The initial analysis (Carlson et al. 2012, 2013) reported in 2012 used best professional judgment to determine the likelihood of the modeled forces of the turbine blade causing damage to the skin and underlying tissues of the SRKW. The outcome of the 2012 analysis was that the turbine blade, under the scenario tested, is unlikely to break the skin of the SRKW, but may impart stress to the underlying blubber in such a way as to cause minor hemorrhaging, or the equivalent of a bruise under the skin.

Tissue from two stranded SRKWs became available after the initial analyses were completed: a juvenile female and a neonatal male. Analysis of the skin and blubber of both whales yielded some insights into preferred methods for tissue testing and yielded some additional biomechanical information to inform a second round of modeling. However, due to uncertainties in the impacts of degraded tissue, freezing, and thawing, the tissue samples did not provide a clear and definitive understanding of SRKW tissue behavior in tension.

By the time the carcass of the juvenile was discovered, the whale had degraded; the animal had probably been dead for several days before necropsy and tissue collection. Post collection, the tissue was frozen for a year until testing took place in January 2013. The neonatal tissue was collected within a day of stranding and was frozen for 1 to 2 days before being transported to FHL for testing. The condition of the juvenile tissue was noticeably degraded; a substantial odor of decomposition was noted and portions of the thin outer layer of skin were observed to slough off under stress. In comparison to the fresher neonatal tissue, the juvenile skin tissue was visually more wrinkled, rough, and less stretchy.

The juvenile and neonatal blubber and skin tissues were tested under tension at FHL in several different orientations. The testing procedure involved clamping small sections of tissue securely, then pulling the tissue. Clamping and compression of the sample placed increased stress on the ends of the specimen, noticeably weakening the tissue. The samples often slipped slightly in the clamps as the tests proceeded.

5.1 Interpretation of Engineering and Biomechanical Analyses

Translating material properties and forces (such as those calculated by the engineering model) into a level of injury an animal might sustain as the result of a known force is challenging. Even if the tissue-testing analyses had yielded significantly more biomechanical information, it would nonetheless remain difficult to determine the specific type of injury that might occur to the animal. For example, SRKW skin

might be calculated to exceed the elastic region and be permanently deformed; however, for living tissue, that exceedance might manifest as a wrinkle (such as might occur in the crease of a human finger, or as a stretch mark). It is difficult to determine what forces might actually cause tearing, bruising, stretching, or splitting of the SRKW skin. The strain of the material in the engineering model, compared to the strain produced in testing, may aid in understanding the type of injury.

As expected with biological materials, the tissue-testing data were highly variable. The available tissue sample for the juvenile was small, resulting in a small sample size for each tissue test; the neonate sample was larger, allowing for larger sample sizes. Though the neonate condition was fresher, it is unclear how the properties of skin and blubber tissue in whales change as the animal ages. This uncertainty makes it difficult to use analysis of neonatal tissue data to extend, compare or extrapolate the juvenile data. PNNL provided average values for the material properties, as well as standard deviations, as input to SNL's engineering model; raw data stress/strain curves for blubber and skin were also provided to place the values in context.

Based on the expertise of the FHL and PNNL biologists, neither set of tissue samples (juvenile and neonate) provided clear indications of what might be expected in a living animal. The degradation of the juvenile samples and the young age of the neonate do not provide a clear pathway to understanding the biomechanical properties of even a dead adult whale, much less a living one.

Using the results of the tissue testing SNL reran the blade strike simulators, applying significantly more detail to the skin and blubber layers of the simulated SRKW. The FY13 analyses predict tissue damage at high-speed blade impacts under a worst case scenario. The speeds indicating potential tissue damage are at 3 m/s or higher, which occur less than the 6% of the operating time, further decreasing the likelihood of such an event. It is not clear however whether the degraded condition of the tissue samples make these results credible. The outcome of the worst case scenario at the maximum blade velocities for the Admiralty Inlet turbine is expected to consist of damage to the subcutaneous tissues (i.e., blubber layer) of the animal, resulting in minor hemorrhaging in the tissues (or the equivalent of a bruise) and perhaps some level of damage (such as bruising or tearing) to the skin. The biomechanical properties of the juvenile and the neonate tissues are highly uncertain and variable but appear to bracket the biomechanical properties estimated from the literature in the 2012 modeling efforts.

Based on our best professional judgment, it is expected that in the case of the proposed worst case scenario strike, under typical turbine blade velocities, SRKW skin tissue and the underlying soft tissue would deform, absorb the force of the strike, and return to its normal condition, as described in the FY12 results. The only published data on the strike pressure needed to fracture the mandibular bone (jawbone) of a cetacean comes from a North Atlantic right whale (NARW). Although the NARW is much larger than a SRKW and has a more massive mandible, in the absence of other data this analysis assumes that the SRKW mandibles have similar biomechanical properties to those of NARWs. This assumption is considered appropriate because SRKWs are thought to have sturdy mandibles, based on observations of SRKWs using their rostrums to batter prey animals and battle conspecifics. Applying this assumption, the stresses predicted by the model are highly unlikely to result in the fracture of a SRKW mandible. The mandible of an orca is partially hollow, which could increase the vulnerability of the animal to damage; however there are no data that will assist with this assessment at this time. The available literature and best professional judgment of marine veterinarians did not differ from the outcome of the analyses.

5.2 Uncertainty of Analyses Outcomes

The overall uncertainty of the engineering and biomechanical analyses can best be estimated by assessing the accuracy of each piece of information that informed the analyses. The modeling techniques used are well documented and are unlikely to have introduced significant uncertainty. Table 7 summarizes the uncertainty of each specific information source. Other parts of the analysis are conservative, so the conclusions are still conservative, but the uncertainties cannot be clarified without further study.

Table 7. Level of certainty associated with each input to the FY13 engineering and biomechanical analyses.

Portion of Analysis	Specific Input to Analysis	Accuracy/Level of Certainty of Information	Explanation
Modeling of Strike Forces	Geometry of SRKW approach to turbine	High	Geometry of turbine based on detailed drawings from turbine manufacturer; geometry of SRKW based on reports for several SRKWs studied. Chose “worst case for injury” approach of SRKW swimming directly into outer edge of turbine.
	Speed and forces modeled for turbine, as they vary with tidal current speed	High	Turbine speeds and tidal current values are well known, supplied from manufacturer; multiple model runs to determine forces.
	Orientation of animal with turbine blade, transfer of momentum	Medium	Limited model runs for orientation of animal, to ensure choice of “worst case for injury” scenario. Based on engineering judgment.
	Nonlinear model for materials	Medium	Because almost all of the tissue was tested in tension, the simplest (Neo-Hookean) hyperelastic model was used.
Biomechanics of orca tissues	Information about tissue thickness and properties of skin	Low	Directly measured skin thickness from degraded sample, as well as adapted information from CT scans of SRKW and literature about other species. Tissue testing unreliable due to degradation.
	Information about tissue thickness and properties of blubber	Low	Good geometry values from literature and direct measurement, as well as adapted information from CT scans of SRKW and literature about other species. Tissue testing unreliable due to degradation.
	Information about thickness and properties of bone	Medium	Biomechanics of impact on bone well understood; used other species in absence of information on SRKW. Based on professional judgment.

	Information about tissue thickness and properties of melon	Low	Tissue thickness from CT scan and necropsy data, biomechanical values from literature. Properties from blubber used in model because of similar biomechanical properties.
	Effects of blunt-force trauma	Medium	Good understanding and copious literature for humans and livestock; little information for marine mammals. Some anecdotal information may be gleaned from interviews. Based on professional judgment.
Sensory response to impact	Post-trauma effects on SRKW	Low	No literature on effects. Potential for anecdotal information from interviews. Not used in model. Other scenarios for different life stages of SRKW and different approaches to the turbine that were not analyzed could create different risks, including the potential for delayed effects of head trauma, concussion, injury or death due to infection of lacerations, etc.

5.3 Additional Information to Inform Analyses

In assessing the available blunt-force trauma literature, there appears to be a paucity of data on head injuries in marine mammals that can be associated with a reliable estimate of the forces involved. The best available information is associated with whale–ship collisions and, to a lesser extent, data from underwater detonations. Of the available animal surrogate models, the pig provides the most detailed information on head trauma in a large animal model (Appendix E). Recent studies with rodents and in vitro models coupled to some type of computational analysis appear to offer a tractable alternative to traditional animal testing. However, rodent brains react very differently from those of higher mammals, including cetaceans (R. Campbell-Malone, personal communication, September 2012). The information gleaned from the literature may be of value in future marine mammal assessments in which post-mortem (from stranding or other natural cause of death) brain tissue may become available for testing, and more direct measurements of force-causing trauma can be made, as described in Appendix F.

Although some interesting insights can be drawn from the anecdotes and professional judgment of veterinarians who care for injured marine mammals and perform necropsies on dead animals, no research is available that directly informs the SRKW interaction with a tidal turbine scenario.

5.4 Next Steps

The engineering and biomechanical analyses reported herein indicate that insight can be provided into potential interactions between marine animals and turbines. However, it is clear that the information base of mechanical properties for marine mammal tissues lacks key pieces critical to the analyses. We propose the collection of an enhanced database of marine mammal biomaterial properties. This information could be collected through a coordinated action to recover more biomechanical information about marine mammal tissue and bone as a routine part of the existing necropsies on animals found dead. Also of

importance are data on specific properties and operational modes of turbines that could cause harm to marine animals; for example, material properties that can be used on the leading edges of turbine blades to decrease potential harm to animals. Animal models are needed that can connect the biomechanical properties of marine mammals and design criteria for turbines, allowing for a modeling application to evaluate the design of turbines before deployment.

It is also important to note that the analyses performed here do not necessarily inform interactions between tidal turbine blades from devices with designs different from those of the open-center OpenHydro turbine, nor are these analytical outcomes necessarily transferable to turbine blade interactions with other marine mammals. We propose that analyses of additional turbine designs, interacting with other marine mammals potentially at risk, be performed. Of particular interest are studies that link turbine rotors without ducts (exposed blades) and vertical axis turbines with marine mammals that differ in size, body conformation, and mass from those of the adult SRKW.

5.5 Conclusion from FY13

Little is known about the potential effects of tidal turbine blade impacts on SRKWs; the engineering and biomechanical approach used in this study demonstrates that insight can be provided, even in the absence of definitive data. A SRKW interaction with a turbine in 55 m of water in Admiralty Inlet is unlikely because SRKWs in this region spend 97% of their time at 30 m or shallower. In the rare occurrence of a whale strike, modeling the speed and potential force exerted by an OpenHydro tidal turbine blade allowed SNL to estimate the maximum force of tidal turbine blunt-edge blades acting upon soft tissue of a SRKW. At each step in the process (scenario development, modeling the maximum speed of the turbine blades, and maximum whale swimming speed) a conservative approach was used so that the results might be expected to provide a “worst-case scenario” for harm to a SRKW.

Understanding that the likelihood of a SRKW encountering a bottom-mounted tidal turbine is extremely small, the additional information that was added to the estimate of potential harm to the whale in the proposed worst-case scenario from a turbine blade strike on the rostrum can be summarized as follows:

1. The uncertainty surrounding the tissue testing analyses makes it impossible to determine with any certainty how extensive damage to the SRKW might be.
2. The engineering modeling outcome of a blade strike to the head of a SRKW inspecting the turbine suggests that a catastrophic injury is not likely.
3. The modeling analysis predicts that a break in the skin could occur at blade speed of 3 m/s or above (which occurs less than 6% of the time in Admiralty Inlet), and indicates that damage such as bruising to deeper underlying tissues is a more likely outcome.
4. Taking the most likely outcome of the engineering model analysis, the logical interpretation is to expect that under a worst-case scenario (as described earlier), a SRKW struck by a turbine blade will experience some damage to the underlying tissue with the possibility of laceration to the skin at very high blade speeds.
5. Results of the FY12 analysis, using literature values and surrogate properties to represent the biomechanics of the SRKW tissues, and with the simpler engineering model, reach a similar

conclusion as the FY13 analysis: the improbable encounter of a SRKW with an OpenHydro blade in Admiralty Inlet is most likely to result in minor recoverable injury, such as bruising.

PNNL/SNL analyses could not provide insight into the potential for subtler changes to SRKWs from an encounter with a turbine, such as changes in behavior. Other scenarios that could be investigated further include: a potential encounter of different life stages of the SRKW (neonate, juvenile, subadult, smaller adult female), as well as an encounter of other body parts with the turbine blade (fin, fluke, ventral surface).

6.0 References

References include those cited in the appendices

Admiralty Inlet Pilot Tidal Project. 2012. Application for a new pilot project license (minor water power project): FERC No. 12690. Vol. IV: Draft Biological Assessment. Public Utility No. 1 of Snohomish County, Everett, Washington.
(http://www.snopud.com/Site/Content/Documents/tidal/ai_final/FLA_Volume_IV_412.pdf)

Baird RW, MB Hanson, EE Ashe, MR Heithaus, and GJ Marshall. 2003. *Studies of Foraging in "Southern Resident" Killer Whales During July 2002: Dive Depths, Bursts in Speed, and the Use of a "Cittercam" System for Examining Sub-Surface Behavior*. National Marine Fisheries Service, National Marine Mammal Laboratory, Seattle, Washington.

Campbell-Malone R. 2007. *Biomechanics of North Atlantic Right Whale Bone: Mandibular Fracture as a Fatal Endpoint for Blunt Vessel-Whale Collision Modeling*. Massachusetts Institute of Technology, Woods Hole Oceanographic Institution, Woods Hole, Massachusetts.

Campbell-Malone R, SG Barco, PY Daoust, AR Knowlton, WA McLellan, DS Rotstein, and MJ Moore. 2008. Gross and histologic evidence of sharp and blunt trauma in north atlantic right whales (*eubalaena glacialis*) killed by vessels. *Journal of Zoo and Wildlife Medicine* 39(1):37–55.

Carlson, T.J, JL Elster, ME Jones, BE Watson, AE Copping, M Watkins, R Jepsen, and K Metzinger. 2012. Assessment of Strike of Adult Killer Whales by an OpenHydro Tidal Turbine Blade. (US Department of Energy, Trans.) (pp. 44), Pacific Northwest National Laboratory. Carlson T, R Jepsen, and A Copping. 2013. Potential Effects of the Interaction between Marine Mammals and Tidal Turbines – An Engineering and Biomechanical Analysis. Paper presented at the European Wave and Tidal Energy Conference, Aalborg, Denmark.

Dunn DG, SG Barco, DA Pabst, and WA McLellan. 2002. Evidence for infanticide in bottlenose dolphins of the western north atlantic. *Journal of Wildlife Diseases* 38(3):505–510.

Durban J, H Fearnbach, D Ellifrit, and K Balcomb. 2009. Size and Body Condition of Southern Resident Killer Whales. Contract report to the Northwest Regional Office, National Marine Fisheries Service. Order number AB133F08SE4742, Requisition Number NFFP5000-8-43300.

Endangered Species Act of 1973. Public Law 93-205, as amended, 16 USC 1531 *et seq.*

Fearnbach H, J Durban, D Ellifrit, K Balcomb 2011. Size and long-term growth trends of Endangered fish-eating killer whales. *Endangered Species Research* 13:173–180.

Hanson MB. 2001. An evaluation of the relationship between small cetacean tag design and attachment durations: a bioengineering approach. Ph.D. dissertation, University of Washington, Seattle, Washington.

Hendriks FM. 2001. Mechanical behavior of human skin in vivo, a literature review. Report 2001/820, Koninklijke Philips Electronics, N.V. Amsterdam, the Netherlands.

Huggins, J, D Duffield, and D Lambourn. 2012. Examination of dead killer whale on Long Beach Peninsula, February 12, 2012. http://www.cascadiaresearch.org/examination_of_dead_killer_whale-12Feb2012.htm

Kipps EK, WA McLellan, SA Rommel, and DA Pabst. 2002. Skin density and its influence on buoyancy in the manatee (*trichechus manatus latirostris*), harbor porpoise (*phocoenca phocoena*), and bottlenose dolphin (*tursiops truncatus*). *Marine Mammal Science* 18(3):765–778.

Koteras JR, AS Gullerud, NK Crane, and JD Hales. 2006. *Presto User's Guide Version 2.6*. SAND2006-6093, Sandia National Laboratories, Albuquerque, New Mexico.

Lightsey JD, SA Rommel, AM Costidis, and TD Pitchford. 2006. Methods used during gross necropsy to determine watercraft-related mortality in the Florida manatee (*Trichechus manatus latirostris*). *Journal of Zoo and Wildlife Medicine* 37(3):262–275.

McKenna MF. 2005. Comparative morphology of the odontocete melon: Functional and evolutionary interpretations. Masters of Science thesis, San Diego State University, San Diego, California.

NMFS (National Marine Fisheries Service). 2008. *Recovery Plan for Southern Resident Killer Whales* (*Orcinus orca*). National Marine Fisheries Service, Northwest Region, Seattle, Washington.

Noren DP. 2011. Estimated field metabolic rates and prey requirements of resident killer whales. *Marine Mammal Science* 27(1):60–77.

Oremland MS and BM Allen. 2010. Mandibular fractures in short-finned pilot whales, *Globicephala macrorhynchus*. *Marine Mammal Science* 26(1): –16.

Patterson IA, RJ Reid, B Wilson, K Grellier, HM Ross, and PM Thompson. 1998. Evidence for infanticide in bottlenose dolphins: an explanation for violent interactions with harbour porpoises? *Proceedings of the Royal Society - Biological Sciences* 265(1402):1167–1170.

Rommel SA, AM Costidis, TD Pitchford, JD Lightsey, RH Snyder, and EM Haubold. 2007. Forensic methods for characterizing watercraft from watercraft-induced wounds on the Florida manatee (*Trichechus manatus latirostris*). *Marine Mammal Science* 23(1):110–132.

Schaefer RJ. 2009. Mechanical Properties of Rubber. In *Harris' Shock and Vibration Handbook* (5th edition). AG Piersal and TL Paez (eds), pp 1108-1125. McGraw Hill, New York.

- Silver FH, JW Freeman, and D DeVore. 2001. Viscoelastic properties of human skin and processed dermis. *Skin Research and Technology* 7(1):18–23.
- Soldevilla MS, MF McKenna, SM Wiggins, RE Shadwick, TW Cranford, and JA Hildebrand. 2005. Cuvier's beaked whale (*Ziphius cavirostris*) head tissues: physical properties and CT imaging. *Journal of Experimental Biology* 208:2319–2332.
- Tsukrov I, JC DeCrew, K Baldwin, R Campbell-Malone, and MJ Moore. 2009. Mechanics of the right whale mandible: full scale testing and finite element analysis. *Journal of Experimental Marine Biology and Ecology* 374(2):93–103.
- Williams R and DP Noren. 2009. Swimming speed, respiration rate, and estimated cost of transport in adult killer whales. *Marine Mammal Science* 25:327–350.
- Williams R and Lusseau D. 2006. A killer whale social network is vulnerable to targeted removals. *Biology Letters* 2:497–500.
- Winn JP. 2006. *Modeling Large Whale Entanglement Injuries: An Experimental Analysis of the Influence of Tissue Compliance, Line Tension, and Draw-Length on Epidermal Abrasion Resistance*. Masters of Science thesis, University of Maine, Orono.
- Winn JP, Woodward B, Moore MJ, and Peterson ML. 2008. Modeling whale entanglement injuries: An experimental study of tissue compliance, line tension, and draw-length. *Marine Mammal Science* 24:326–340.

Appendix A – Head Morphology of SRKW

A.1 Head Morphology of SRKW

The engineering analysis modeled an adult killer whale that was approximately 650 cm in length, not considering the whale's flukes, and weighed 4,000 kg. PNNL was able to locate CT scan data for the head of an adult female that weighed approximately 5,300 kg and was roughly 670 cm in length, including the flukes. Because of the similarity in size to the modeled case, the CT scan data is a reasonable example of the size and location of features in the head of a killer whale of the size modeled in the engineering analysis. The yet unpublished CT scan data presented in this report were made available by Ted Cranford of Quantitative Morphology Consulting, Inc., and are reproduced here with his permission.

Figure A. 1 shows a sagittal slice through the head of the whale. The location of the transverse slice shown in Figure A. 2 is located approximately 40 cm from the anterior tip of the whale's head. The intersection of the transverse slice line and the upper surface of the whale's head is the approximate location modeled as the location of impact of the turbine blade on the upper surface of the whale's head.

Figure A. 2 shows the CT scan for a transverse slice through the head of the whale, as indicated in Figure A. 1. This slice intersects the lower mandibles of the whale's jaw, which are the "hook"-shaped images to the right and left of center. The hollow voids in the whale's lower mandibles are filled with acoustic fat and other soft tissue and are believed to have a function in the reception of sound by the whale.

The whale's head is approximately 912 mm thick along the transverse slice line shown in Figure A. 1. In Figure A. 1, it appears that the mouth of the whale may have been somewhat agape when the head was scanned. However, even considering this condition, it is clear from Figure A. 1 and Figure A. 2 that the outline of the whale's head is oblong in shape, being compressed laterally. These images and data were not available when the finite element model of the whale's head used in the engineering analysis was constructed or when assessment of the extent of exposure of the whale's head to the turbine's blades was made. Given the turbine blade spacing of 550 mm shown in Figure A. 1, assuming that the approach of the whale would be straight toward the blade assembly, it seems that whales the size of this adult female would most likely not be able to extend their head into the blade assembly (blade length on the order of 1,250 mm) to the extent used in the model, even more so if the turbine's shroud were considered in the analysis. Modeling the location of blade strike further forward on the whale's head makes the assessment of the force of the strike absorbed by tissue conservative because the amount of blade strike energy that would have gone into "pushing" the whale away from the blade is increased as the location of strike is moved away from the center of mass of the whale. However, there is less soft tissue on the anterior of the head, so that a strike in this location might result in more severe consequences. Stranded pilot whales have been noted to sustain the greatest number of injuries on the forward (ventral) third of their heads, however no indication is clear as to the cause of the injuries. Most of the injuries were shown to be non-lethal (Oremland and Allen 2010).

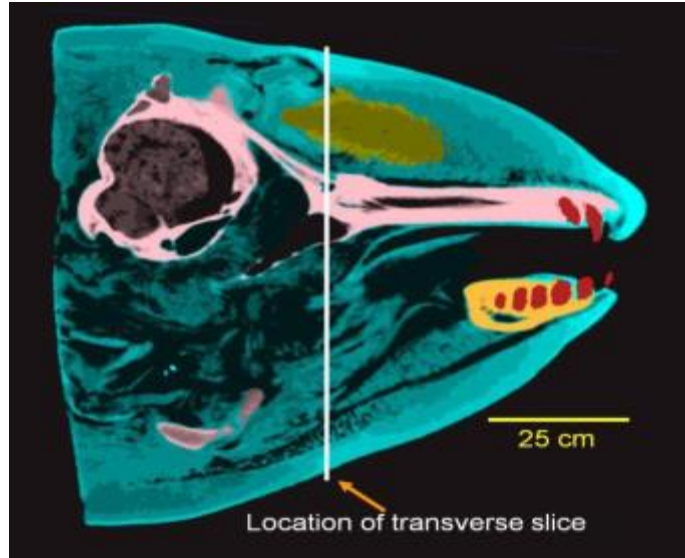


Figure A. 1. A sagittal CT scan of the head of an adult killer whale. Bone is shown as pink with the lower mandible in orange, teeth as red, voids are black, and other tissues in various other colors. Portions of the upper mandible of the whale's jaw and a cross section through the whale's skull are clear.

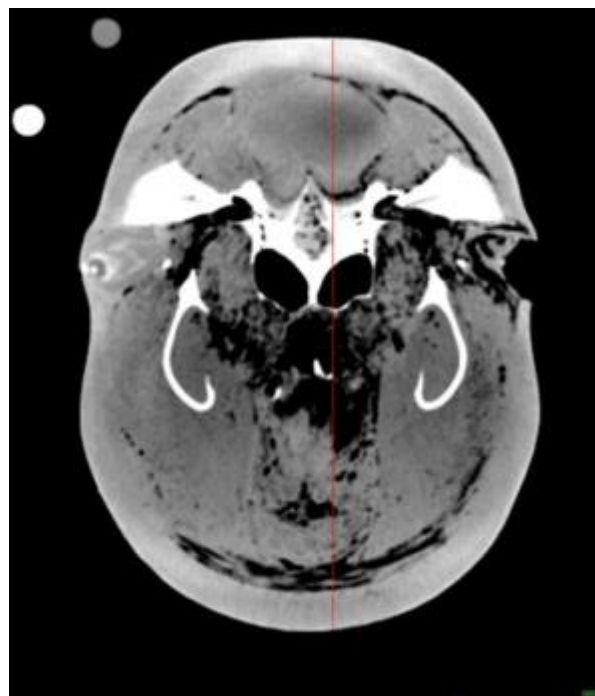


Figure A. 2. CT scan of a transverse slice through the head of a killer whale approximately 40 cm from the tip of the whale's snout. The red line identifies a transect through the slice where CT scan image intensity values were sampled. In this figure, bone is white, voids are black, and other tissues are gray.

Figure A. 3 shows the CT scan image intensity data along a vertical transect through the transverse CT scan slice shown in Figure A. 2. CT scan image intensity data is proportional to the density of the tissue and bone. The x -axis is incremented in index units that correspond to a physical length through the head of the whale of approximately 2.5 mm each. The y -axis indicates the transmissivity of the tissue to the radiation. In Figure A. 3, the first data points on the left are for higher-density skin and fibroelastic connective tissues, followed by lower-density adipose and other tissue. Bone has the highest image pixel

intensity. These data can be used to estimate the thickness of various tissues and the location of bone relative to the surface of the whale’s head. Along this transect, it is estimated that the high-density tissue of the whale’s skin and fibroelastic tissue are approximately 50 mm thick, and the lower-density adipose and connective tissue between this layer and the maxilla bones is on the order of 200 mm thick. In total, there is approximately 250 mm (9.8 in.) of tissue with varying density and biomechanical properties between the upper surface of the whale’s head and upper mandible bone, along the transect shown in Figure A. 2. The tissues overlying the mandible in whales probably act as a “bumper” that absorbs and redistributes stresses applied to the surface of the whale (Campbell-Malone 2007).

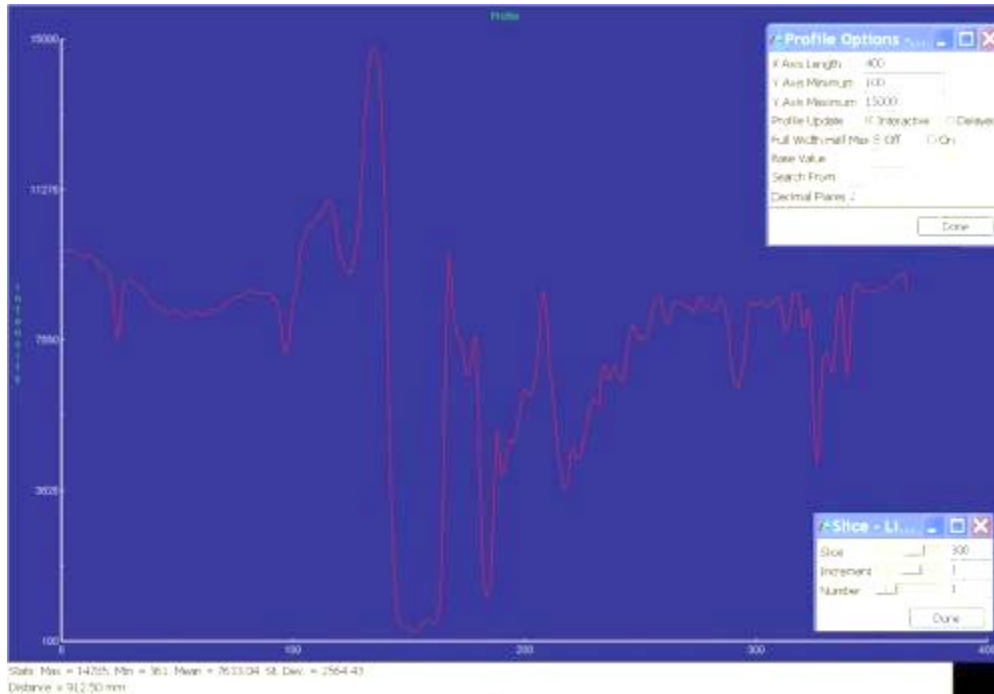


Figure A. 3 Intensity values along a vertical transect through a transverse slice of CT scan data for the head of a killer whale

Appendix B – Biomechanical Properties of Tissue

B.1 Biomechanical Literature Review

In the FY12 report (Carlson et al. 2012), a literature review was performed to understand the biomechanical properties of complex tissues like SRKW epidermis. Biomechanical data obtained by testing skin and blubber tissue from stranded SRKW was used in all engineering analysis presented in this report. The biomechanical data of similar tissues obtained by the literature review provided a context for evaluating SRKW biomechanical test data.

B.2 Biomechanical Properties of Tissue

The literature review determined that very little information exists for mechanical properties of whale skin. J.P. Winn (2006), in a master's of science thesis that investigated the physical response of whale tissue to entanglement as well as a peer reviewed article on the same topic (Winn et al. 2008), reported that

The dermal layer is composed of an extensively cross-linked network of collagen fibers that may function as an elastic recoil mechanism during swimming activities. However, to date the only structural studies on cetacean epidermis have been measurements of epidermal thickness and evaluations of surface properties, including surface roughness and resistance to biofouling. Epidermal thickness ... ranging from a minimum of 1.4 mm to a maximum of 25 mm in fin (*Balaenoptera physalus*) and bowhead whales (*Balaena mysticetus*) respectively.

Table B. 1 Comparative epidermal ranges reported for baleen whale species (Winn 2006, Table 1)

Epidermis Thickness:								
Species	Gender	Length (cm)	Maximum Thickness (mm)	Source	Gender	Length (cm)	Minimum Thickness (mm)	Source
Balaena mysticetus	-	-	25.0	Haldiman <i>et al.</i> 1985	-	-	8.6	Haldiman <i>et al.</i> 1985
Balaenoptera acutorostrata	-	-	3.0	Singarajah 1984	-	-	3.0	Singarajah 1984
Balaenoptera acutorostrata	F	708	3.0	Sokolov 1982	F	708	1.4	Sokolov 1982
Balaenoptera physalus	M	156	3.9	Sokolov 1982	F	160	2.5	Giacometti 1967
Eubalaena glacialis	M	107	13.2	Sokolov 1982	F	163	8.6	Sokolov 1982
Megaptera novaeangliae	M	857	5.6	Jones and Pfeiffer 1994	M	857	4.3	Jones and Pfeiffer 1994

Winn's thesis contains results from abrasion tests on whale epidermis using 6.4-mm and 9.5-mm float line. Tests used straight pull and oscillatory pull under load to evaluate the effects of movement of rope across whale skin. The intent of the experiments was to model injury to the skin of whales struggling to free themselves from entanglement.

Observations from both bowhead and right whales indicate that the primary strength in the epidermis is oriented in a vertical direction while laterally the structure is more elastic with lower strength. From a structural standpoint, this type of fiber integration would have several mechanical advantages. Strong vertically oriented fibers would both increase the abrasion resistance of the epidermis and may help to decrease the compressibility of the layer (Figure B. 1). As a lateral abrading force is applied to the surface of the epidermis, the strong vertical fibers would start to bend, orienting in the direction of the applied load. This flexure would allow the load to be applied in line with the vertical fibers that are anchored through the entire epidermal layer. Retaining elastic elements between these vertical fibers would maintain the flexibility needed in the epidermis allowing the epidermis to stretch during normal swimming activities. This elasticity may be graded through the stratum intermedium as the degree of keratinization and flattening of the epidermal cells has been noted to increase with distance from the stratum germinativum.

Winn also reports that

The depth of penetration and character of the dermal papillae may also substantially influence the strength of the epidermis as a unit. Assuming that a more multidirectional orientation of collagen fibers in the dermal material enhances the tensile properties of the dermis, the volume of this dermal material interwoven within the epidermis would substantially influence the structural characteristics of the layer.

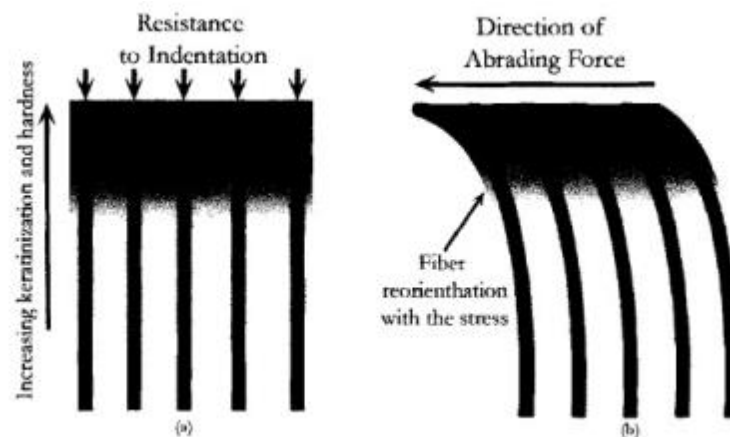


Figure B. 1. Structural advantages of a vertical fiber orientation within the epidermis. Fibers provide resistance to: (a) indentation and (b) lateral abrasion. (Winn 2006)

Based on the information from Winn (2006), in the absence of biomechanical data for whale skin, hyperelastic material was used to examine the SRKW skin layer as a baseline comparison. Figure B. 2 and Table B. 2 show properties of rubber and various elastomers.

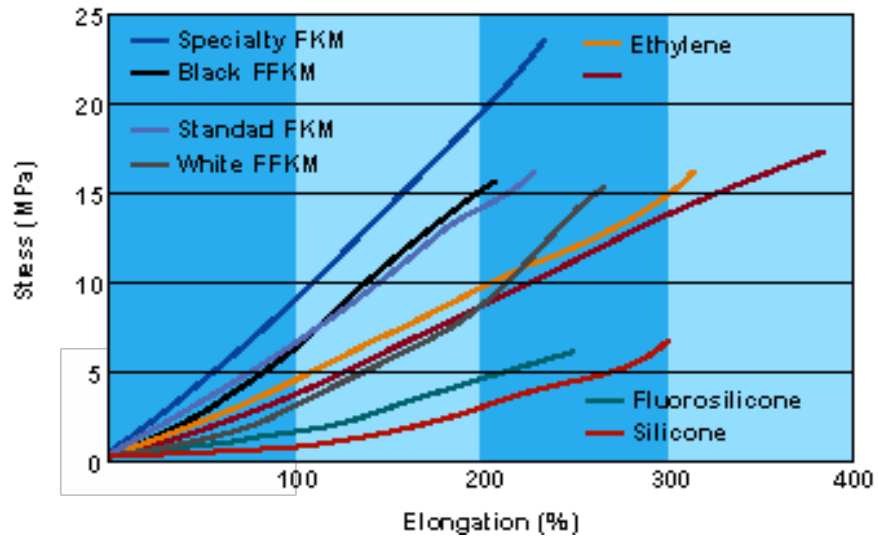


Figure B. 2. Examples of stress-strain characteristics for some manmade elastomers (*The Physics of Rubber*, <http://www.allsealsinc.com/allseals/Orings/or13.htm>)

Table B. 2. Properties of various elastomers (Schaefer 2009, Table 33.2)

ASTM designation	NR	BR	SBR	HIR CIIR	EPM EPDM	CSM	CR	NBR	HNBR	ACM ANM	T	FKM	FVMQ	VMO MQ, PMQ, PVMQ	AU EU	GPO	CO ECO
Durometer range	30-90	40-90	40-80	40-90	40-90	45-100	30-95	40-95	35-95	40-90	40-85	60-90	40-80	30-90	35-100	40-90	40-90
Tensile max, psi	4500	3000	3500	3000	2500	4000	4000	4000	4500	2500	1500	3000	1500	1500	5000	3000	2500
Elongation max., %	650	650	600	850	600	500	600	650	650	450	450	300	400	900	750	600	350
Compression set	A	B	B	B	B-A	C-B	B	B	B-A	B	D	B-A	C-B	B-A	D	B-A	B-A
Creep	A	B	B	B	C-B	C	B	B	B	C	D	B	B	C-A	C-A	B	B
Resilience	High	High	Med.	Low	Med.	Low	High	Med.-Low	Med.	Med.	Low	Low	Low	High-Low	High-Low	High	Med.-Low
Abrasion resistance	A	A	A	C	B	A	A	A	A	C-B	D	B	D	B	A	B	C-B
Tear resistance	A	B	C	B	C	B	B	B	B	D-C	D	B	D	C-B	A	A	C-A
Heat aging at 212°F	C-B	C	B	A	B-A	B-A	B	B	A	A	C-B	A	A	A	B	B-A	B-A
T _b , °C	-73	-102	-62	-73	-65	-17	-43	-26	-32	-24, -54	-59	-23	-69	-127, -86	-23, -34	-67	-25, -46
Weather resistance	D-B	D	D	A	A	A	B	D	A	A	B	A	A	A	A	A	B
Oxidation resistance	B	B	C	A	A	A	A	B	A	A	B	A	A	A	A	B	B
Ozone resistance	NR-C	NR	NR	A	A	A	A	C	A	B	A	A	A	A	A	A	A
Solvent resistance																	
Water	A	A	B-A	A	A	B	B	B-A	A	D	B	A	A	A	C-B	C-B	B
Ketones	B	B	B	A	B-A	B	C	D	D	D	A	NR	D	B-C	D	C-D	C-D
Chlorohydrocarbons	NR	NR	NR	NR	NR	D	D	C	C	B	C-A	A	B-A	NR	C-B	A-D	A-B
Kerosene	NR	NR	NR	NR	NR	B	B	A	A	A	A	A	A	D-C	B	A-C	A
Benzol	NR	NR	NR	NR	NR	C-D	C-D	B	B	C-B	C-B	A	B-A	NR	C-B	NR	B-A
Alcohols	B-A	B	B	B-A	B-A	A	A	C-B	C-B	D	B	C-A	C-B	C-B	B	C	A
Water glycol	B-A	B-A	B	B-A	A	B	B	B	A	C-B	A	A	A	A	C-B	B	C
Lubricating oils	NR	NR	NR	NR	NR	A-B	B-C	A	A	A	A	A	A	B-C	A-B	D	A

A = excellent, B = good, C = fair, D = use with caution, NR = not recommended
 SOURCE: *Seals Eastern, Inc.*

Table B. 3 shows mechanical properties from Matbase and Matweb for a wide variety of elastomers. To understand the effects of the whale skin layer from turbine blade impact, it would be advantageous to run multiple engineering models with hyperelastic materials. Materials such as natural rubber and fluorosilicone rubber fall into this category and have properties that bound those of the materials in this category.

Table B. 3. Mechanical properties of various elastomers (<http://www.matbase.com> and <http://www.matweb.com/>)

Material	Ultimate Yield Stress (kPa)	Elongation/Strain %	Young's Modulus (MPa)
Butadiene Rubber	15000	200–400	
Chloroprene Rubber (CR)	25000	100–400	
Chlorosulph PE	20000	200–500	2–15
Ethenepropenediene Rubber	20000	250–500	2–10
Liquid Silicon Rubber	7000	250–550	—
Natural Rubber (NR)	30000	750–850	1–5
Nitrile Rubber (NBR)	20000	200–500	2–5
Silicon Rubber (SI, Q, VMQ)	8000	200–800	1–5
Styrenebutadiene Rubber (SBR)	25000	250–700	2–10
Urethane Rubber	30000	300–400	2–10
Butyl Rubber (IIR, CIIR, BIIR)	17000	400–800	—
Chlorosulfonated Polyethylene Rubber	21000	200–500	—
Epichlorohydrin Rubber (CO, ECO)	17000	150–500	—
Ethylene Propylene Rubber (EPM, EPDM)	17000	600	—
Fluorosilicone Rubber (FMQ, FVMQ, FSI)	8600	100–400	—
Hydrogenated Nitrile Rubber (HNBR)	30000	100–400	—
Natural Rubber, Not Vulcanized (NR, IR,	27600	500	—
Natural Rubber, Vulcanized (NR, IR,	28000	100–800	—
Polybutadiene Rubber (BR)	17000	300–800	—
Polychloroprene Rubber (CR)	28000	100–800	—
Polynorbornene Rubber (PNR)	24000	—	—
Polyphosphazene Rubber (PZ, FZ)	14000	—	—
Propylene Oxide Rubber (GPO)	17000	—	—

B.3 Biomechanics of Human Skin

Human skin has the same basic construction as SRKW skin, with an epidermis, dermis, hypodermis, and a fourth layer connecting the skin to underlying tissue. Human skin has been found to behave as a nonhomogeneous, anisotropic, nonlinear viscoelastic material (Hendriks 2001). A basic function of the skin is to protect the body from mechanical injury.

The stress-strain relationship for human skin is shown in Figure B. 3. The top line in Figure B. 3 is the true stress-strain curve for human skin; the two below are elastic and viscous stress-strain curves.

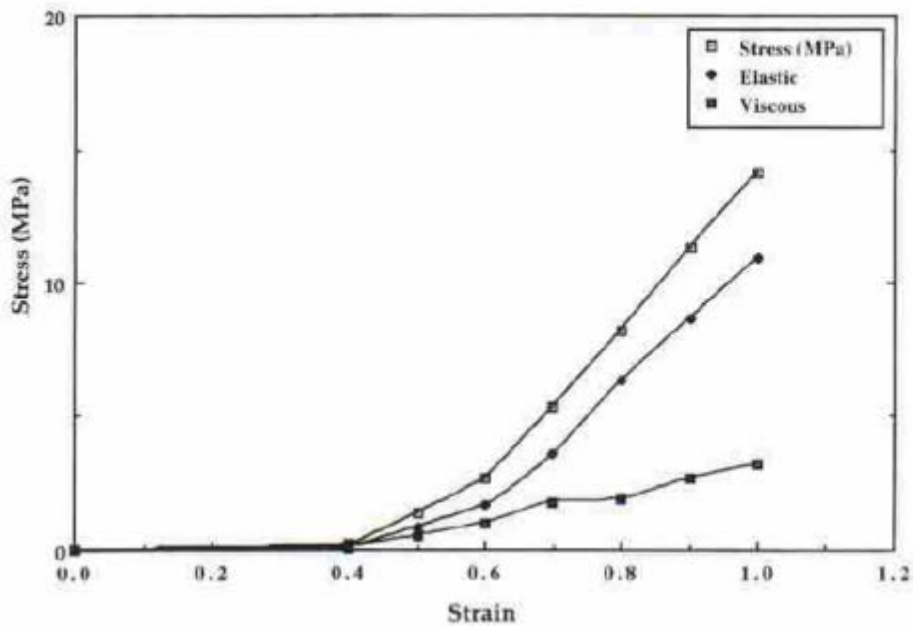


Figure B. 3. Relationship between stress and strain for human skin showing true stress (unfilled squares), elastic (diamond symbols), and viscous (filled squares) components (after Silver et al. 2001, Figure 2)

B.4 Material Properties for SRKW

Material properties for a Cuvier’s beaked whale are available via tissue sample testing and CT scanning from Soldevilla et al. (2005). Table B. 4 shows the elastic modulus for several tissue types.

Table B. 4. Elastic moduli (kPa) for several whale tissue types (Soldevilla et al. 2005, Table 4)

Stress (kPa)	Forehead tissues			Mandible tissues	
	Blubber	Acoustic fat	Connective tissue	Blubber	Acoustic fat
2.5	59	75	124	158	78
5	208	153	149	220	215
10	411	212	279	400	303
20	712	412	618	650	420
30	1006	626	1030	913	587
40	1200	739	1295	991	726
50	1410	910	1510	1174	934

These stresses are somewhat lower than what is expected for the impact scenario analysis, and extrapolation may be required to determine the elastic modulus at higher stress states. Figure B. 4 shows the curve developed by Soldevilla et al. (2005) for stress versus strain of the whale blubber. The data in Figure B. 4 suggest that the strain and stress for Cuvier’s beaked whale tissue reach an asymptote near 1.8 MPa. In addition, the blubber and connective tissue have very similar elastic moduli, and the same value could be reasonably used to represent each. 1.8 MPa was used as a conservative estimate for the whale-blubber complex in the 2012 strike analysis. In the 2013 analysis biomechanical data for skin and blubber obtained from testing SRKW tissue was used in the strike analysis (Appendix C).

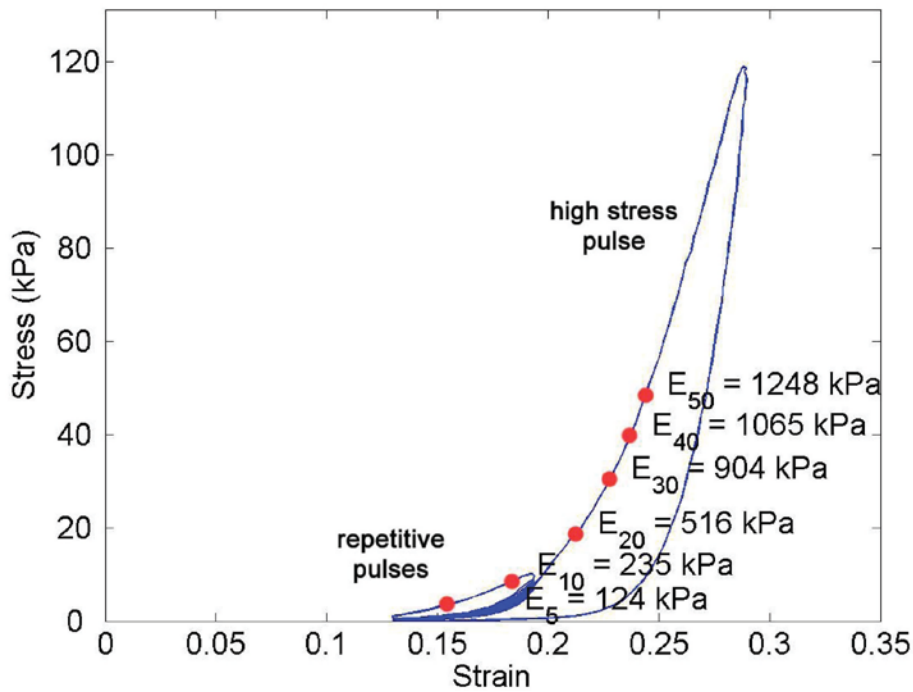


Figure B. 4. Stress-strain curve for whale blubber (Soldevilla et al. 2005, Figure 7)

Data provided by PNNL for the structure of the head region from McKenna (2005) provide sufficient detail to reconstruct the dimensions of bone matter in the head for use in the finite element model. The material properties of the bone matter can be extracted from Table 4.5 in Campbell-Malone (2007), which provides several values for elastic moduli of right whale (*Eubalaena glacialis*) mandible bone as a function of direction. Although the NARW is much larger than a SRKW and has a more massive mandibular, in the absence of other data, this analysis assumed that the SRKW mandibles have similar biomechanical properties to those of right whales. This assumption is considered to be appropriate as SRKWs are thought to have sturdy mandibles, based on the animals' observed behavior using their rostrums to batter or ram prey animals. The average value is approximately 300 MPa for both directional and bone type (trabecular or cortical); this value was used for the finite element analysis.

Appendix C – SRKW Tissue Analysis

C.1 SRKW Tissue Testing Methods

Two samples of orca (*Orcinus orca*) skin (epidermis plus underlying blubber or hypodermis) were obtained through NOAA's marine mammal stranding network. One sample of skin was from L-112, a 3 year old juvenile female that died in February 2011. The tissue sample had been kept frozen for 11 months before biomechanical testing began. The skin sample was 20 cm x 15 cm and came from the right dorsal lateral side, anterior to the whale's blow hole (Figure C. 1).



Figure C. 1. Photo of SRKW L-112 (aka Sooke). Red square indicates approximate location of skin section.
http://www.beamreach.org/wp-content/uploads/L-112-20110816-KCB_SJ1-176.jpg (Photo by: Ken Balcomb, Center for Whale Research, copyright 2013)

A second skin sample was obtained from a newborn (neonatal) male SRKW from the SRKW J-pod that died in January of 2013. The sample consisted of a continuous piece of skin that began just above the upper jaw and continued over the top of the neonate's head, and included the blowhole (Figure C. 2). The neonate tissue sample was frozen for three weeks before testing.



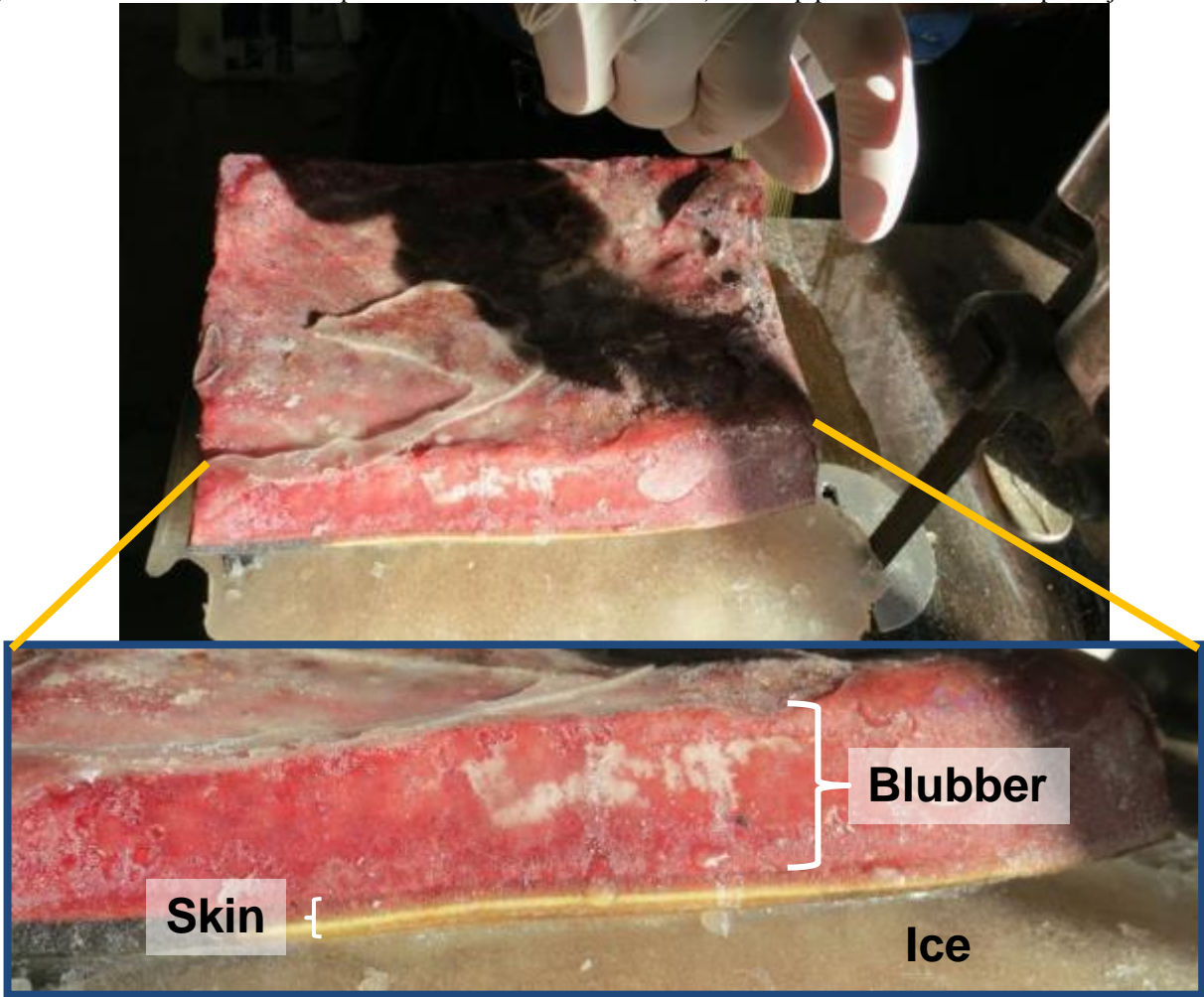
Figure C. 2. Necropsy of SRKW neonate carcass. The skin sample was the entire head region above the jaw including the blowhole. Note: the neonate's skin was debrided (likely due to surf and sand) on the right side of the animal's head, jaw, and throat area. (Photo by: Kim Parsons, NOAA Fisheries)

Biomechanical testing of juvenile and neonate tissue was conducted in January 2013. Whale tissue was kept frozen until tested. All tissue preparation and biomechanical testing was performed at Friday Harbor Laboratories (FHL).

C.2 Frozen Tissue Sample Preparation

The protocol for processing skin samples began each day with cutting the portion of skin sample needed for the day's testing from the total block of tissue. This was done using a band saw (Figure C. 3). This process was completed quickly so that the total block of tissue was out of the freezer a very short time to avoid any thawing of the primary block of tissue.

Figure C. 3. Juvenile orca skin sample and associated blubber (frozen). The top photo is the total sample of juvenile



orca skin and blubber. The lower photo shows the layers of skin (on the bottom, cream and black) and blubber (on top, red).

The second stage of sample processing was to separate the epidermis from underlying blubber. In whales the blubber and epidermal layer are tightly bound together with interconnecting fiber like tissue forming an integrated composite consisting of two layers with different biological and biomechanical properties (reference). The blubber layer is tough and oily, quite different from the almost rubber like consistency of the epidermal layer. Because of the nature of whale skin, the two layers needed to be cut apart. Figure C. 4 shows how the blubber was separated from the epidermis using a band saw. After the blubber was separated from the epidermis it was returned to the freezer for storage until it was scheduled for processing.



Figure C. 4. The photo shows the second stage of processing of a frozen subsample of juvenile skin tissue where the blubber and epidermal layers are separated using a band saw. The blubber remained frozen through this process and was returned to the freezer for later use immediately after being separated from the epidermis.

C.2.1 Epidermis (Skin) Layer Sample Preparation

Following cutting from the frozen primary block of tissue, the subsample to be processed during the day was in fresh flowing seawater (32 ppt) at ~ 12°C for at least one hour, and processed within 12 hours of thawing.

The neonate skin samples had to be prepared for processing using a different method than that used for the juvenile tissue because of the relatively thinner layer of blubber and to provide a uniform blubber tissue sample thickness for testing (C.2.2 Hypodermis (Blubber) Layer Test-Sample Preparation). For the neonate samples the blubber was separated from the epidermis using a meat slicer as shown in the photograph of Figure C. 5B. Some of the neonate skin tissue came from portions of the whale's body that

were rounded (Figure C. 5A), which could not be processed using the meat slicer. For these sample segments the blubber layer was separated from the epidermal layer by hand using a scalpel

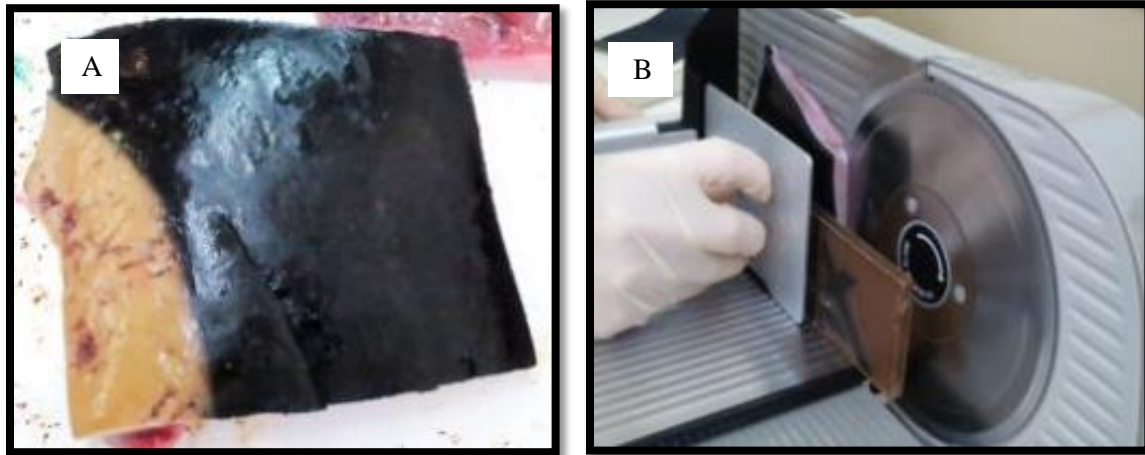


Figure C. 5. A test-sample of neonate skin showing both curved (A) where blubber was removed by hand and flatter segments (B) where a meat slicer was used to prepare a sample of neonate skin tissue.

Two different die-cut punches, dogbone and rectangular, were manufactured in the laboratory and used to prepare tissue samples for testing (Figure C. 6). The punches were made of aluminum and hold microtome (razor) blades to cut the tissues. The two punches were used to test different properties of the material. A dogbone punch is more appropriate for a maximum strength of the material, as the shape concentrates the stress in the smallest cross section of the sample and therefore breaks more consistently. The rectangular shape was more appropriate for understand the elastic modulus of the tissue.



Figure C. 6. Dogbone and rectangular tissue punches are shown above. Samples prepared with the rectangular punch were 40 mm long and 7 mm wide. Those prepared with the dogbone punch were 40 mm long and were 15 mm wide at the top and bottom and 7 mm wide in the narrower middle section.

Test-samples were extracted from tissue block by first punching the outline of the sample in the tissue then extracting the test-sample from the tissue block using a scissors and scalpel (Figure C. 7). In the case of epidermal samples, the thickness of the block of tissue was always thicker than the punch blades were long, even when much of the blubber layer was removed with the band saw or meat slicer during preparation of the block of sample tissue. The remaining thickness of blubber was cut away from the sample of epidermis by hand to extract the final test-sample (Figure C. 8).

To control for possible anisotropic material properties the orientation (i.e., left/right and nose-to-tail directions) of sample blocks and the test-sample cut from them was documented.

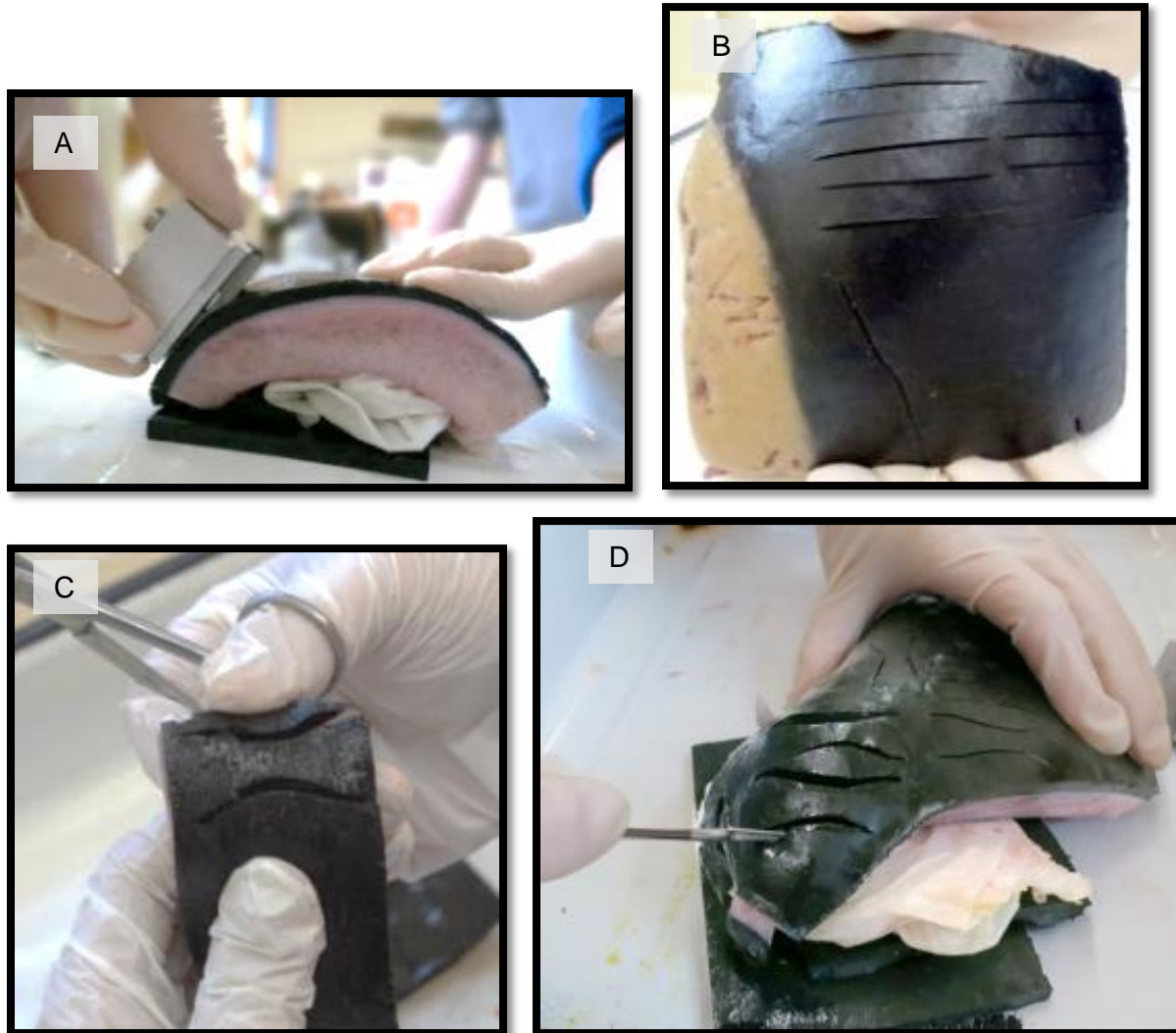


Figure C. 7. Rectangular and dogbone test-sample extraction from blocks of epidermal tissue. Panel A shows the rectangular punch being used to make the initial cut into the tissue block. Panel B shows the results of the punch use shown in panel A. Panel C and D shown the results of use of the dogbone punch on blocks of epidermal tissue and the use of a scalpel to complete removal of test-samples from the block of epidermal tissue.



Figure C. 8. The final step in epidermal test-sample preparation was removal of blubber. Because the blubber layer is firmly attached to the skin layer it had to be cut away using a scalpel.

Test-samples ready to test were wrapped in seawater soaked paper towels to keep them hydrated until they were processed.

C.2.2 Hypodermis (Blubber) Layer Test-Sample Preparation

Blubber is extremely tough, strong, and difficult to cut; it has a high fat content that makes it oily and slippery. For the tissue samples from both the neonatal and juvenile SRKW, as needed, samples of the thick blubber section cut away from the skin sample were thawed in seawater, then sliced into 3-5 mm thick layers using a meat slicer (Figure C. 9).

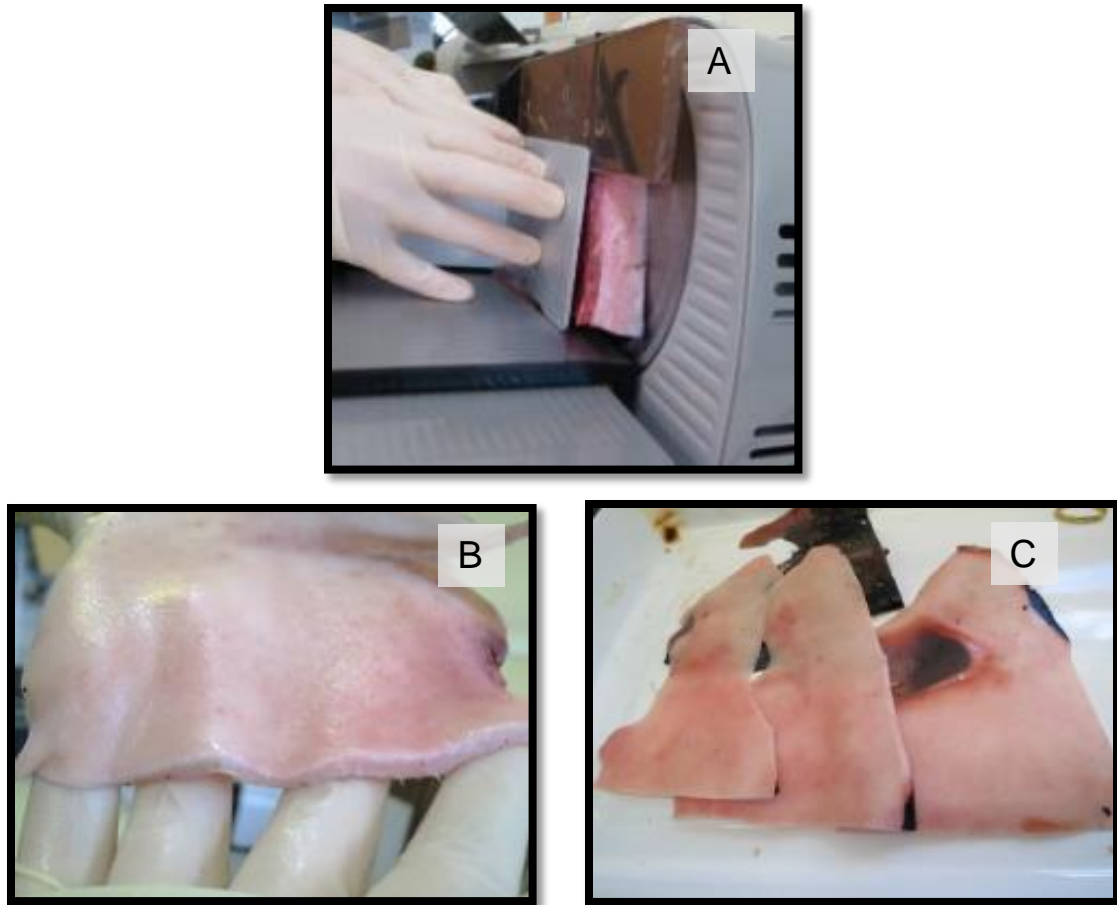


Figure C. 9. Panel A shows a section of blubber being prepared for sectioning using a meat slicer. Panels B and C show the resulting slices of blubber. As many as three slices of blubber 3-5 mm thick could be obtained from a block of blubber tissue..

Test-samples of blubber were cut from blubber slices using the dogbone and rectangular punches following the same test-sample preparation protocols as those used for epidermal skin tissue samples. The steps for preparation of dogbone samples from a slice of blubber tissue are shown in Figure C. 10.

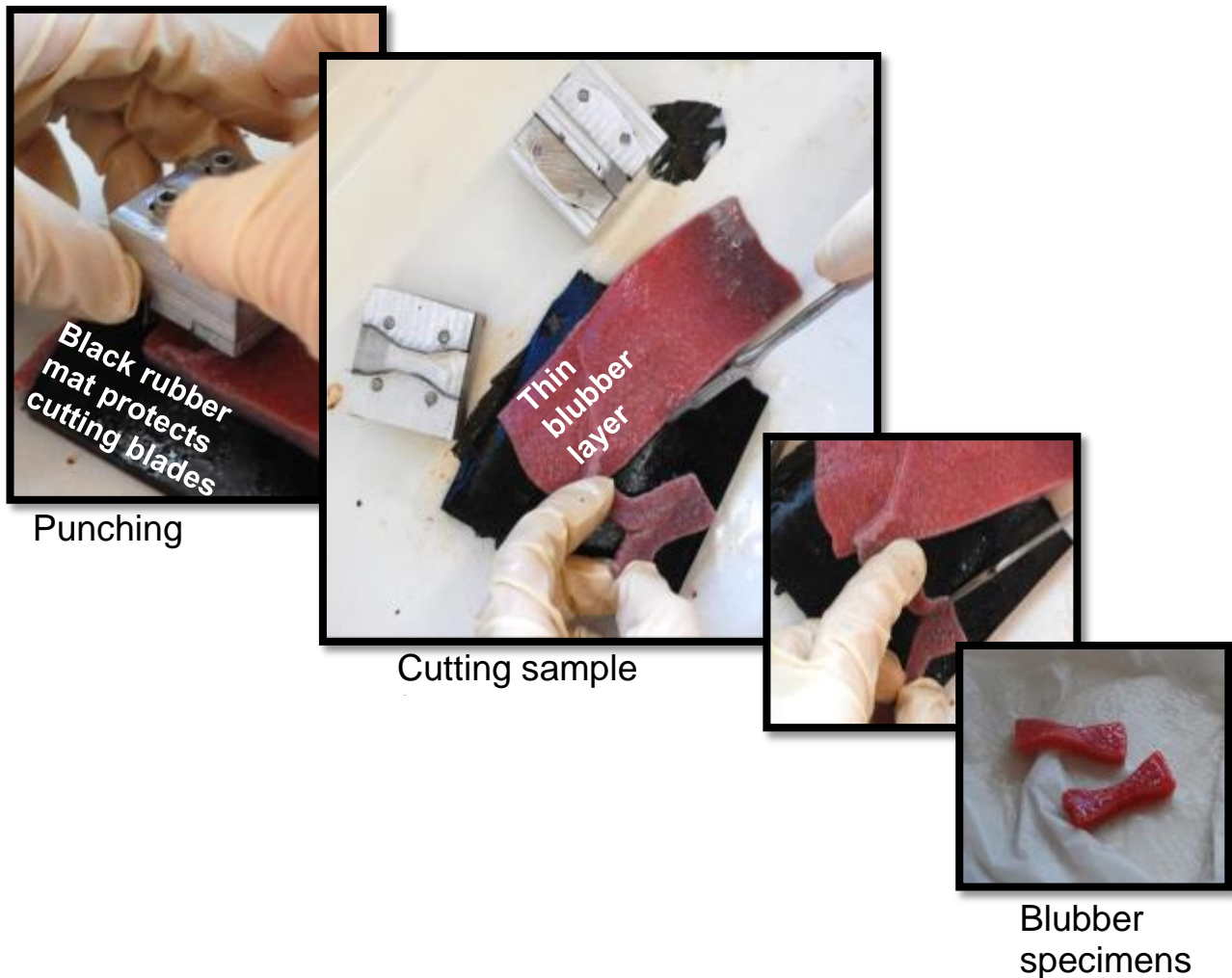


Figure C. 10. The steps in preparation of dogbone samples for tension testing from a slice of blubber are shown. The first panel shows the use of the dogbone punch on the blubber slice. The second and third panels show steps in using a scapel to finishing cutting the test-samples from the slice. The fourth panel shows the completed dogbone blubber test-samples.

As was the case for the test-samples of epidermal tissue, blubber test-samples were kept moist with seawater soaked paper towels.

C.2.3 Testing Equipment

A Materials Testing System (MTS) Synergie 100 was used with a 500 N load cell and .TestWorks 4 software running on a Dell computer to operate the system during test, and to acquire and record data. Acquired data was digitally stored for later analysis. The MTS was used for tensile, indentation (compression), and Poisson's ratio testing.

C.2.4 Tensile test

Uniaxial tension testing of a material determines the strain a material experiences (i.e. how much the material elongates relative to its original length) as a function of the stress (i.e. tensile force) applied to

the material (Ozkaya and Nordin, 1999). In the case of many biological tissues, such as whale skin, which are viscoelastic, the rate at which the force (stress) is applied is also important. For this reason the materials were tested a several crosshead speeds.

Each tissue specimen (epidermis or hypodermis) was loaded into the MTS (Figure C. 11) by clamping one end of the test-sample to the static lower head of the MTS using a clamp designed to hold biological tissue samples. The other end of the test-sample was clamped to the movable upper head of the MTS. The clamps were adjusted so that 5-10 mm of each end of the test sample was contained within the jaws of the clamps. This left a 20 mm gage length of the sample between the clamps. The MTS was then operated to bring the sample into tension and the thickness of the middle of the sample was measured using a caliper (Figure C. 11).

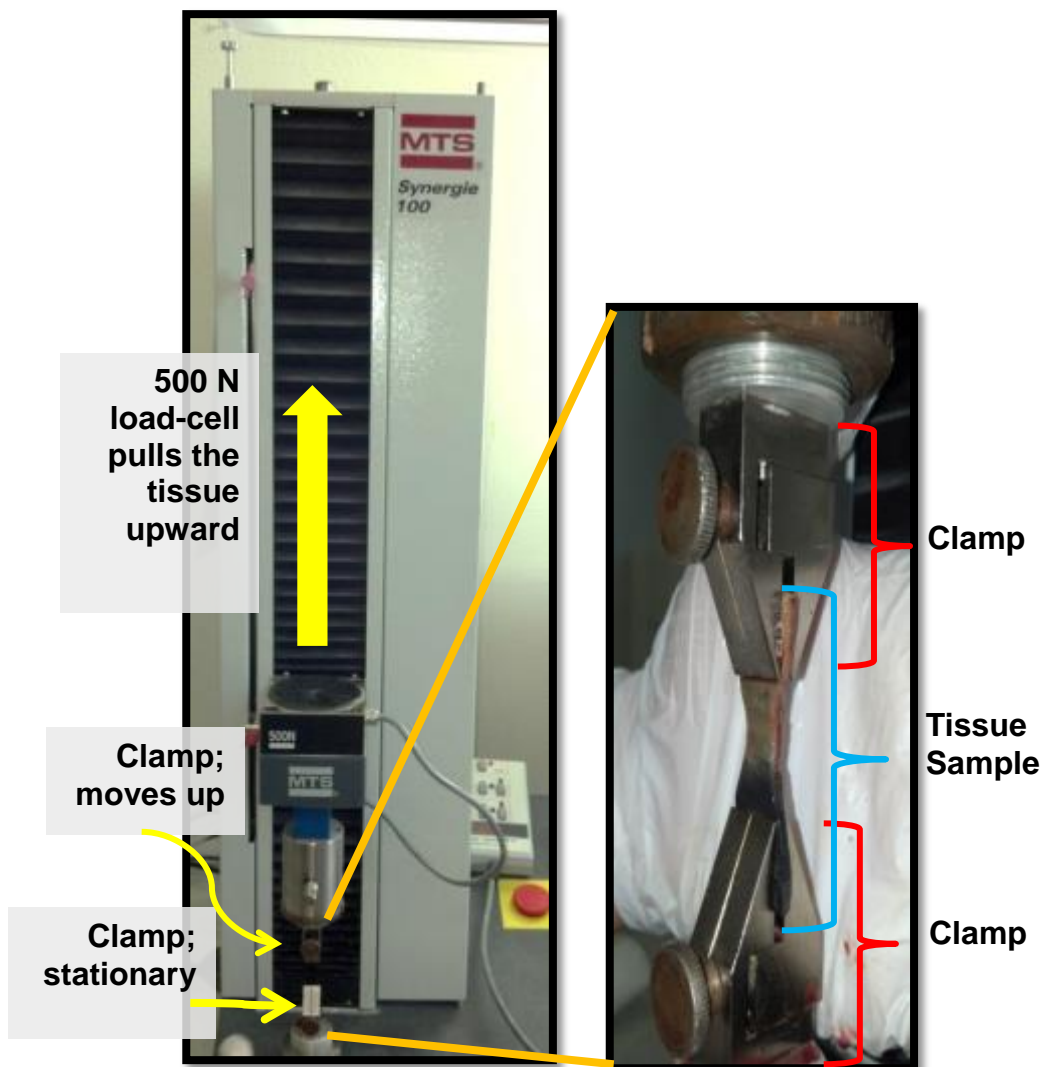


Figure C. 11. The MTS system shown with a test-sample held by the upper and lower clamps under slight tension immediately prior to testing. The left panel shows the MTS with the clamps in their starting positions. The right panel is a close up of a sample of epidermal tissue held at tension between the MTS clamps prior to testing.



Figure C. 12 Following loading of the test specimen its thickness was measured to the nearest 0.001 mm as shown above using a digital caliper.. The sample thickness was entered into the MTS software program at the beginning of a test.

Tests were run at several crosshead speeds. Juvenile samples were tested at crosshead speeds of 0.1, 1.0 and 10.0 mm/s. A crosshead speed of 1 mm/s was a 5%/s strain rate. The neonatal samples were tested at crosshead speeds of 0.001, 0.1, 1.0, 5.0, 10.0, and 15.0 mm/s. The majority of samples were tested at a crosshead speed of 1 mm/s. The dogbone test- samples had a higher likelihood than the rectangular test- samples of failure in the middle of the specimen. Both sets of tests produced load-displacement data. The data from the dogbone sample testing were used to determine failure strength. The data from testing the rectangular test- samples were used to estimate modulus and strain to failure. Failure of a test-sample was defined as a 50% drop from the maximum stress recorded. While the test was in progress, the test- samples were observed for slippage in the clamps. If a test-sample slipped in a clamp, the test was stopped, and the test-sample reset in the clamp and the test resumed.

C.2.5 Examples of Tissue at Tensile Test Endpoints

All tissues were pulled (stressed) until the tissue “failed” by tearing in two or exhibiting otherwise that it had reached its mechanical limits (Figure C. 13). This point was defined as the maximum stress for the sample. The failure point of a sample was reported as the strain when the stress had dropped to 50% of its maximum value. There was a wide range of mechanical failure modes (rips, tears, breaks) for tissue samples. If a test-sample failed at the end of a clamp during a test, the test was discarded.

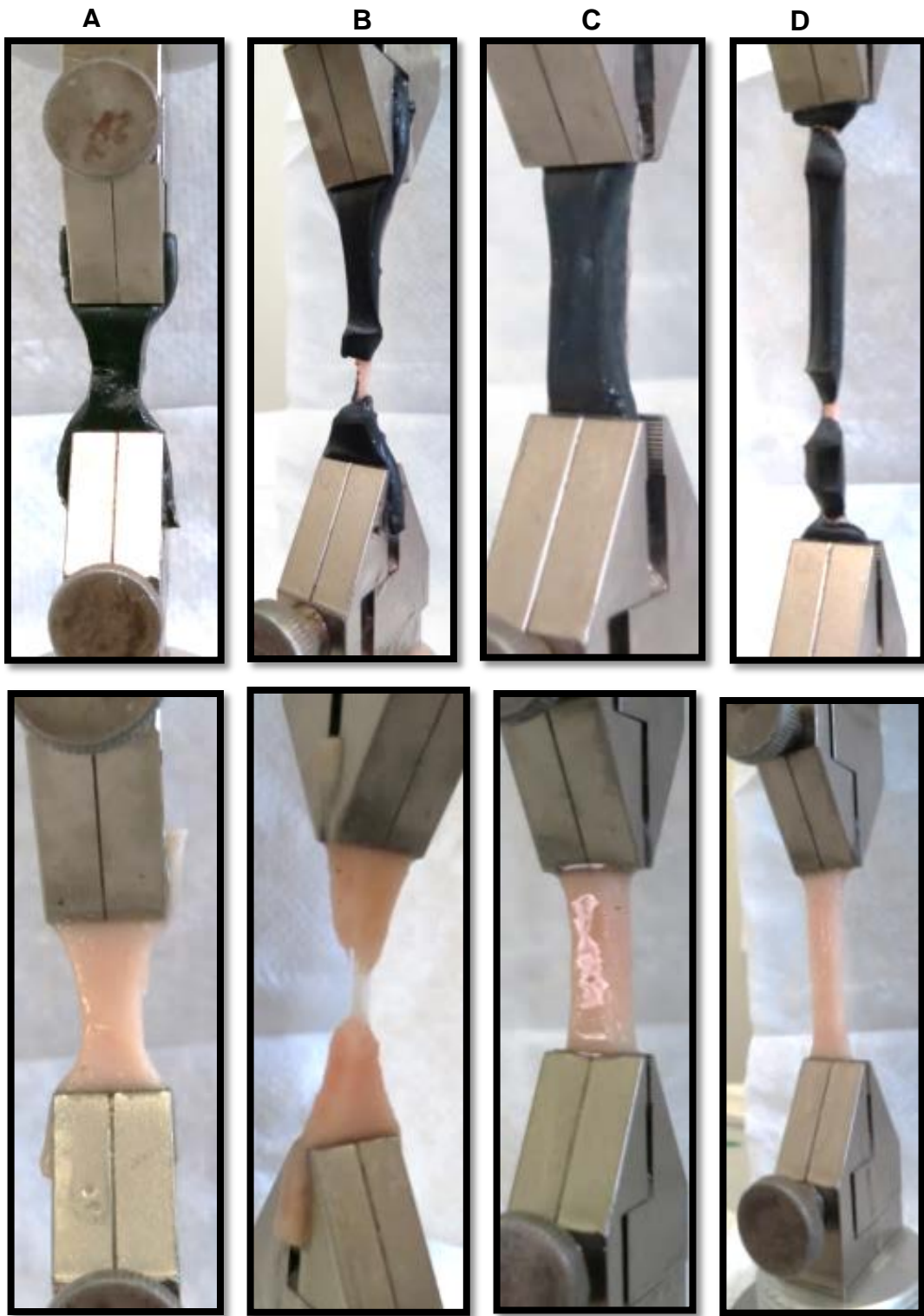


Figure C. 13. The panels in this figure show dogbone and rectangular test-samples of epidermal and blubber skin tissue at the initiation and conclusion of test. In the top row panels A and B are for a dogbone sample of epidermal tissue and C and D for a rectangular sample of epidermal tissue. The bottom row of panels show dogbone and rectangular samples of blubber (hypodermal) tissue at the initiation and conclusion of testing. At the initiation of testing samples are under a very slight stress and at conclusion exhibit signs of mechanical failure of the tissue such as rips, tears, or breaks.

C.2.6 Indentation test

An indentation test was performed with the MTS using a 31.7 mm sphere on samples of intact neonate skin consisting of unmodified epidermal and blubber layers. A skin sample was placed on the platform at the base of the MTS ram and at initiation of testing the sphere was pressed onto the dorsal surface of the skin to a maximum depth of 5 mm (Figure C. 14). At initiation of testing a force was applied to the sphere and was this force was maintained through the test. As the test progressed the skin tissue relaxed and “cupped” around the sphere (Figure C. 14). The test was stopped when the tissue sample had been compressed to 50% of its original thickness. The test purpose was to imitate a more full body response to stress.

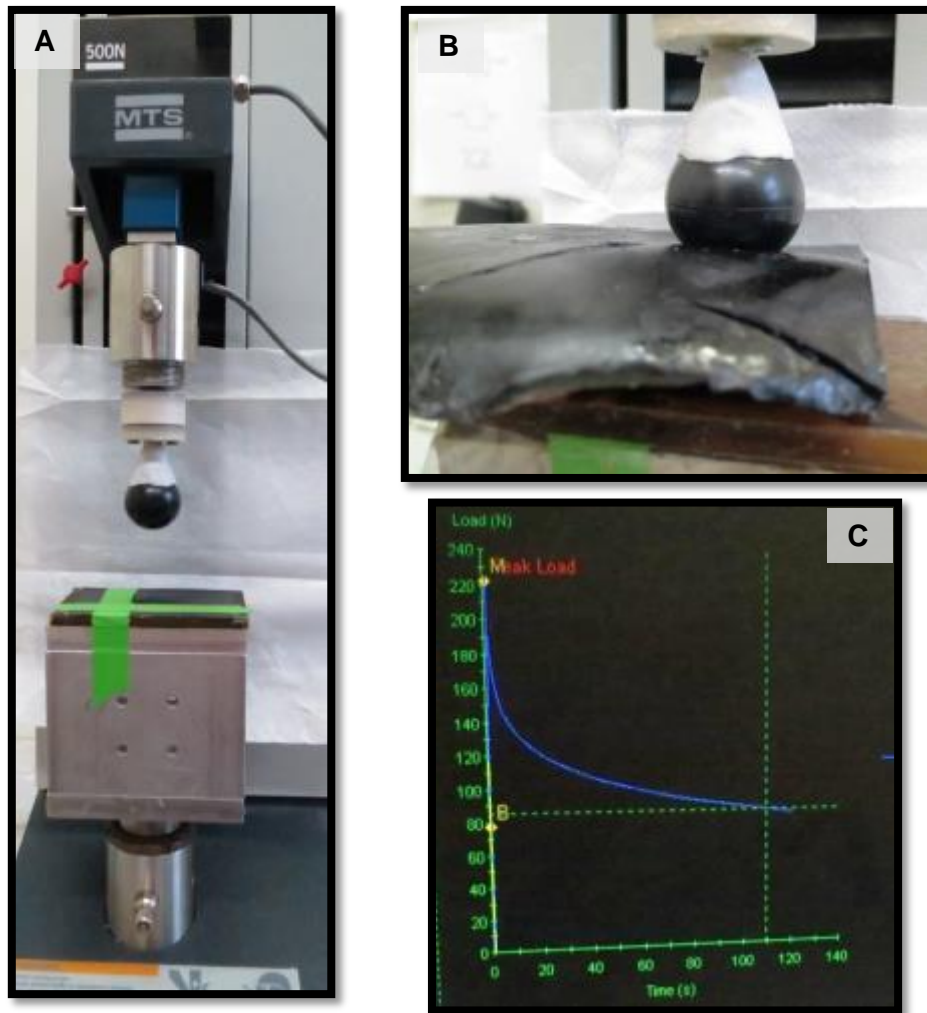


Figure C. 14. The MTS apparatus set up to conduct compression testing is shown in the first panel of the figure. The sphere used for the test and the platform on which the tissue samples were placed are shown. The top right panel shows a sample of skin tissue during compressive testing with the sphere indenting the surface of the tissue. The bottom right panel shows the output of the testing which is the force in N applied to the sample as a function of time in seconds.

Additional compression tests were conducted on 2 cm square slugs of juvenile whale blubber. The slugs of blubber were compressed between flat plates using the MTS. A slug of blubber was loaded on the lower plate and the top plate brought into contact and a very light load was applied. The thickness of the

slug was measure and this value loaded into the MTS operating software. Force was applied to the tissue slug at a rate so that the slug was compressed at a rate of 5% of its thickness per second. The test was stopped when the tissue slug had been compressed to 50% of its initial thickness.

C.2.7 Estimation of Poisson's Ratio

When a sample of tissue is subjected to uniaxial tension (pulled in a one direction) the sample elongates and its cross sectional area simultaneously decreases (laterally contracts). The ratio of lateral and axial strain in a tissue sample is a constant that has been given the name Poisson's Ratio.

An extensometer was used with the MTS so that lateral and axial strains could be simultaneously measured for samples of neonate epidermal tissue. The tests were conducted using rectangular test-samples of neonate epidermal tissue. A test-sample would be clamped into the MTS, the extensometer attached and testing began by applying an axial force to the test-sample (Figure C. 15). Through the test, until the tissue being tested broke in two, both axial and lateral strain was observed as a function of applied stress.



Figure C. 15. The figure shows the MTS with a sample of neonate epidermal tissue within its clamps and an extensometer attached to the sample to measure lateral strain through the test.

C.3 Results

The MTS software, Testworks 4 recorded stress strain data as each test was in progress. FHL provided stress/strain curves based on the tissue testing; PNNL calculated material properties for the skin and blubber tissues. As expected with biological materials, the tissue testing data were highly variable. The available tissue sample for the SRKW sub-adult (L112) was small, resulting in a small sample size

for each tissue test; the neonate sample was larger, allowing for a larger sample size. PNNL provided average values for the material properties, as well as standard deviations, as input to SNL’s engineering model; raw data stress strain curves for blubber and skin were also provided to place the values in context.

In the opinion of the FHL experts and PNNL biologists, the combination of the degradation of the L112 samples and the effects of the testing set up probably led to less resistant values for the resiliency of the tissue than would be expect as a response from a living whole animal. The tissue test results for the neonate are expected to be more representative of living tissue, although the very young age of the animal presents a challenge to compare these tissues to those of an adult SRKW.

For the engineering analysis performed by SNL, only data at the 1 mm/s crosshead speed from 90° rectangular samples were taken into consideration. Strain to failure applies only to rectangular samples, since they have a uniform strain.

C.3.1 Uniaxial Tension Testing

C.3.1.1 Neonatal Skin Tissue

Neonatal Skin (epidermal) Dogbone Samples by Crosshead Speed

Table C. 1. Neonatal Skin (epidermal) Dogbone Samples by Crosshead speed

Dogbone Tests						
<i>Crosshead Speed (mm/s)</i>	<i>Series Name</i>	<i>Peak Stress Mean (MPa)</i>	<i>Peak Stress Stdev (MPa)</i>	<i>n</i>	<i>Orientation</i>	<i>Figure #</i>
0.01	NSD_0.01_0	0.880	0.286	5	0	Figure C. 17
0.1	NSD_0.1_0	0.640	0.152	5	0	Figure C. 18
1	NSD_0	1.213	0.500	8	0	Figure C. 19
1	NSD_45	1.038	0.207	8	45	Figure C. 20
1	NSD_90	1.720	0.598	10	90	Figure C. 21
10	NSD_10_0	0.960	0.219	5	0	Figure C. 22
15	NSD_15_0	1.400	0.324	5	0	Figure C. 23

Summary Figures

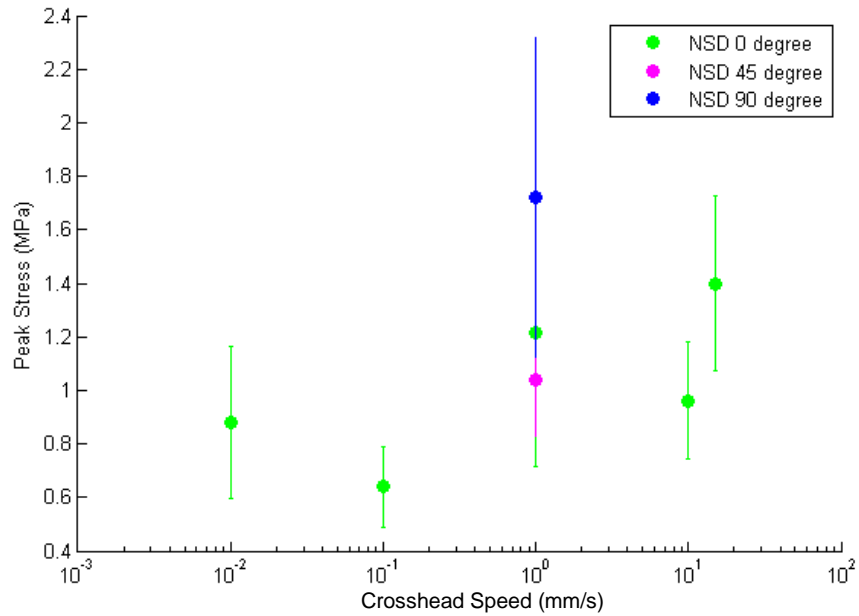


Figure C. 16. Scatter plot of peak stress values by crosshead speed. Trend toward strain-strengthening.

Individual Series Stress-Strain Figures

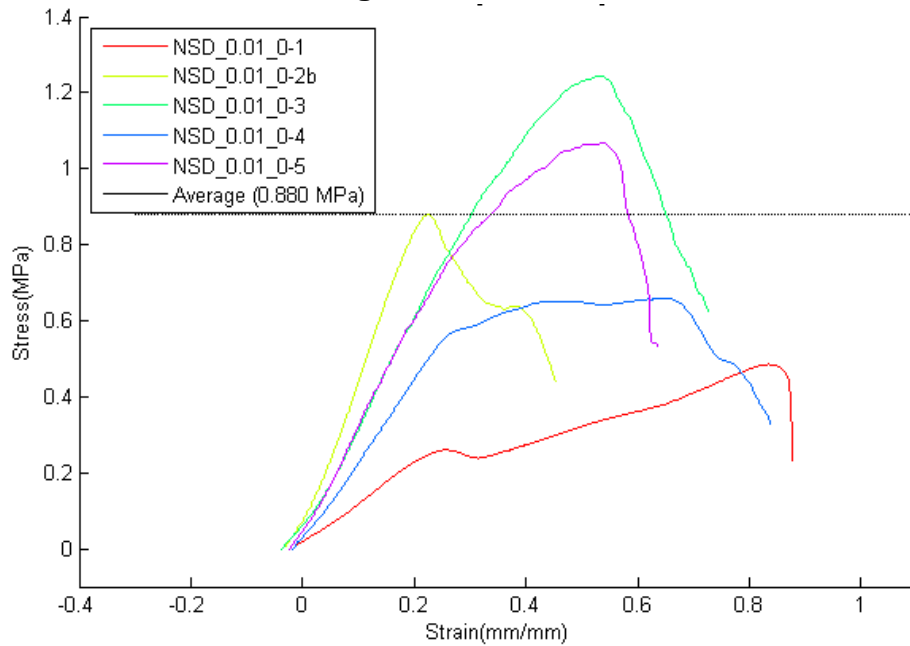


Figure C. 17. Neonatal Skin Dogbone Samples (NSD) in the 0 degree direction. Test performed at a crosshead speed of 0.01 mm/s.

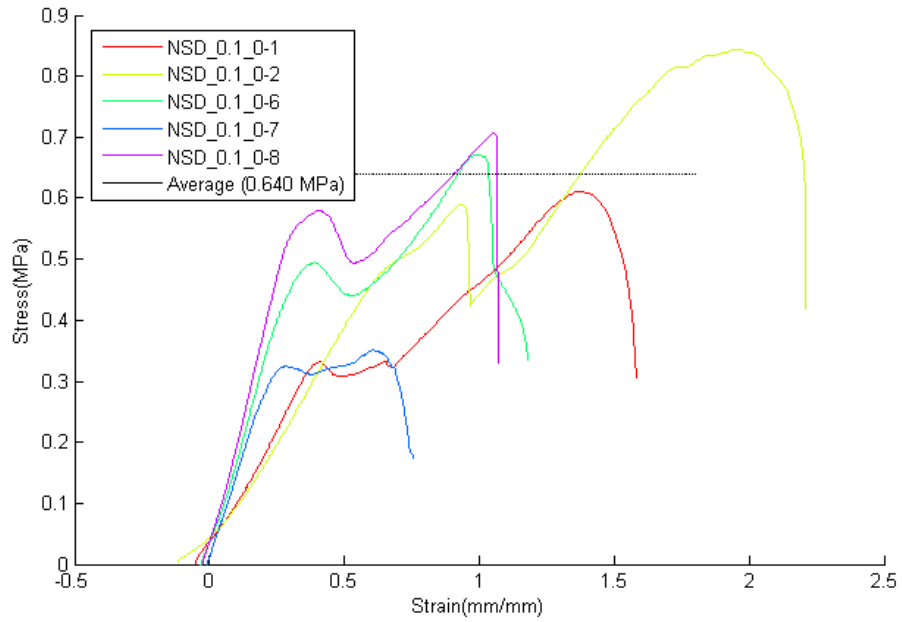


Figure C. 18. Neonatal Skin Dogbone Samples (NSD) in the 0 degree direction. Test performed at a crosshead speed of 0.1 mm/s.

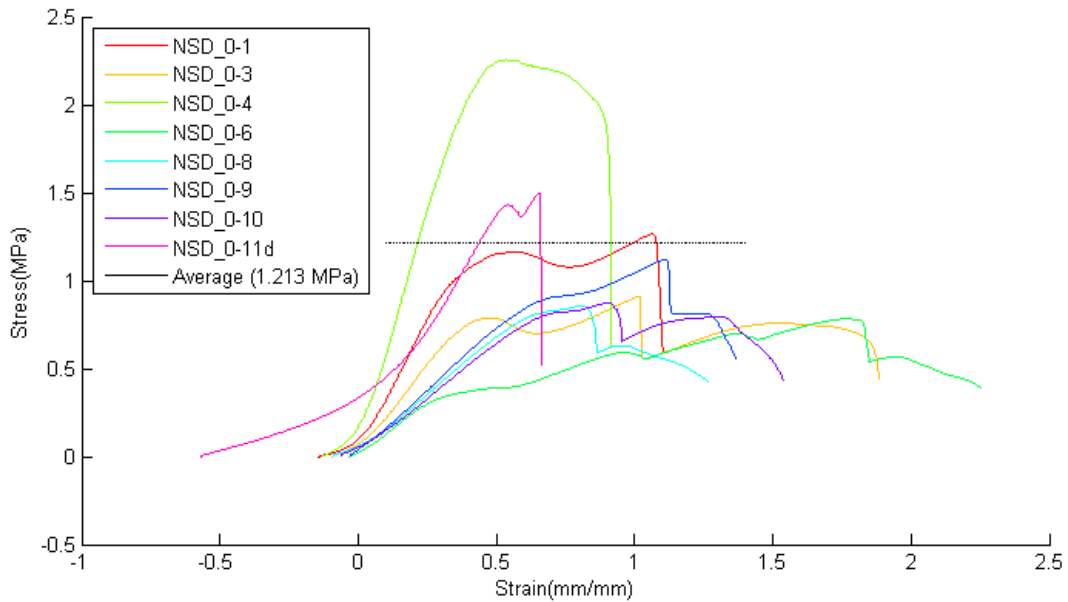


Figure C. 19. Neonatal Skin Dogbone Samples (NSD) in the 0 degree direction. Test performed at a crosshead speed of 1 mm/s

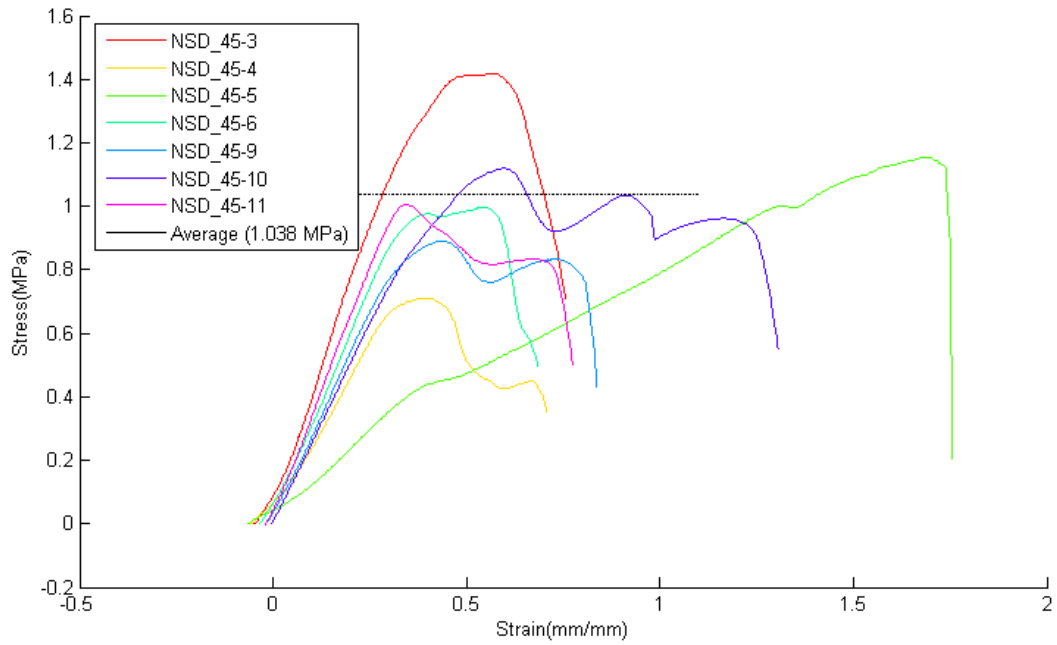


Figure C. 20. Neonatal Skin Dogbone Samples (NSD) in the 45 degree direction. Test performed at a crosshead speed of 1 mm/s.

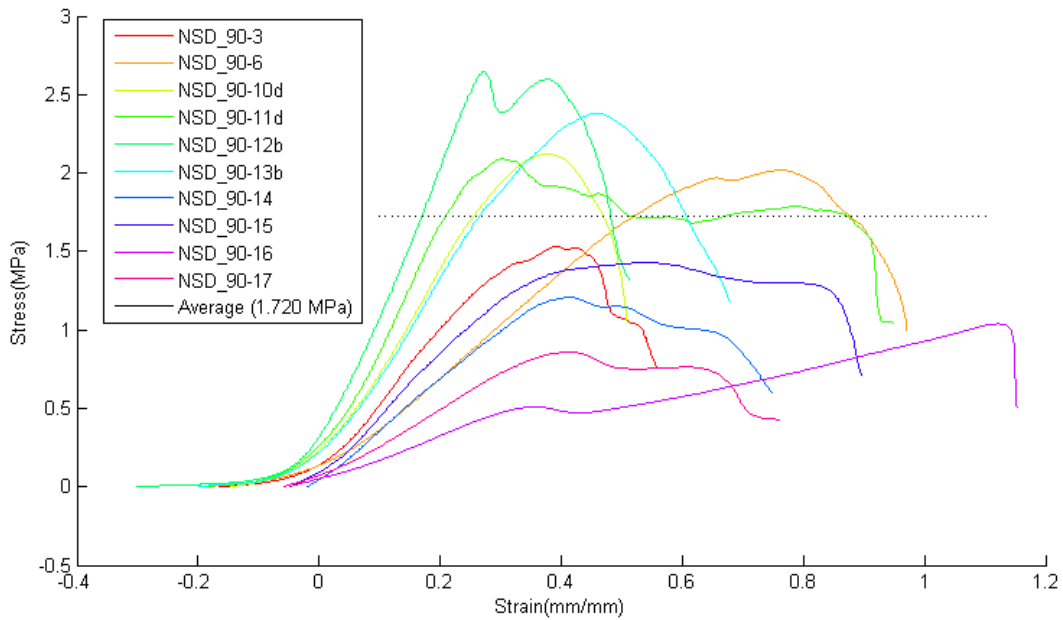


Figure C. 21. Neonatal Skin Dogbone Samples (NSD) in the 90 degree direction. Test performed at a crosshead speed of 1 mm/s.

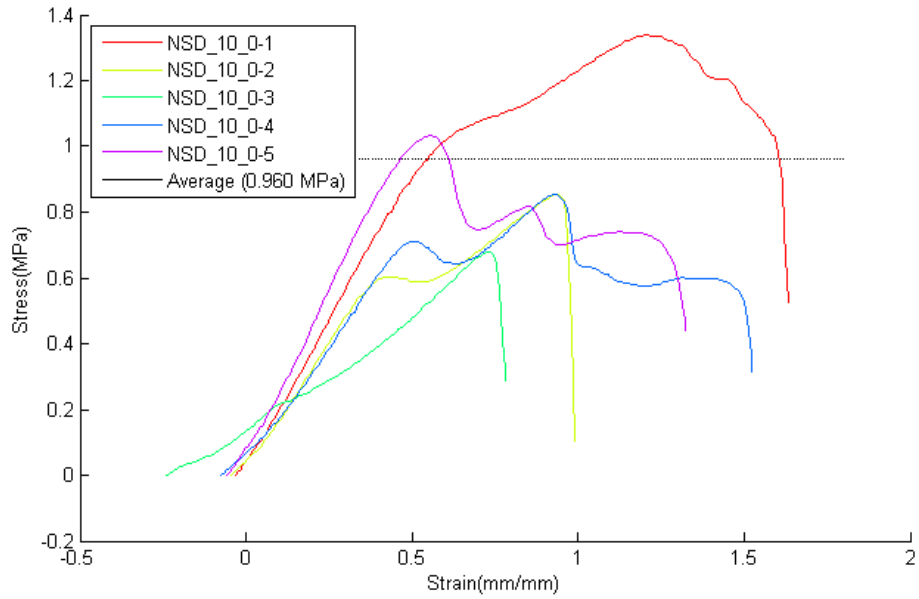


Figure C. 22. Neonatal Skin Dogbone Samples (NSD) in the 0 degree direction. Test performed at a crosshead speed of 10 mm/s.

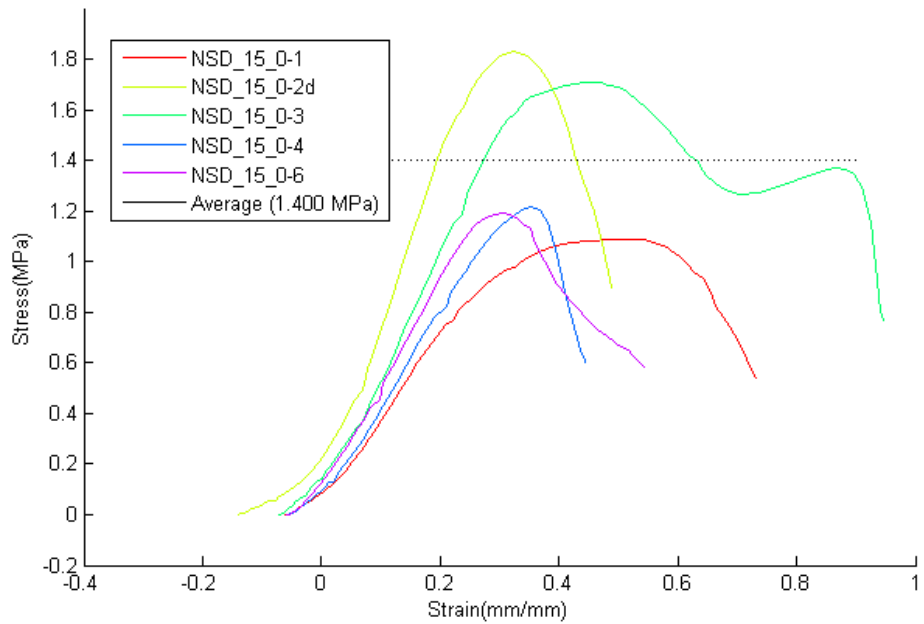


Figure C. 23. Neonatal Skin Dogbone Samples (NSD) in the 0 degree direction. Test performed at a crosshead speed of 15 mm/s.

Neonatal Skin (epidermal) Rectangular Samples

Table C. 2. Neonatal Skin (epidermal) Rectangular Samples

Crosshead Speed (mm/s)	Series Name	Rectangular Tests				Strain to failure (mm/mm)	Figure #
		Elastic Modulus Mean (MPa)	Elastic Modulus Stdev (MPa)	n	Orientation		
0.01	NSR_0.01_0	0.71	0.07	5	0	1.19	Figure C. 26
0.1	NSR_0.1_0	0.78	0.26	5	0	1.48	Figure C. 27
1	NSR_0	2.96	0.51	11	0	1.15	Figure C. 28
1	NSR_45	6.20	2.28	9	45	1.24	Figure C. 29
1	NSR_90	8.02	3.95	11	90	0.63	Figure C. 30
5	NSR_5_0	1.06	—	1	0	0.81	—
10	NSR_10_0	1.71	0.95	5	0	1.98	Figure C. 31
15	NSR_15_0	1.45	0.34	5	0	1.31	Figure C. 32

Summary Figures

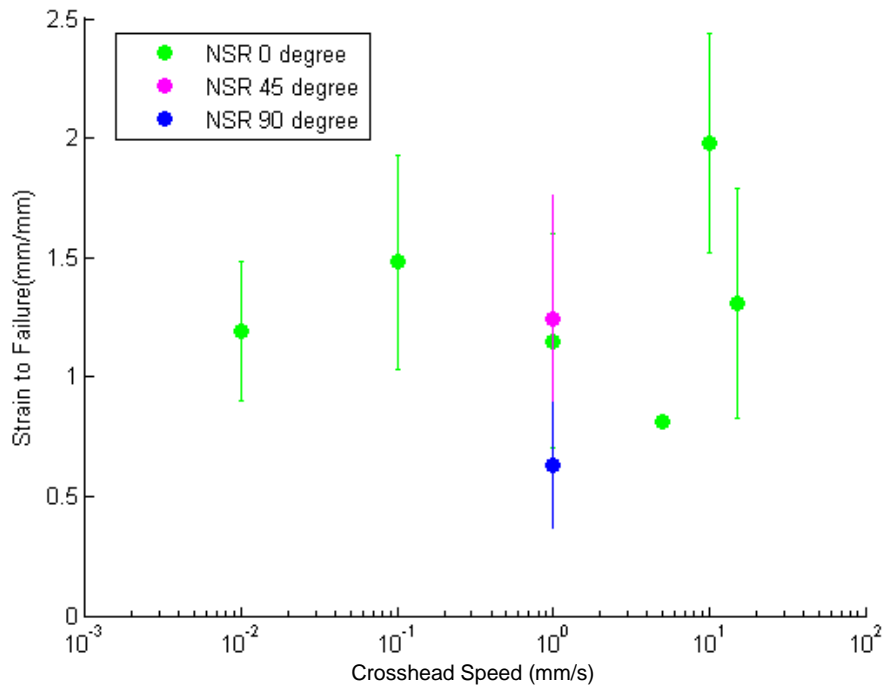


Figure C. 24 Scatter plot of the strain to failure for neonatal skin rectangular samples plotted by crosshead speed.

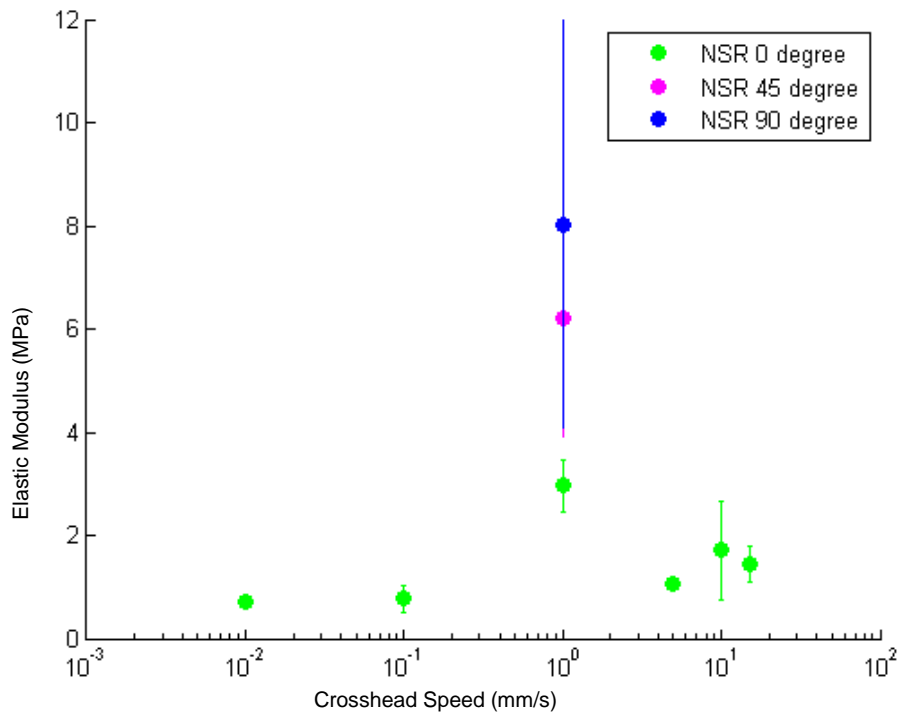


Figure C. 25. Scatter plot of elastic modulus values for neonatal skin rectangular samples by crosshead speed.

Individual Series Stress-Strain Figures

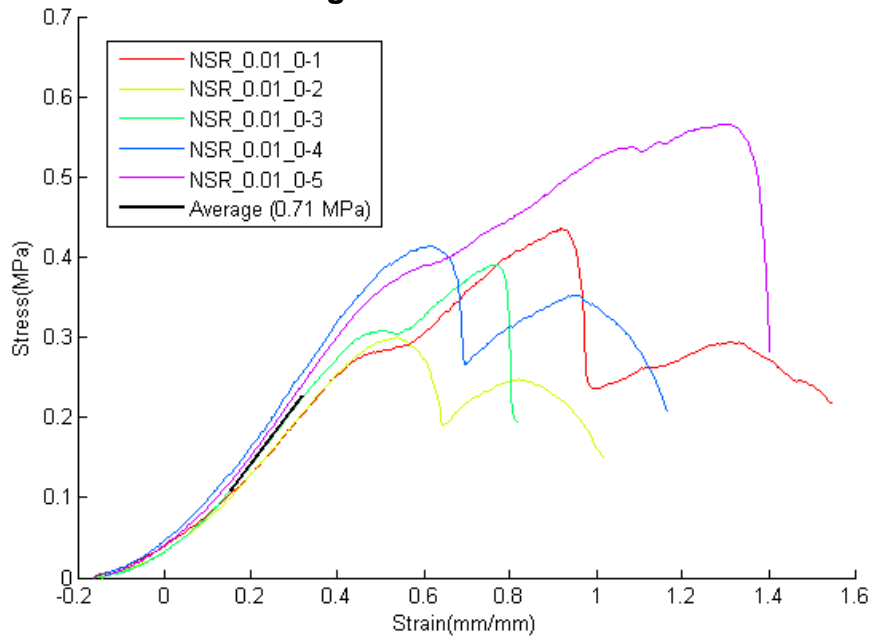


Figure C. 26. Neonatal Skin Rectangular Samples (NSR) in the 0 degree direction. Test performed at a crosshead speed of 0.01 mm/s.

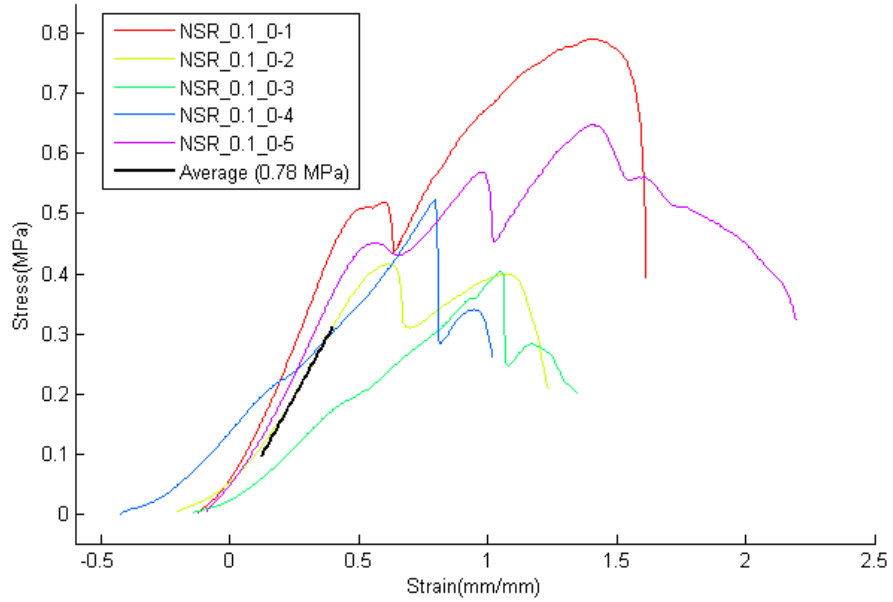


Figure C. 27. Neonatal Skin Rectangular Samples (NSR) in the 0 degree direction. Test performed at a crosshead speed of 0.1 mm/s.

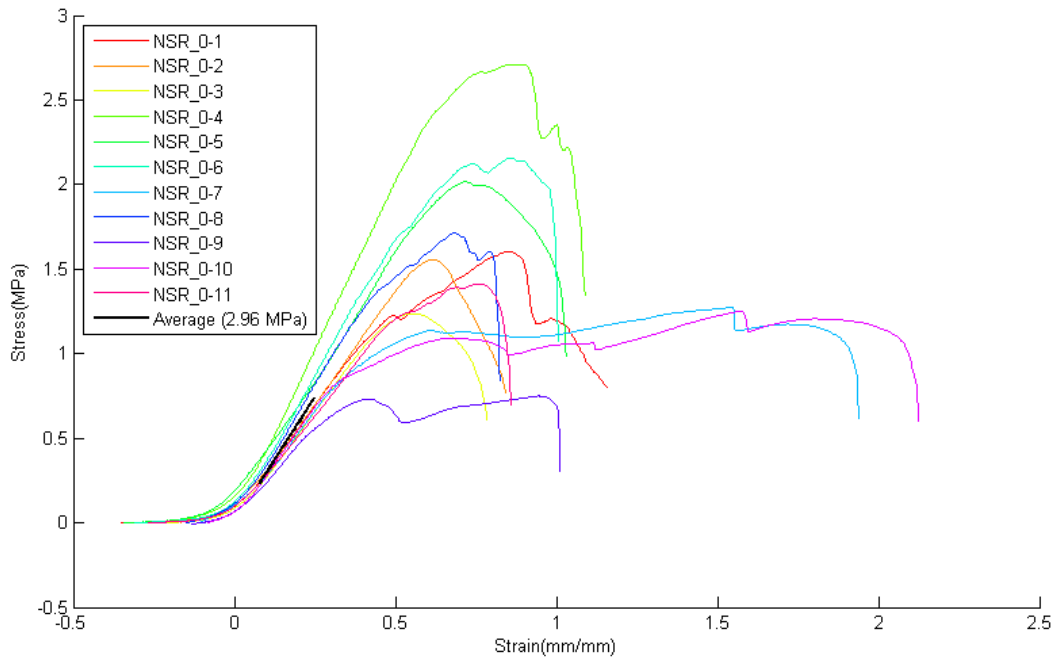


Figure C. 28. Neonatal Skin Rectangular Samples (NSR) in the 0 degree direction. Test performed at a crosshead speed of 1 mm/s.

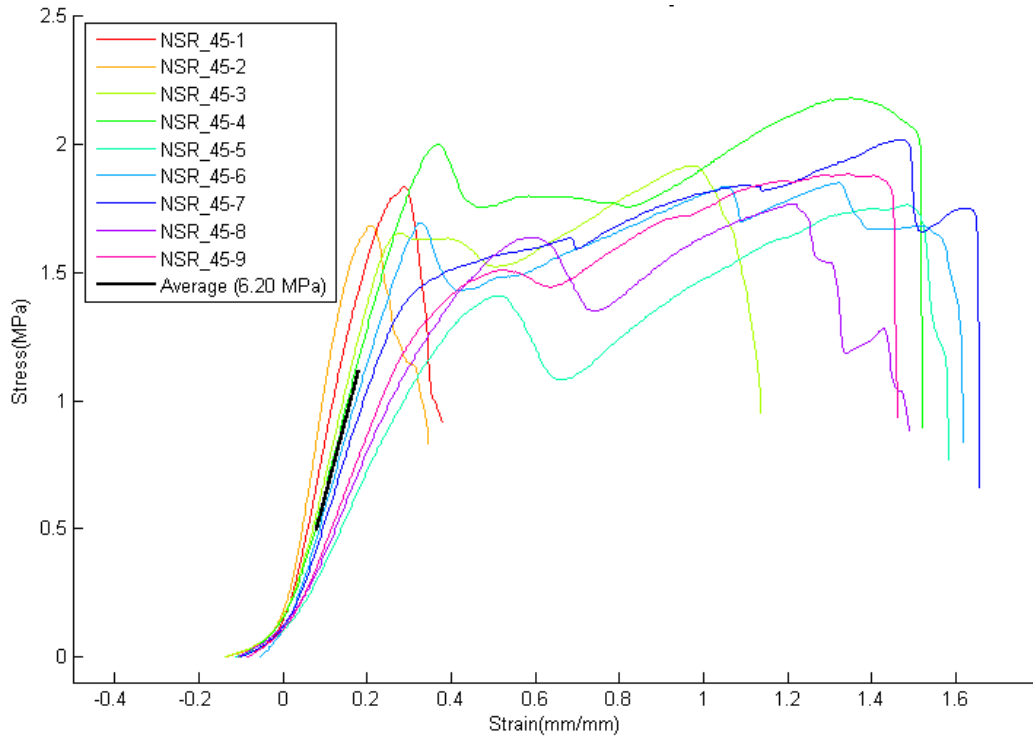


Figure C. 29. Neonatal Skin Rectangular Samples (NSR) in the 45 degree direction. Test performed at a crosshead speed of 1 mm/s.

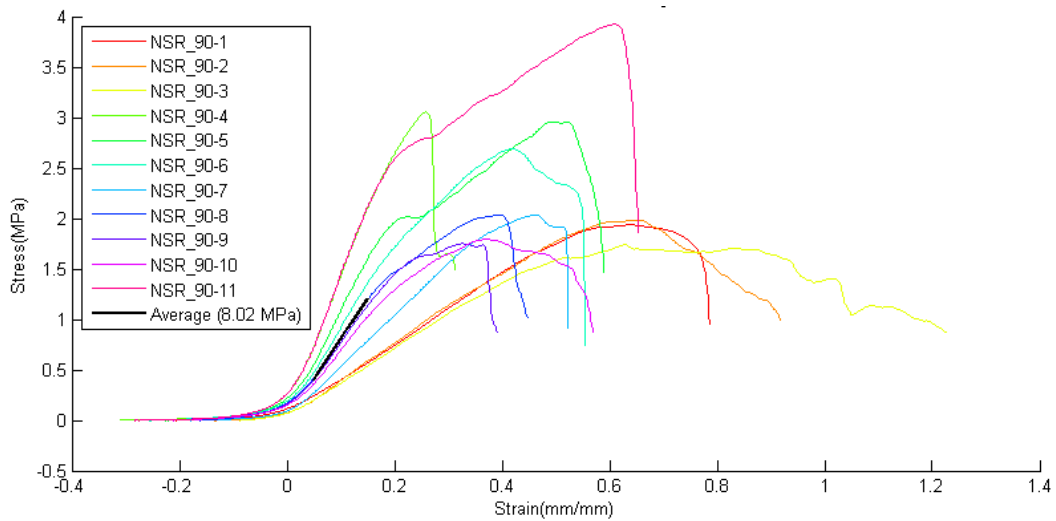


Figure C. 30. Neonatal Skin Rectangular Samples (NSR) in the 90 degree direction. Test performed at a crosshead speed of 1 mm/s.

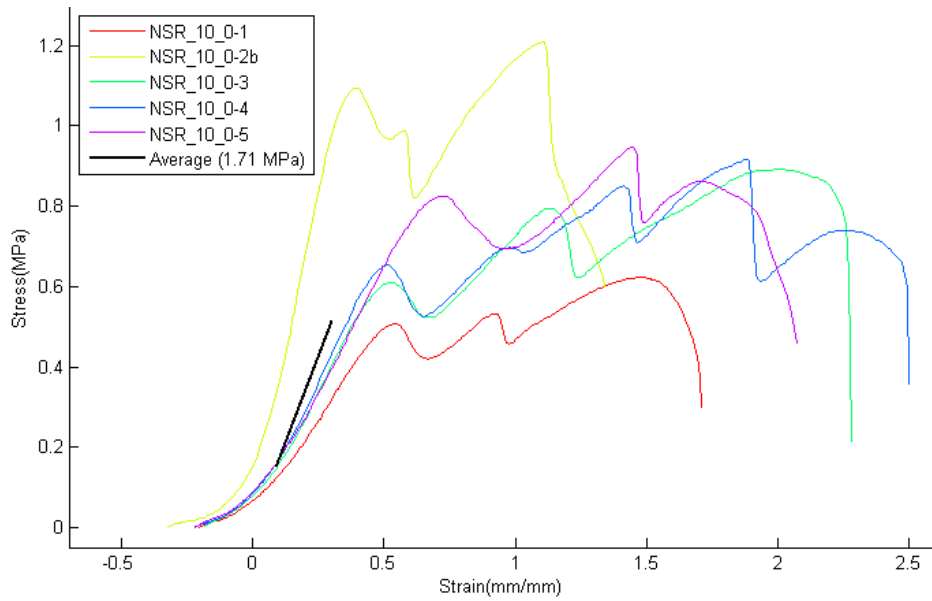


Figure C. 31. Neonatal Skin Rectangular Samples (NSR) in the 0 degree direction. Test performed at a crosshead speed of 10 mm/s.

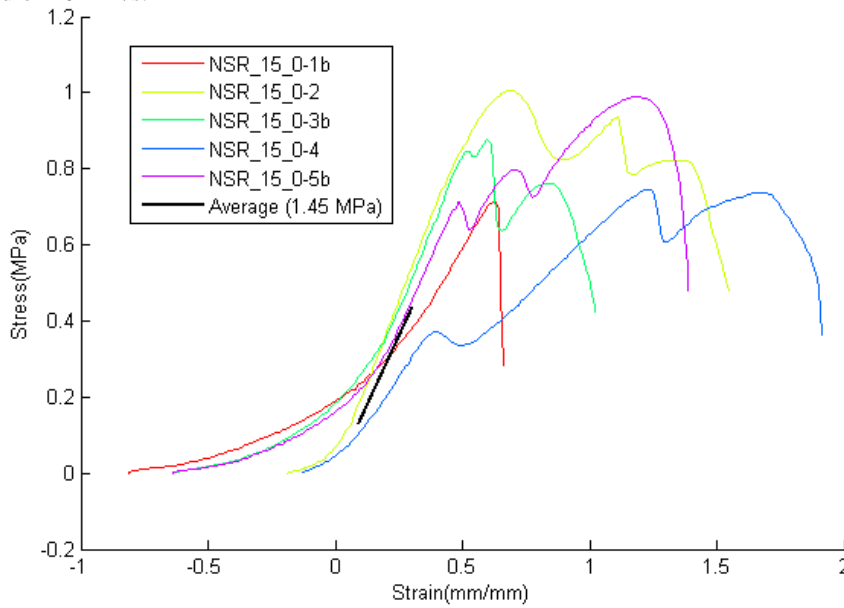


Figure C. 32. Neonatal Skin Rectangular Samples (NSR) in the 0 degree direction. Test performed at a crosshead speed of 15 mm/s.

C.3.1.2 Neonatal Blubber Tissue

Neonatal Blubber (hypodermal) Dogbone Samples

Table C. 3. Neonatal Blubber (hypodermal) Dogbone Samples

Dogbone Tests						
<i>Crosshead speed (mm/s)</i>	<i>Series Name</i>	<i>Peak Stress Mean (MPa)</i>	<i>Peak Stress Stdev (MPa)</i>	<i>n</i>	<i>Orientation</i>	<i>Figure #</i>
0.01	NBD_0.01_0	0.340	0.33	5	0	Figure C. 34
0.01	NBD_0.01_90	0.183	0.00	4	90	Figure C. 35
0.1	NBD_0.1_0	0.420	0.50	5	0	Figure C. 36
0.1	NBD_0.1_90	0.317	0.04	6	90	Figure C. 37
1	NBD_0	0.410	0.14	10	0	Figure C. 38
1	NBD_45	0.367	0.17	9	45	Figure C. 39
1	NBD_90	0.489	0.16	9	90	Figure C. 40
10	NBD_10_0	0.440	0.15	5	0	Figure C. 41
10	NBD_10_90	0.700	0.22	7	90	Figure C. 42
15	NBD_15_0	0.733	0.51	3	0	Figure C. 43
15	NBD_15_90	0.880	0.33	5	90	Figure C. 44

Summary Figures

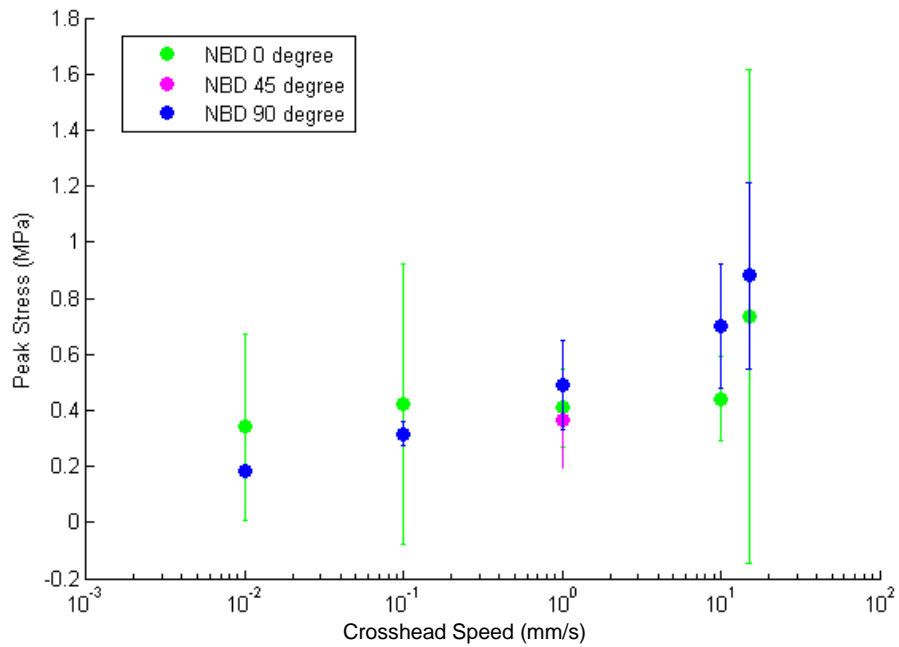


Figure C. 33. Scatter plot of peak stress values for neonatal dogbone blubber samples by crosshead speeds.

Individual Series Stress-Strain Figures

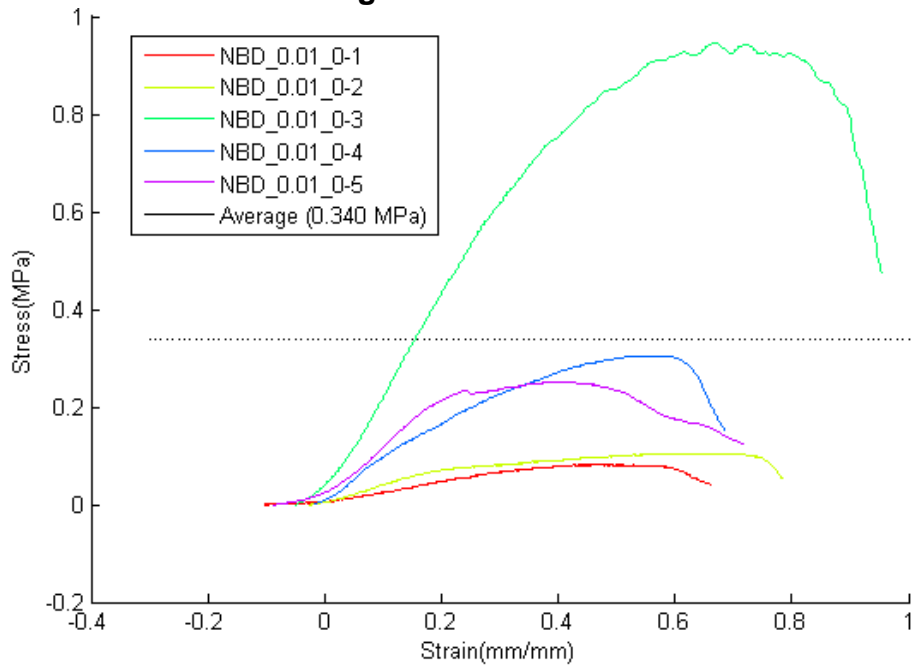


Figure C. 34. Neonatal Blubber Dogbone Samples (NBD) in the 0 degree direction. Test performed at a crosshead speed of 0.01 mm/s.

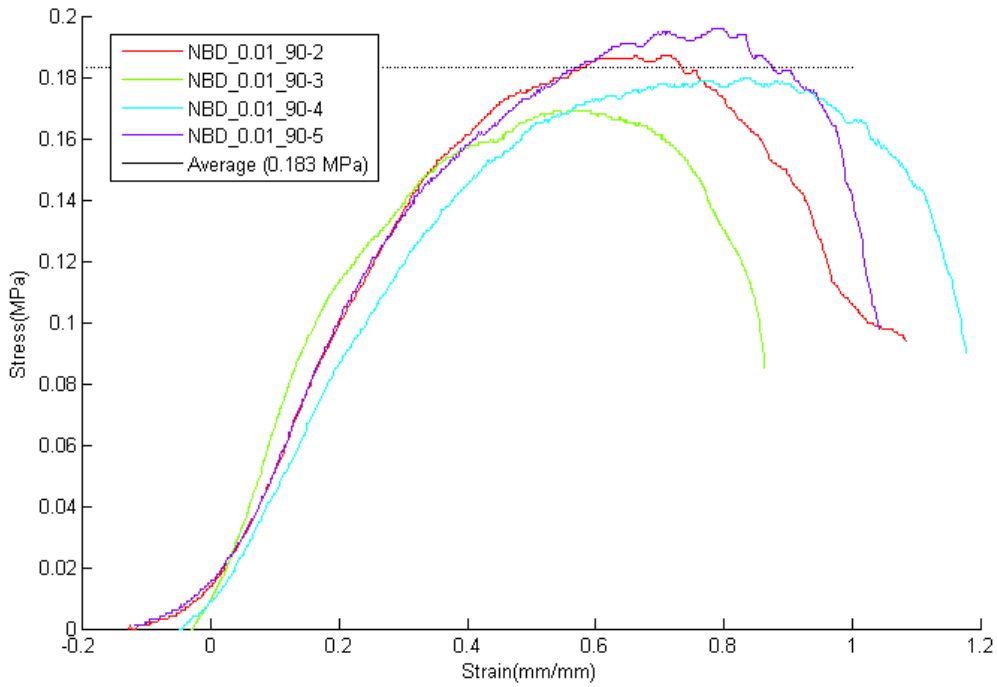


Figure C. 35. Neonatal Blubber Dogbone Samples (NBD) in the 90 degree direction. Test performed at a crosshead speed of 0.01 mm/s.

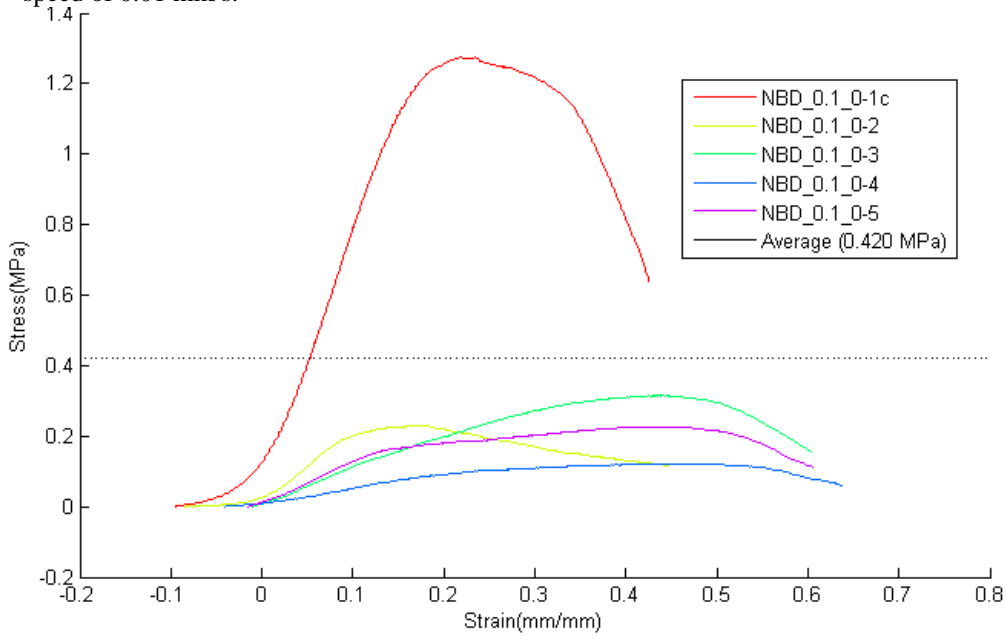


Figure C. 36. Neonatal Blubber Dogbone Samples (NBD) in the 0 degree direction. Test performed at a crosshead speed of 0.1 mm/s.

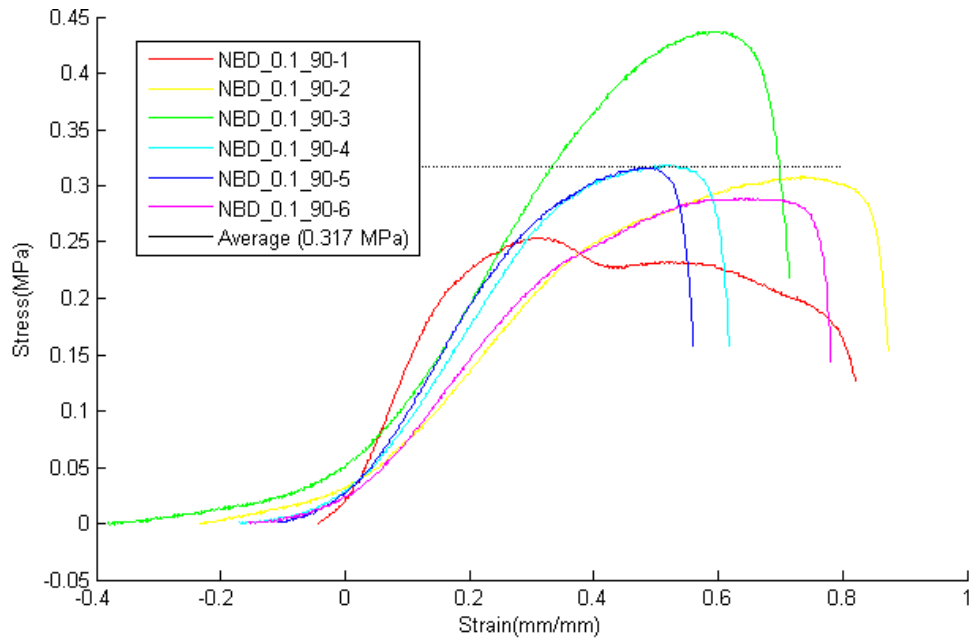


Figure C. 37. Neonatal Blubber Dogbone Samples (NBD) in the 90 degree direction. Test performed at a crosshead speed of 0.1 mm/s.

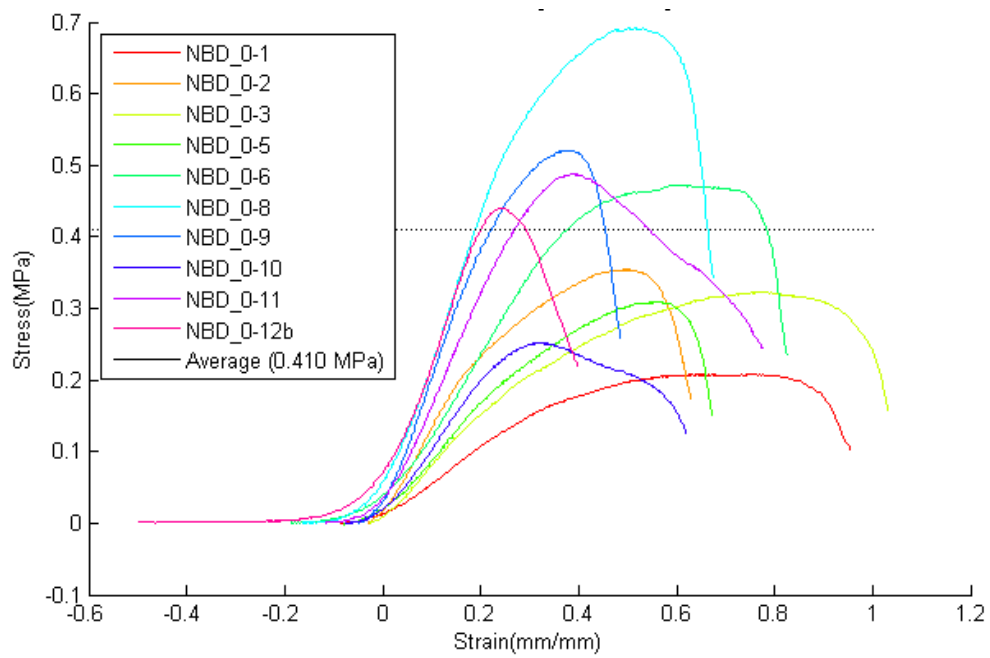


Figure C. 38. Neonatal Blubber Dogbone Samples (NBD) in the 0 degree direction. Test performed at a crosshead speed of 1 mm/s.

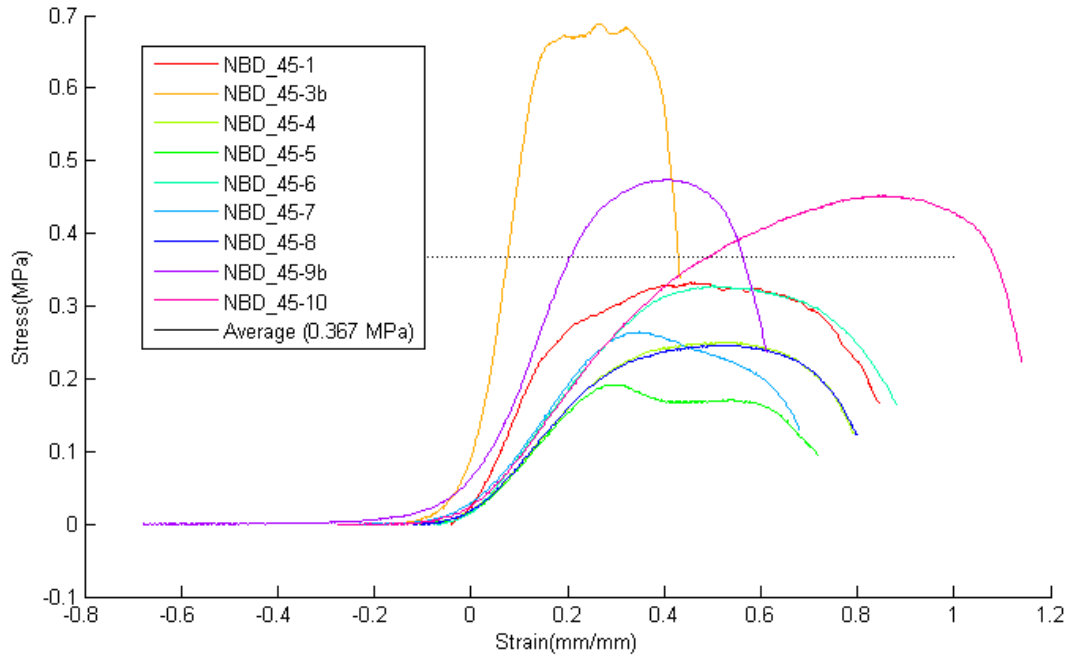


Figure C. 39. Neonatal Blubber Dogbone Samples (NBD) in the 45 degree direction. Test performed at a crosshead speed of 1 mm/s.

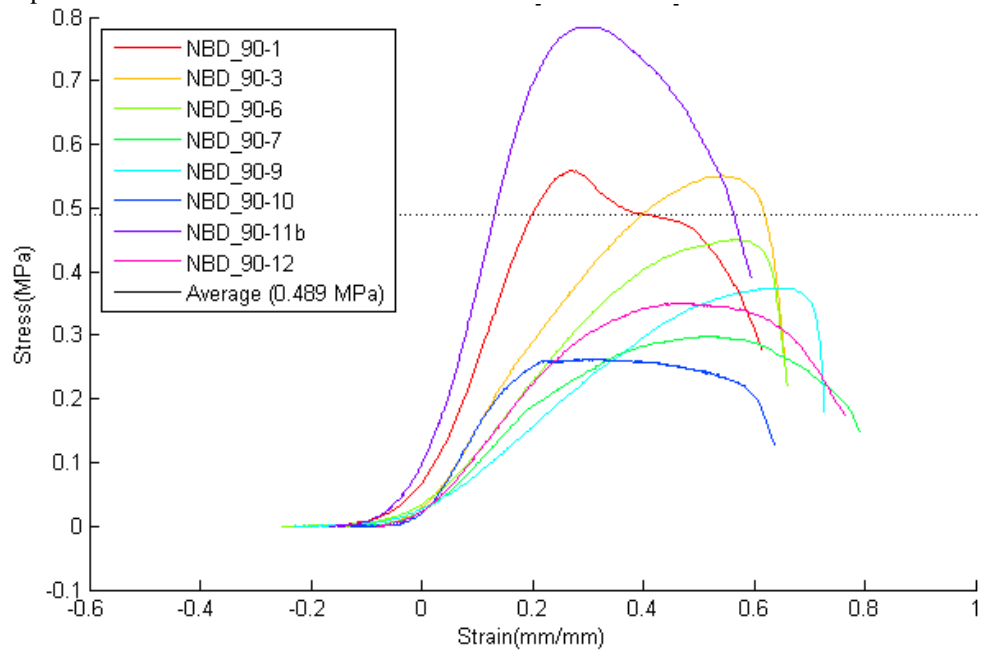


Figure C. 40. Neonatal Blubber Dogbone Samples (NBD) in the 90 degree direction. Test performed at a crosshead speed of 1 mm/s.

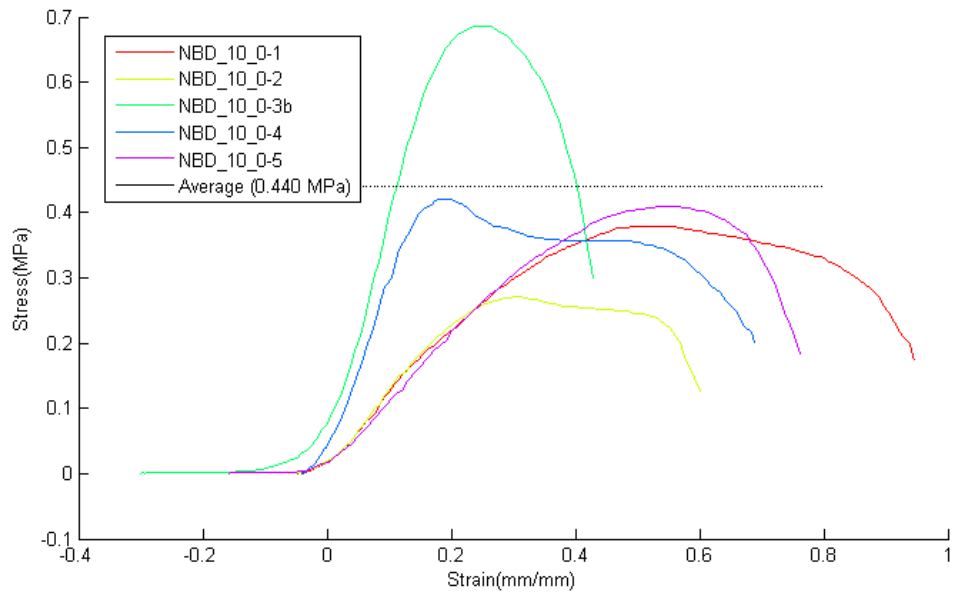


Figure C. 41. Neonatal Blubber Dogbone Samples (NBD) in the 0 degree direction. Test performed at a crosshead speed of 10 mm/s.

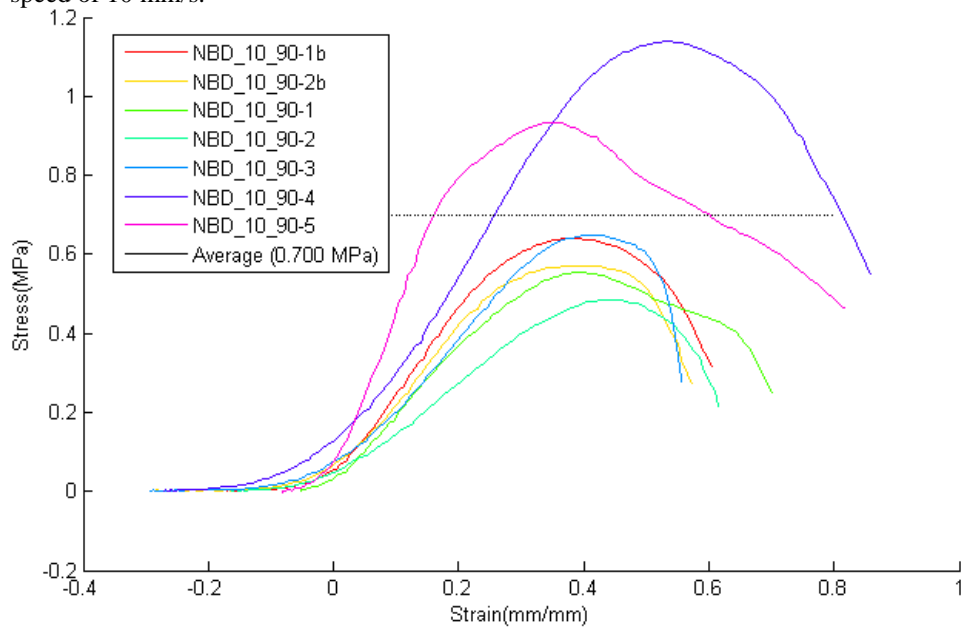


Figure C. 42. Neonatal Blubber Dogbone Samples (NBD) in the 90 degree direction. Test performed at a crosshead speed of 10 mm/s.

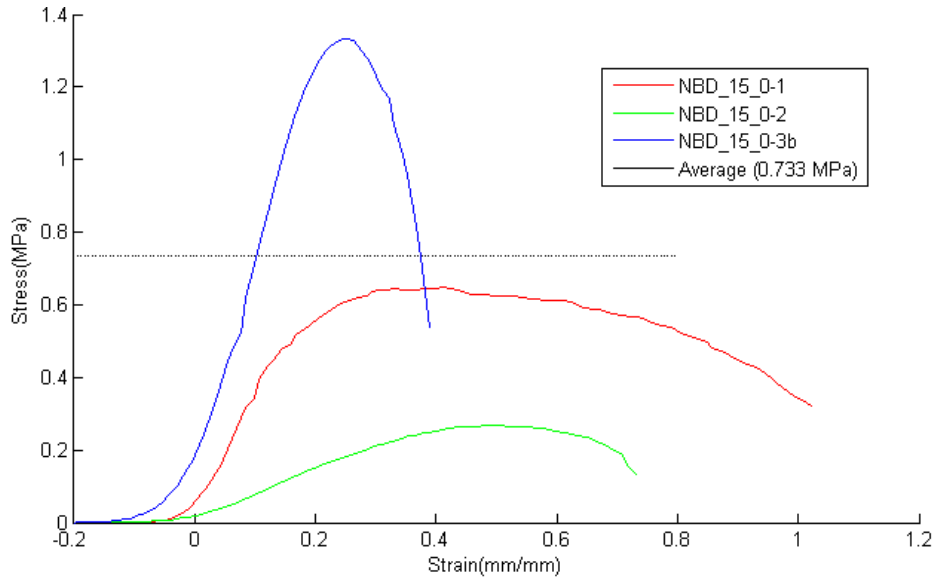


Figure C. 43. Neonatal Blubber Dogbone Samples (NBD) in the 0 degree direction. Test performed at a crosshead speed of 15 mm/s.

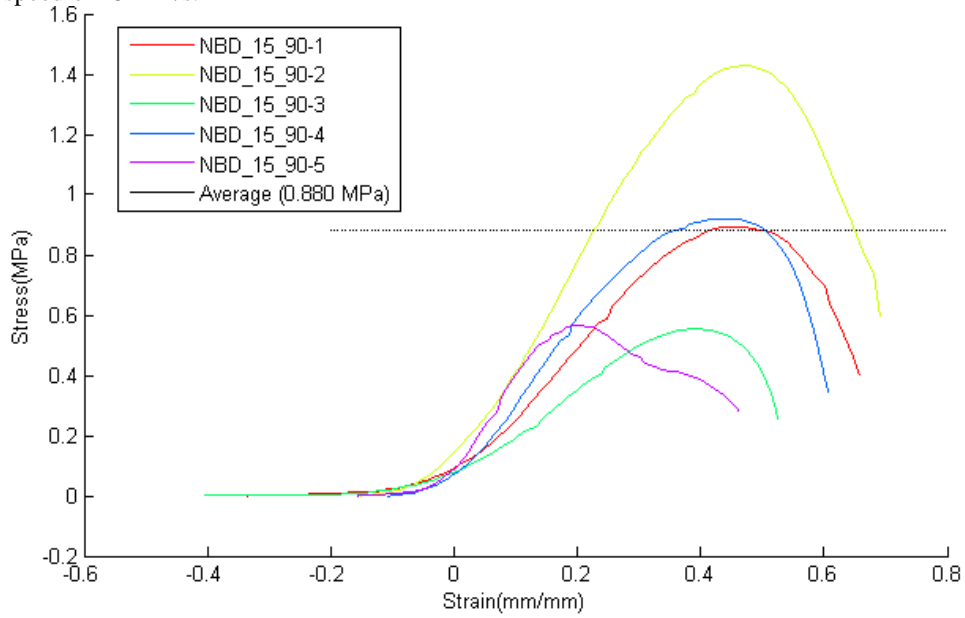


Figure C. 44. Neonatal Blubber Dogbone Samples (NBD) in the 90 degree direction. Test performed at a crosshead speed of 15 mm/s.

Neonatal Blubber (hypodermal) Rectangular Samples

Table C. 4 Neonatal Blubber (hypodermal) Rectangular Samples

<i>Crosshead speed (mm/s)</i>	<i>Series Name</i>	Rectangular Tests				<i>Strain to failure (mm/mm)</i>	<i>Figure #</i>
		<i>Elastic Modulus Mean (MPa)</i>	<i>Elastic Modulus Stdev (MPa)</i>	<i>n</i>	<i>Orientation</i>		
0.01	NBR_0.01_0	0.70	0.79	5	0	0.80	Figure C. 47
0.01	NBR_0.01_90	0.39	0.13	5	90	0.54	Figure C. 48
0.1	NBR_0.1_0	0.90	0.75	5	0	0.94	Figure C. 49
0.1	NBR_0.1_90	0.52	0.14	5	90	0.64	Figure C. 50
1	NBR_0	1.48	0.51	8	0	0.68	Figure C. 51
1	NBR_45	2.59	0.86	8	45	0.62	Figure C. 52
1	NBR_90	1.13	0.56	9	90	0.67	Figure C. 53
5	NBR_5_0	6.30	1.77	2	0	0.70	Figure C. 54
5	NBR_5_90	1.69	0.65	4	90	0.50	Figure C. 55
10	NBR_10_0	1.49	0.96	5	0	0.85	Figure C. 56
10	NBR_10_90	1.40	0.22	5	90	0.60	Figure C. 57
15	NBR_15_0	4.11	3.22	5	0	0.69	Figure C. 58
15	NBR_15_90	1.45	0.35	5	90	0.64	Figure C. 59

Summary Figures

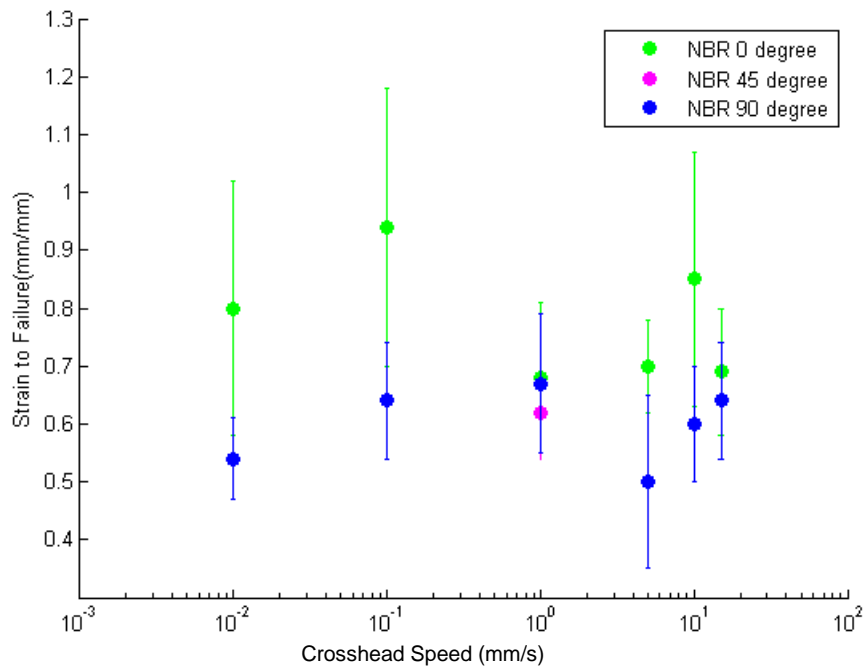


Figure C. 45

shear speed

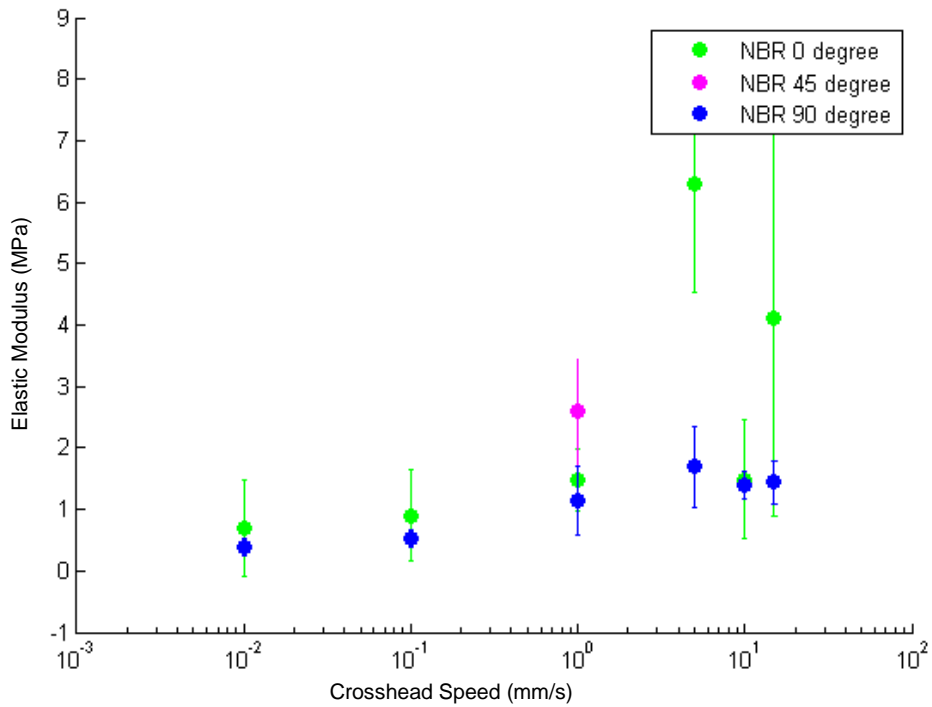


Figure C. 46. Scatter plot of peak stress values for neonatal blubber rectangular samples by crosshead speed.

Individual Series Stress-Strain Figures

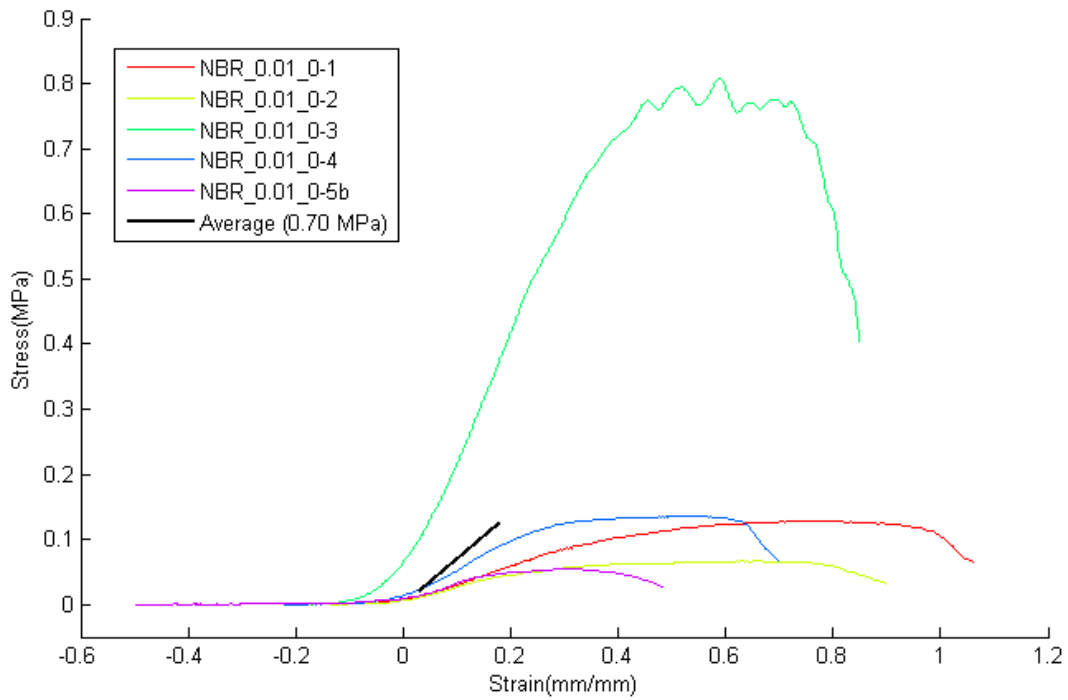


Figure C. 47. Neonatal Blubber Rectangular Samples (NBR) in the 0 degree direction. Test performed at a crosshead speed of 0.01 mm/s.

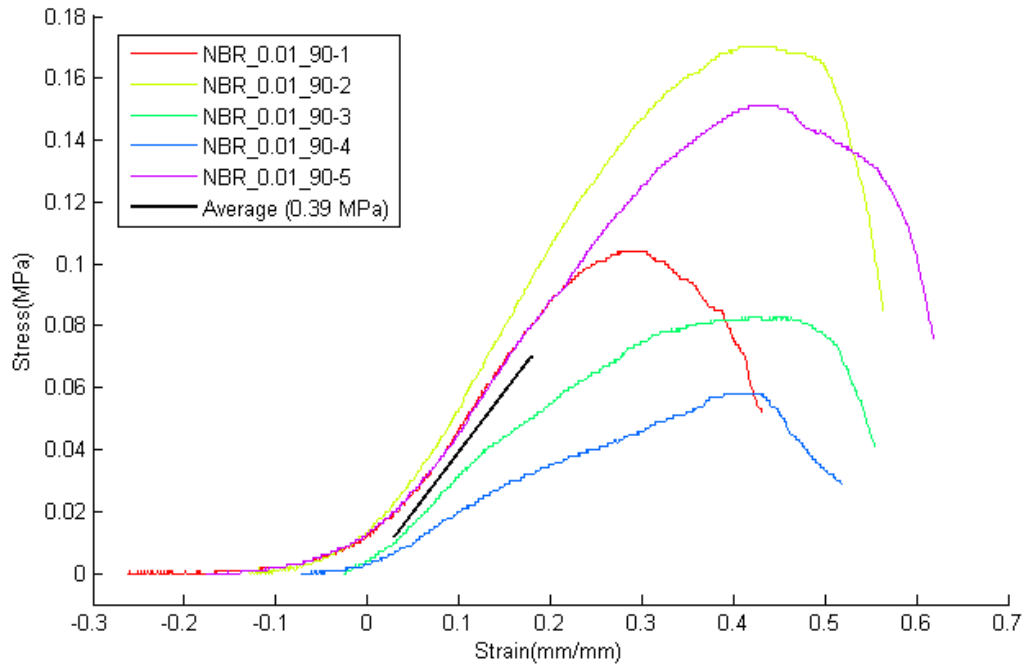


Figure C. 48. Neonatal Blubber Rectangular Samples (NBR) in the 90 degree direction. Test performed at a crosshead speed of 0.01 mm/s.

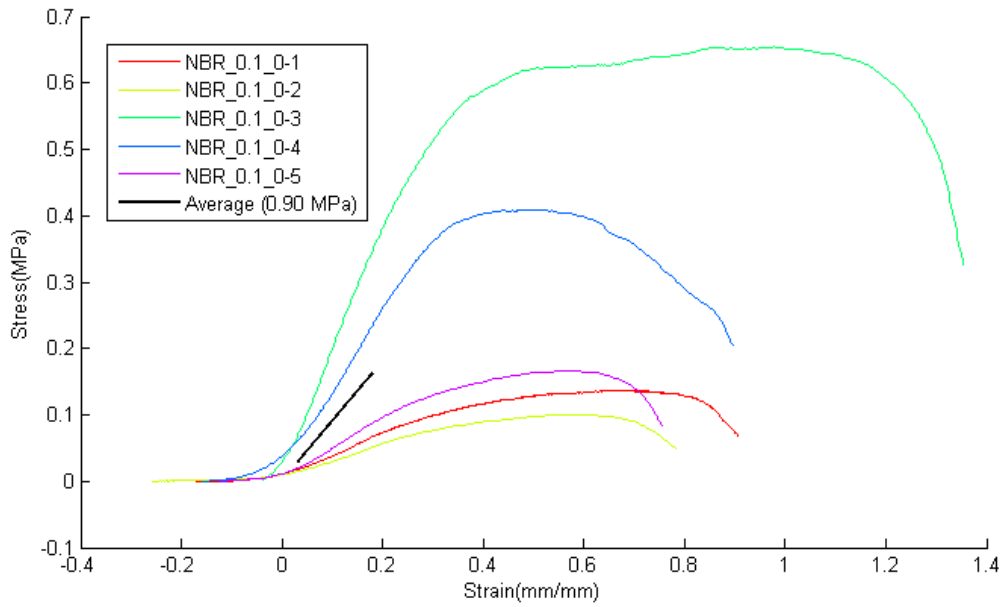


Figure C. 49. Neonatal Blubber Rectangular Samples (NBR) in the 0 degree direction. Test performed at a crosshead speed of 0.1 mm/s.

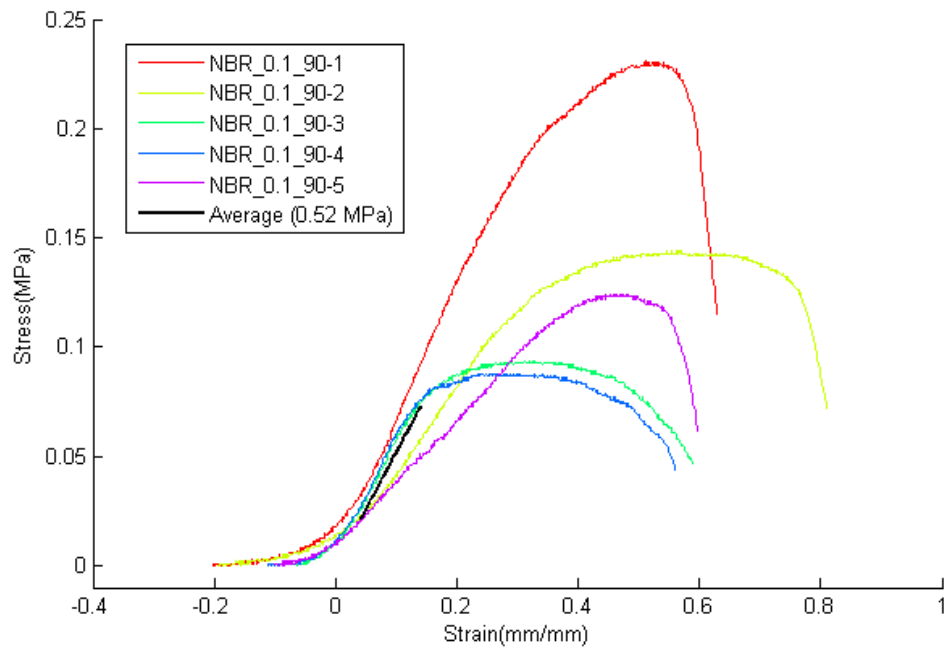


Figure C. 50. Neonatal Blubber Rectangular Samples (NBR) in the 90 degree direction. Test performed at a crosshead speed of 0.1 mm/s.

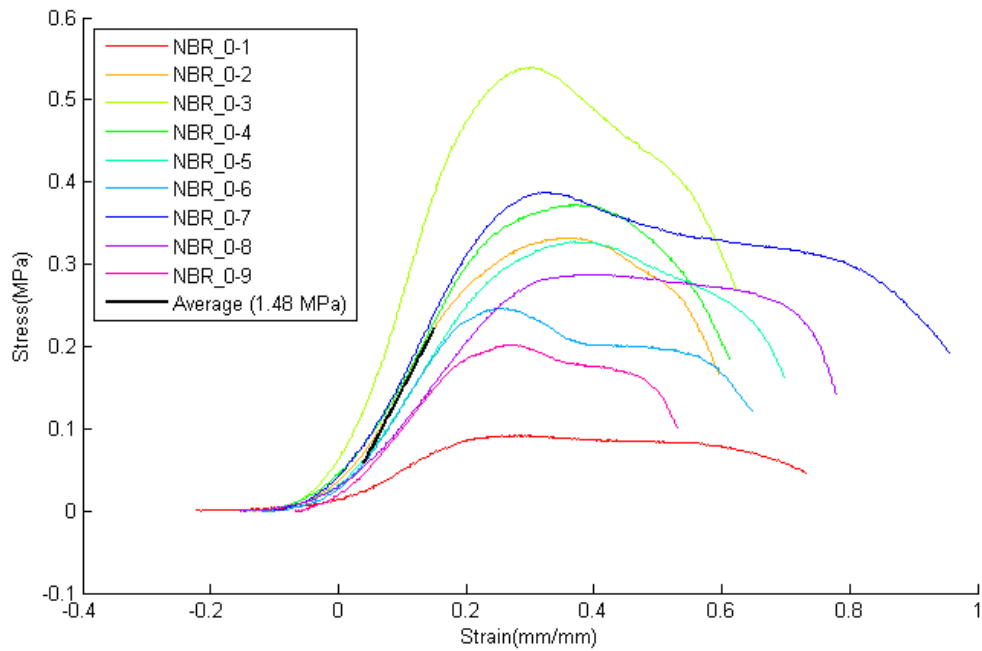


Figure C. 51. Neonatal Blubber Rectangular Samples (NBR) in the 0 degree direction. Test performed at a crosshead speed of 1 mm/s.

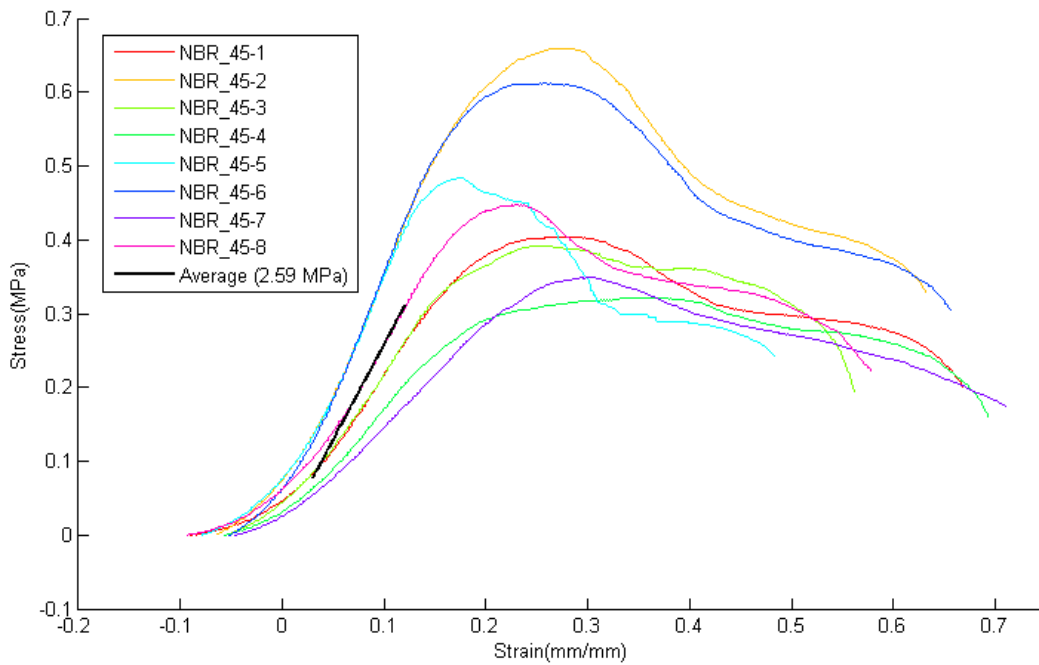


Figure C. 52. Neonatal Blubber Rectangular Samples (NBR) in the 45 degree direction. Test performed at a crosshead speed of 1 mm/s.

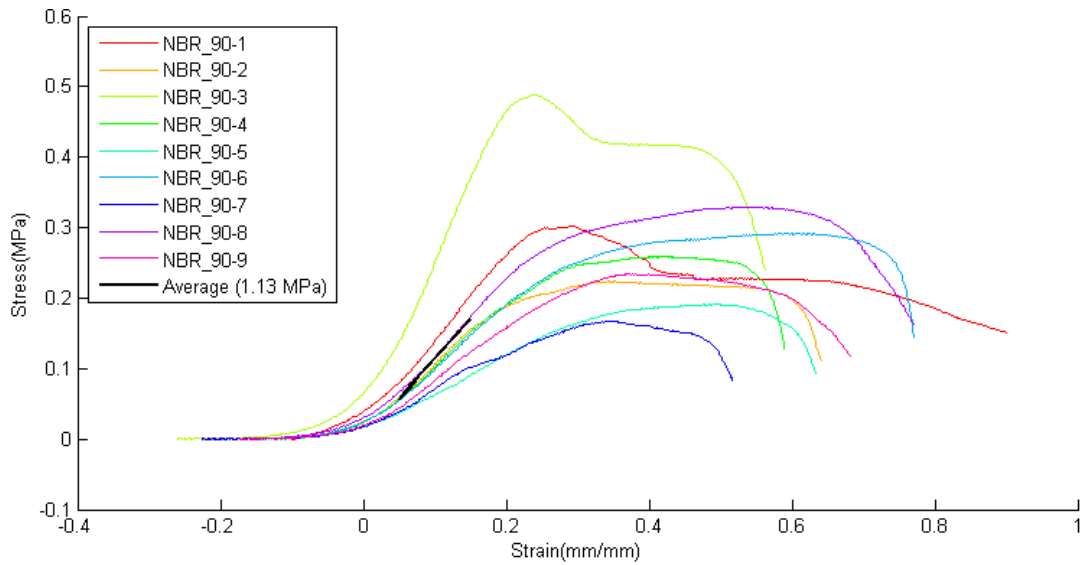


Figure C. 53. Neonatal Blubber Rectangular Samples (NBR) in the 90 degree direction. Test performed at a crosshead speed of 1 mm/s.

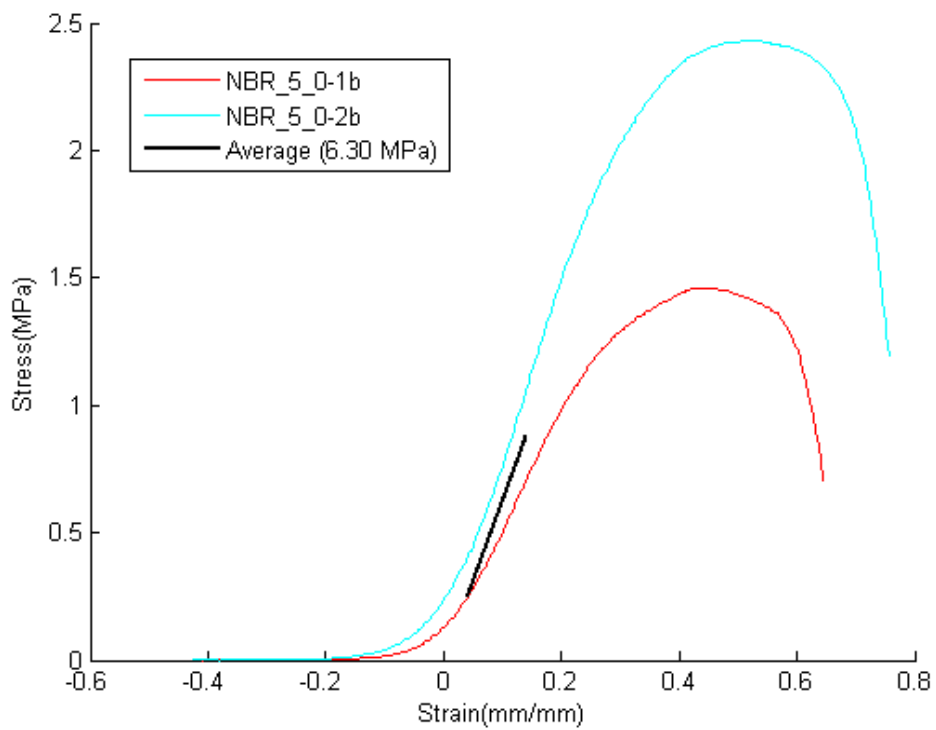


Figure C. 54. Neonatal Blubber Rectangular Samples (NBR) in the 0 degree direction. Test performed at a crosshead speed of 5 mm/s.

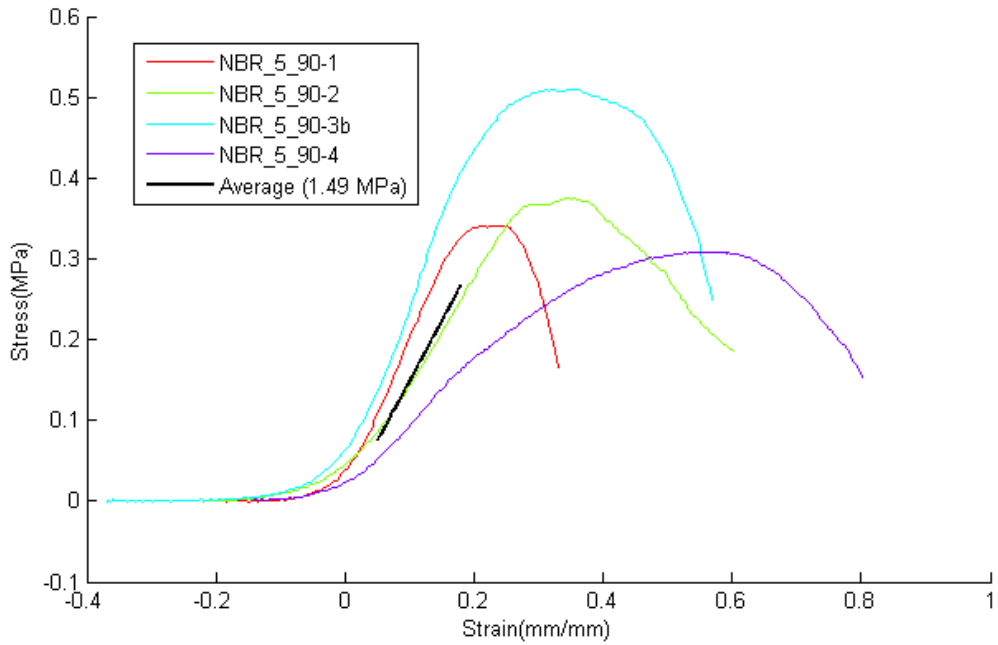


Figure C. 55. Neonatal Blubber Rectangular Samples (NBR) in the 90 degree direction. Test performed at a crosshead speed of 5 mm/s.

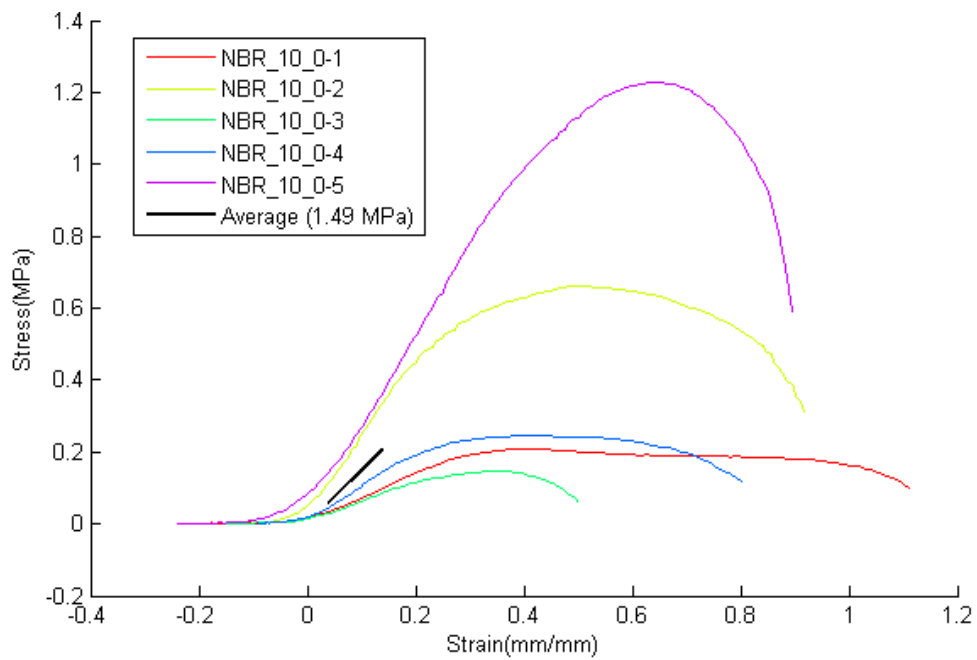


Figure C. 56. Neonatal Blubber Rectangular Samples (NBR) in the 0 degree direction. Test performed at a crosshead speed of 10 mm/s.

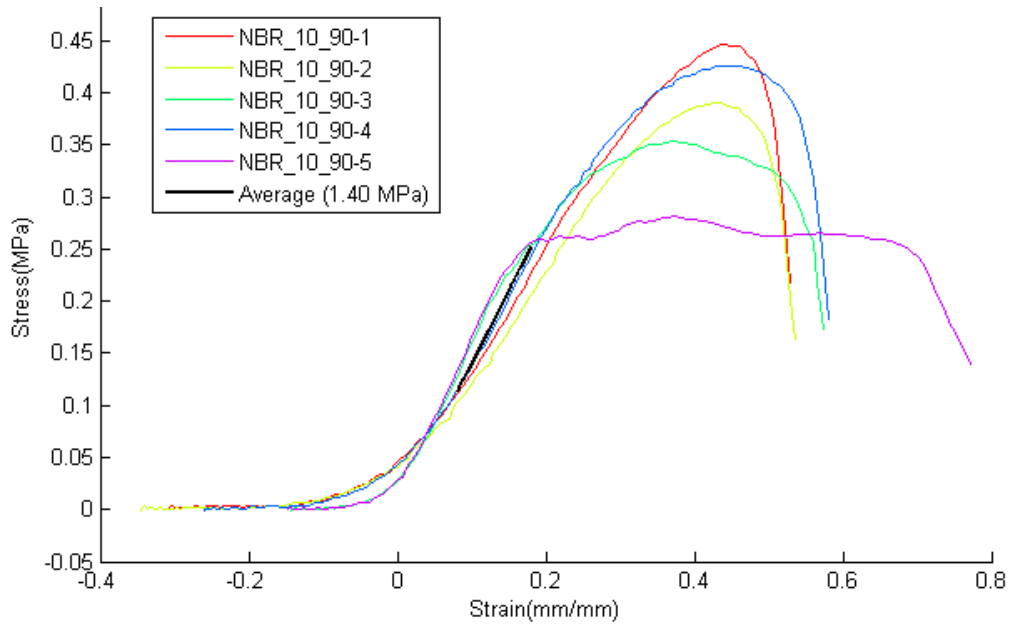


Figure C. 57. Neonatal Blubber Rectangular Samples (NBR) in the 90 degree direction. Test performed at a crosshead speed of 10 mm/s.

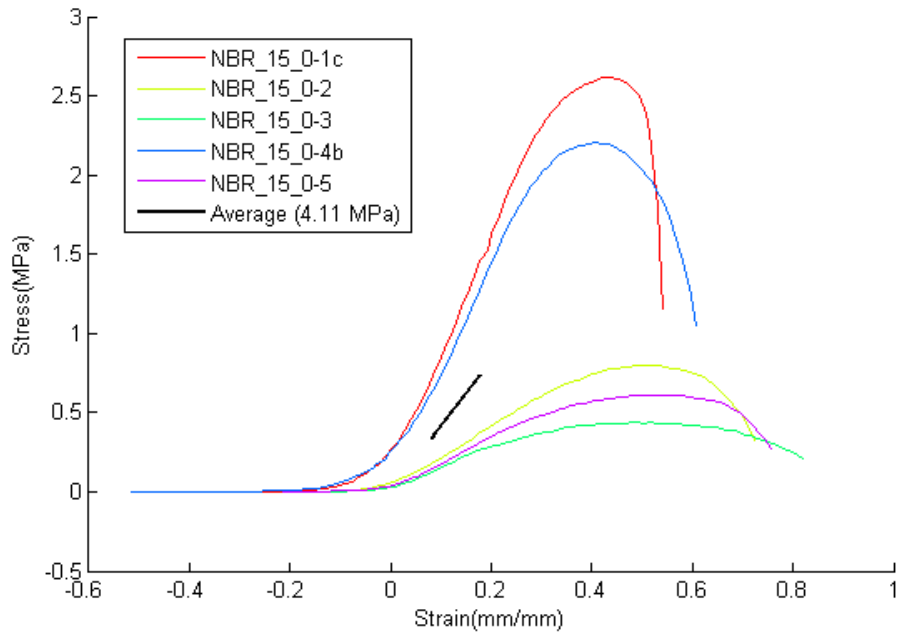


Figure C. 58. Neonatal Blubber Rectangular Samples (NBR) in the 0 degree direction. Test performed at a crosshead speed of 15 mm/s.

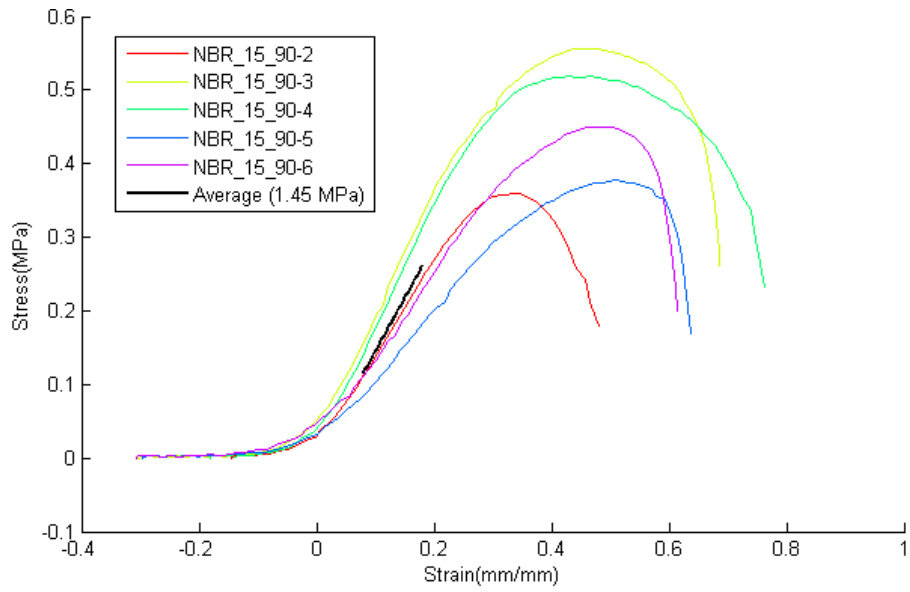


Figure C. 59. Neonatal Blubber Rectangular Samples (NBR) in the 90 degree direction. Test performed at a crosshead speed of 15 mm/s.

C.3.1.3 Neonatal Poisson's Ratio

In materials like tissue, Poisson's ratio changes as the stress and strain changes, and the neonatal epidermis was no exception. Because of the small sample size and strain dependence, no formal statistical analysis was performed to determine Poisson's ratio.

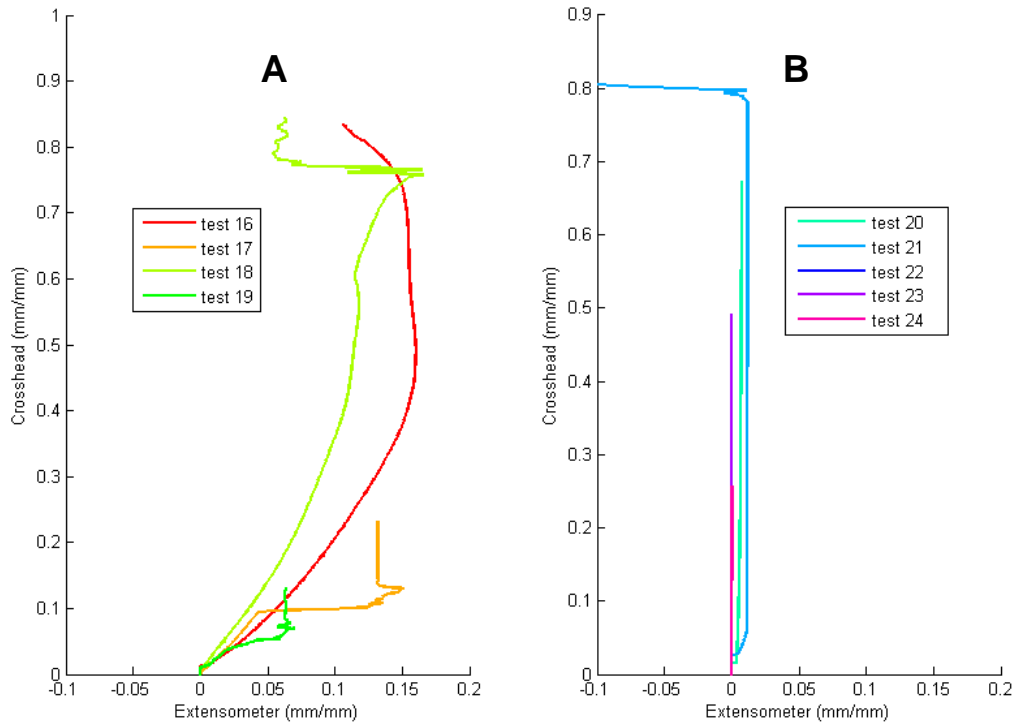


Figure C. 60. Tests in Figure A are tests where the extensometer performed as expected, but many tests, as shown in Figure B, did not show change in the extensometer as the test was performed. Likely the extensometer slipped in these cases.

C.3.1.4 Juvenile Skin Tissue

The juvenile skin samples were the most degraded of all the tissue that was tested. The most outer layer of skin often sloughed off (Figure C. 61.). It is difficult to parse the effects of degradation on the results of tissue testing.



Figure C. 61. Juvenile Skin Rectangular specimen after testing. An example of a thin layer of skin sloughing off can be seen on the bottom clamp. This is a sign of the degradation of the juvenile skin tissue and often happened during tensile testing.

Juvenile Skin (epidermal) Dogbone Samples

Table C. 5 Juvenile Skin (epidermal) Dogbone Samples

Dogbone Tests						
<i>Crosshead speed (mm/s)</i>	<i>Series Name</i>	<i>Peak Stress Mean (MPa)</i>	<i>Peak Stress Stdev (MPa)</i>	<i>n</i>	<i>Orientation</i>	<i>Figure #</i>
1	JSD_0	1.295	0.951	6	0	Figure C. 63
1	JSD_90	2.228	0.861	8	90	Figure C. 64

Summary Figures

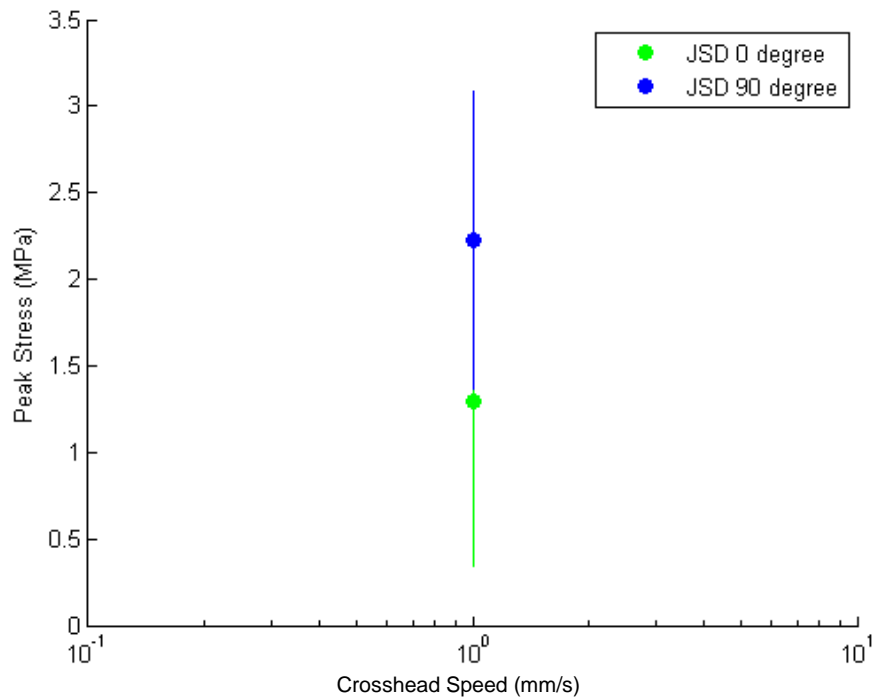


Figure C. 62. Scatter plot of peak stress values for juvenile skin dogbone samples by crosshead speed.

Individual Series Stress-Strain Figures

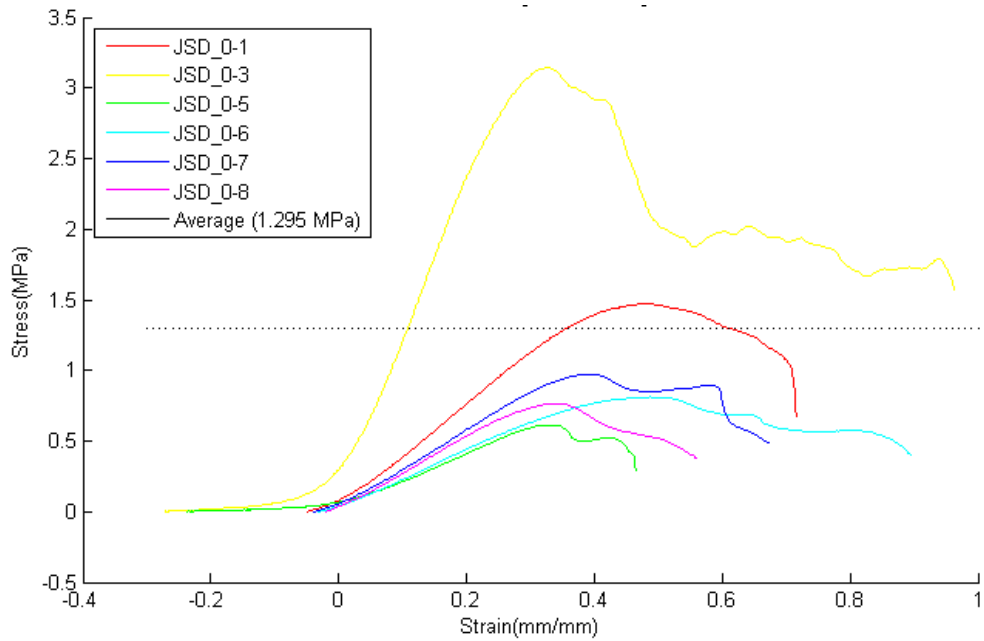


Figure C. 63. Juvenile Skin Dogbone Samples (JSD) in the 0 degree direction. Test performed at a crosshead speed of 1 mm/s.

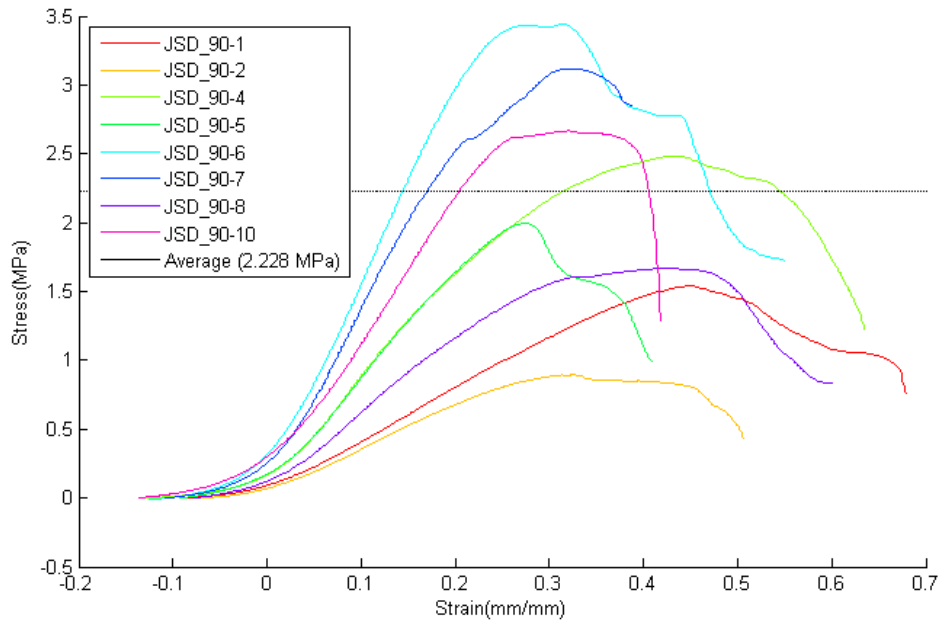


Figure C. 64. Juvenile Skin Dogbone Samples (JSD) in the 90 degree direction. Test performed at a crosshead speed of 1 mm/s.

Juvenile Skin (epidermal) Rectangular Samples

Table C. 6 Juvenile Skin (epidermal) Rectangular Samples

Crosshead speed (mm/s)	Series Name	Rectangular Tests				Strain to failure (mm/mm)	Figure #
		Elastic Modulus Mean (MPa)	Elastic Modulus Stdev (MPa)	n	Orientation		
1	JSR_0	1.75	0.34	4	0	1.13	Figure C. 67
1	JSR_90	6.60	1.81	8	90	0.57	Figure C. 68

Summary Figures

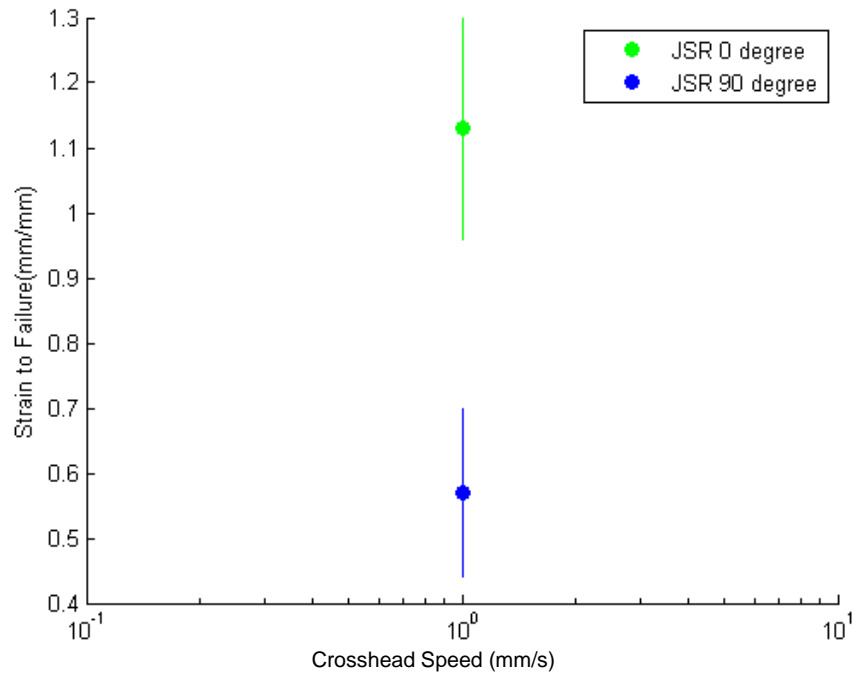


Figure C. 65. Scatter plot of the strain to failure for juvenile skin rectangular samples plotted by crosshead speed.

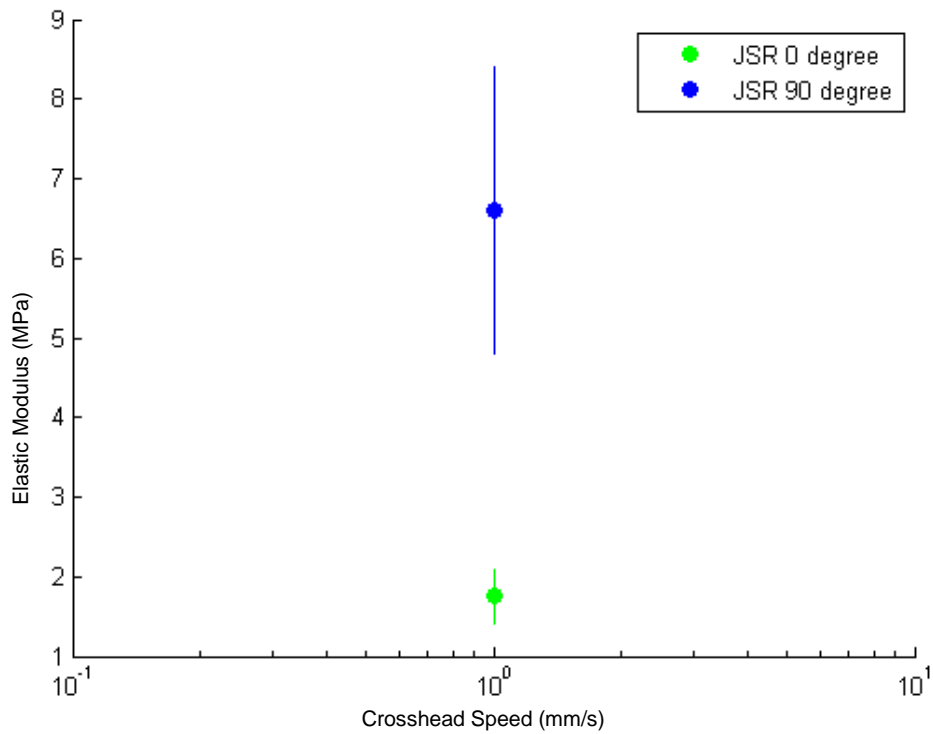


Figure C. 66. Scatter plot of peak stress values for juvenile skin rectangular samples by crosshead speed

Individual Series Stress-Strain Figures

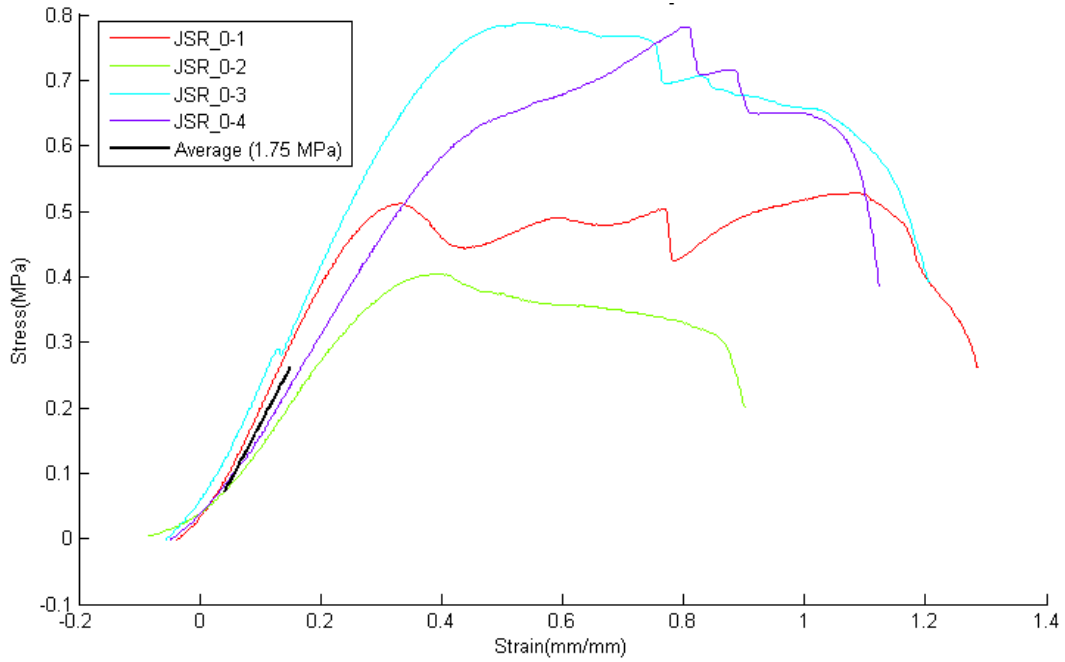


Figure C. 67. Juvenile Skin Rectangular Samples (JSR) in in the 0 degree direction. Test performed at a crosshead speed of 1 mm/s.

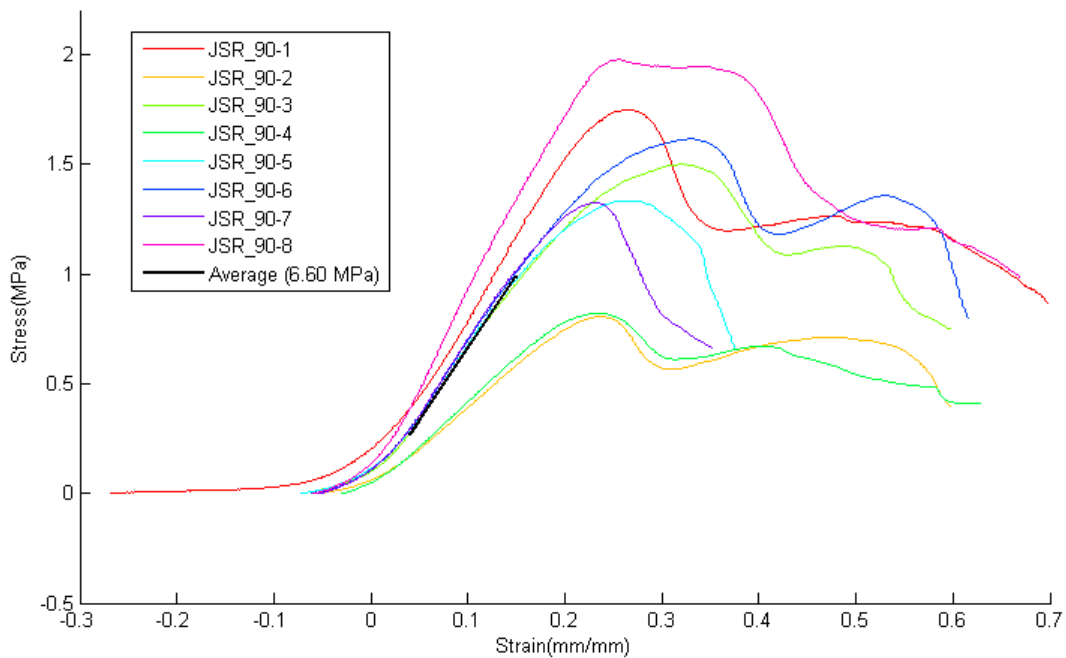


Figure C. 68. Juvenile Skin Rectangular Samples (JSR) in in the 90 degree direction. Test performed at a crosshead speed of 1 mm/s.

C.3.1.5 Juvenile Blubber Tissue

Juvenile Blubber (hypodermal) Dogbone Samples

Table C. 7 Juvenile Blubber (hypodermal) Dogbone Samples

Dogbone Tests						
Crosshead Speed (mm/s)	Series Name	Peak Stress Mean (MPa)	Peak Stress Stdev (MPa)	n	Orientation	Figure #
1	JBD_0	0.534	0.38	8	0	Figure C. 70
1	JBD_45	0.576	0.33	8	45	Figure C. 71
1	JBD_90	1.185	0.67	8	90	Figure C. 72

Summary Figures

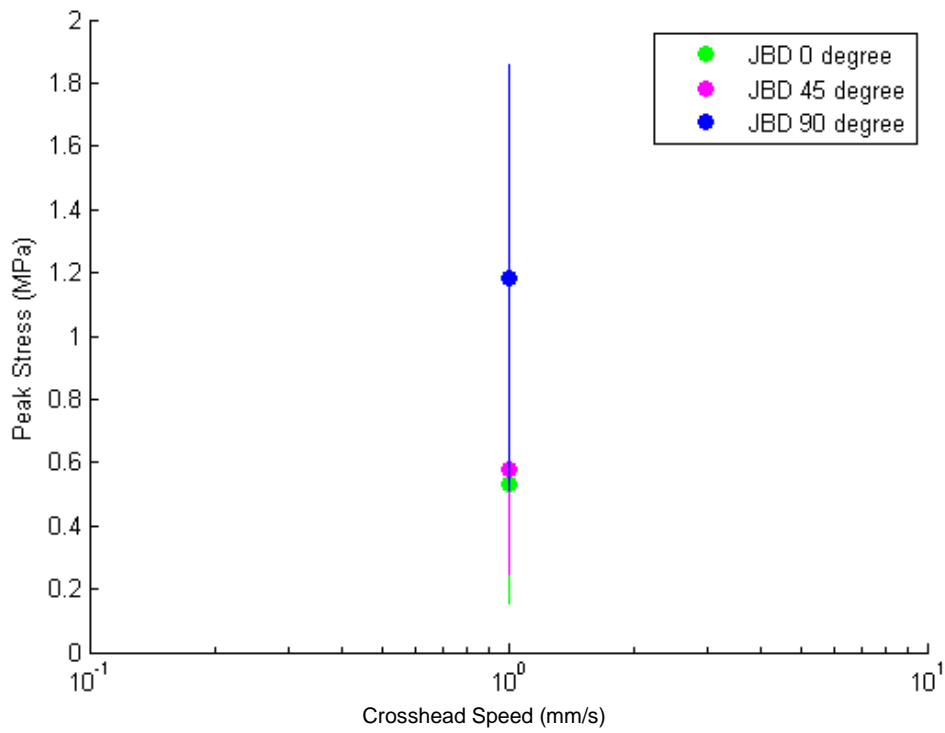


Figure C. 69. Scatter plot of peak stress values for juvenile skin dogbone samples by crosshead speed

Individual Series Stress-Strain Figures

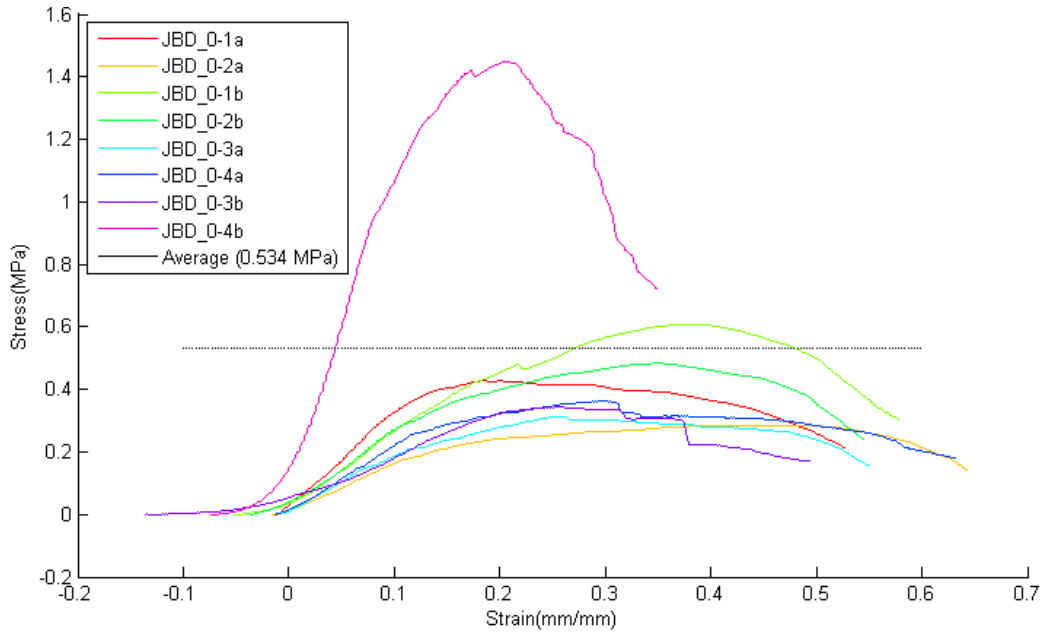


Figure C. 70. Juvenile Blubber Dogbone Samples (JBD) in in the 0 degree direction. Test performed at a crosshead speed of 1 mm/s.

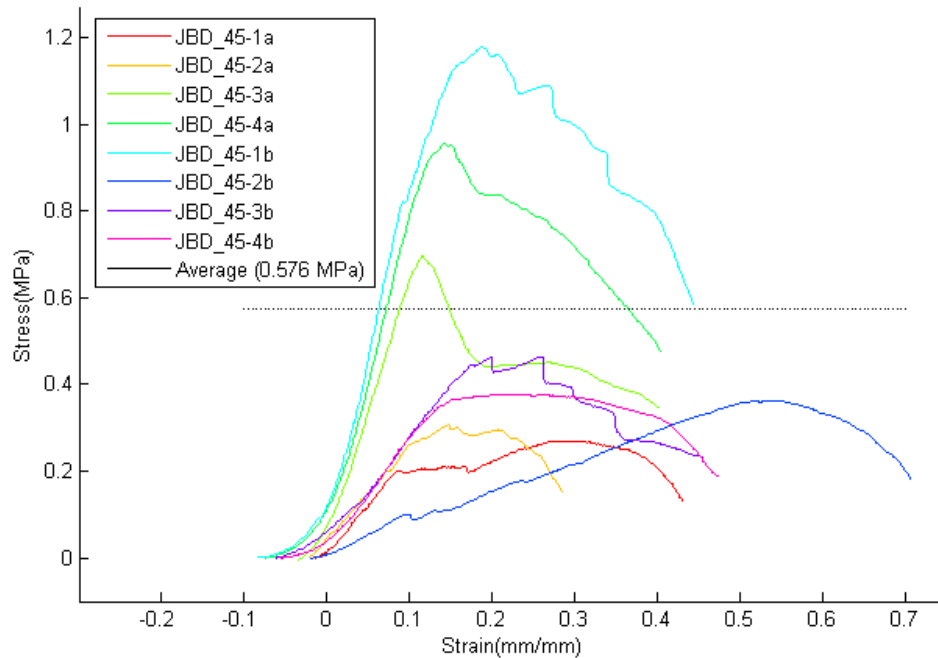


Figure C. 71. Juvenile Blubber Dogbone Samples (JBD) in in the 45 degree direction. Test performed at a crosshead speed of 1 mm/s.

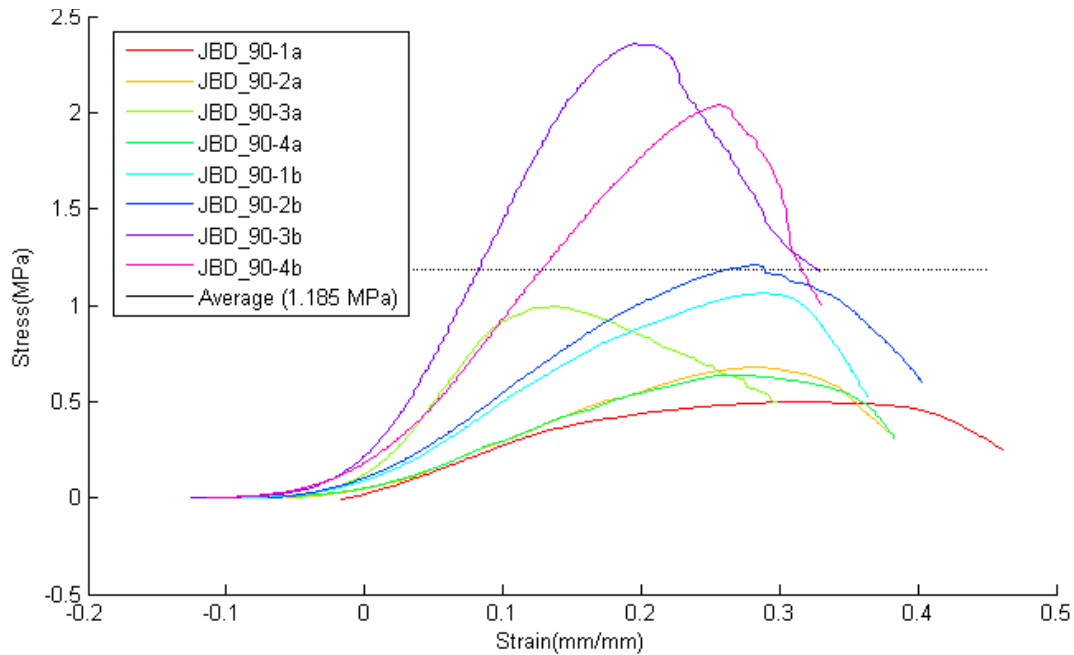


Figure C. 72. Juvenile Blubber Dogbone Samples (JBD) in the 90 degree direction. Test performed at a crosshead speed of 1 mm/s

Juvenile Blubber (hypodermal) Rectangular Samples

Table C. 8 Juvenile Blubber (hypodermal) Rectangular Samples

Crosshead Speed (mm/s)	Series Name	Rectangular Tests					Figure #
		Elastic Modulus Mean (MPa)	Elastic Modulus Stdev (MPa)	n	Orientation	Strain to failure (mm/mm)	
0.1	JBR_0.1_0	3.05	1.28	8	0	0.735	Figure C. 75
0.1	JBR_0.1_90	4.75	2.21	8	90	0.371	Figure C. 76
1	JBR_0	3.70	3.26	8	0	0.614	Figure C. 77
1	JBR_90	11.80	9.96	8	90	0.374	Figure C. 78
10	JBR_10_90	10.96	6.64	8	90	0.381	Figure C. 79

Summary Figures

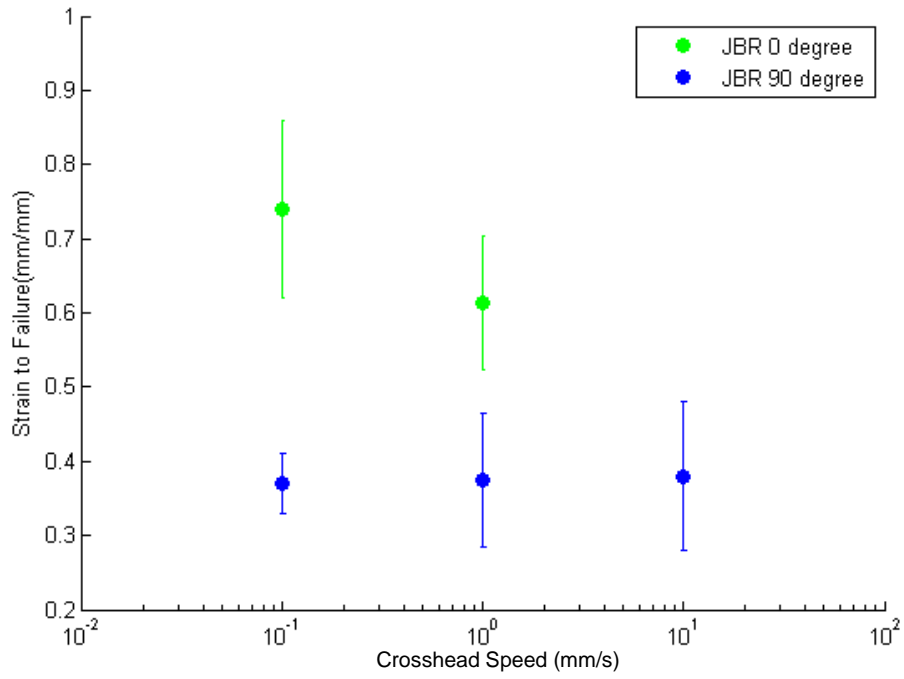


Figure C. 73. Scatter plot of the strain to failure for juvenile skin dogbone samples plotted by crosshead speed.

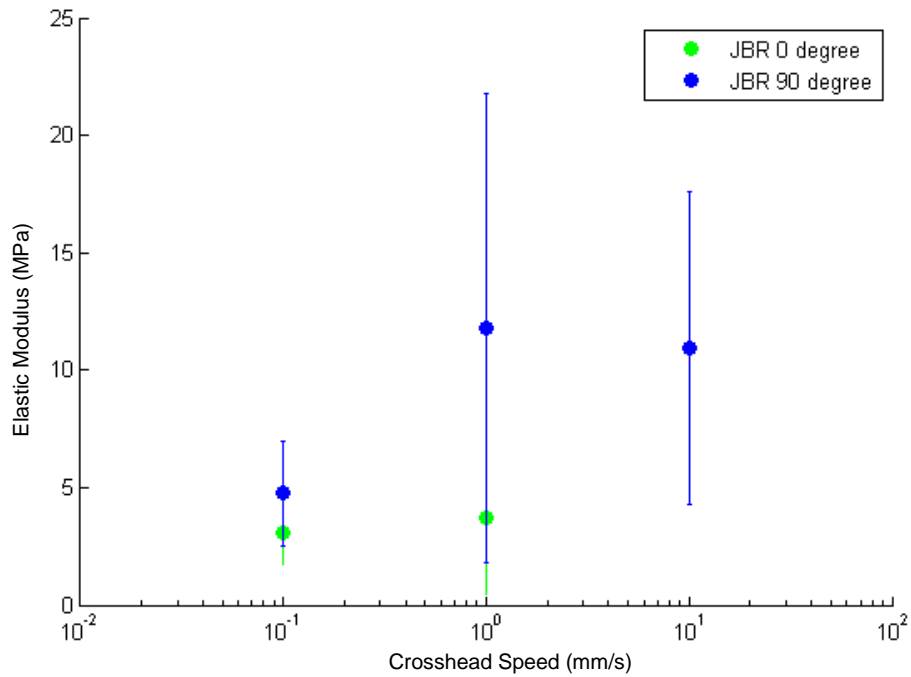


Figure C. 74. Scatter plot of peak stress values for juvenile skin dogbone samples by crosshead speed.

Individual Series Stress-Strain Figures

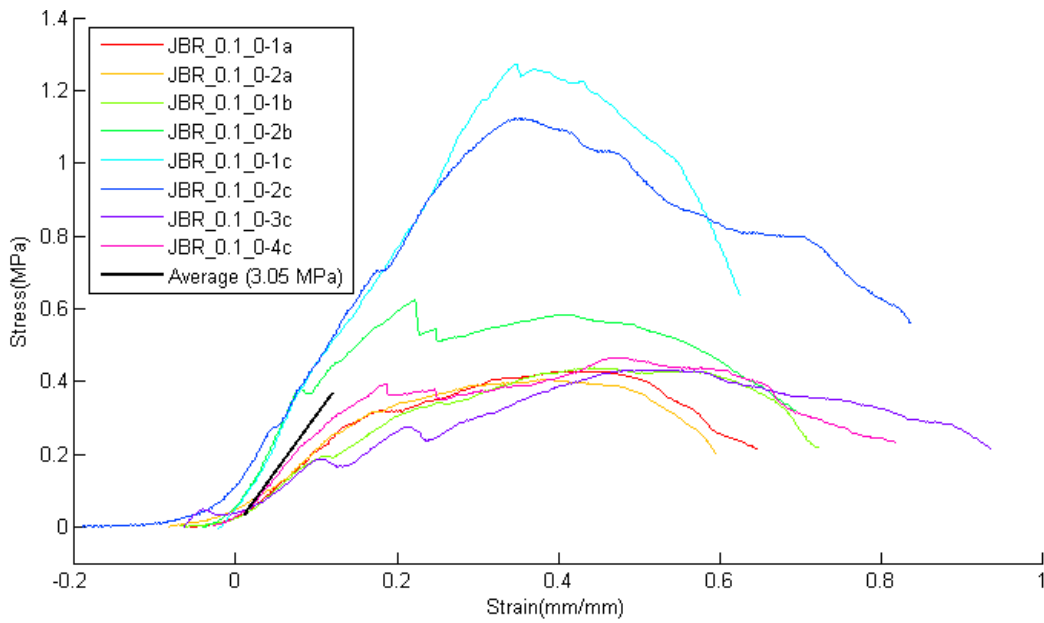


Figure C. 75. Juvenile Blubber Rectangular Samples (JBR) in in the 0 degree direction. Test performed at a crosshead speed of 0.1 mm/s.

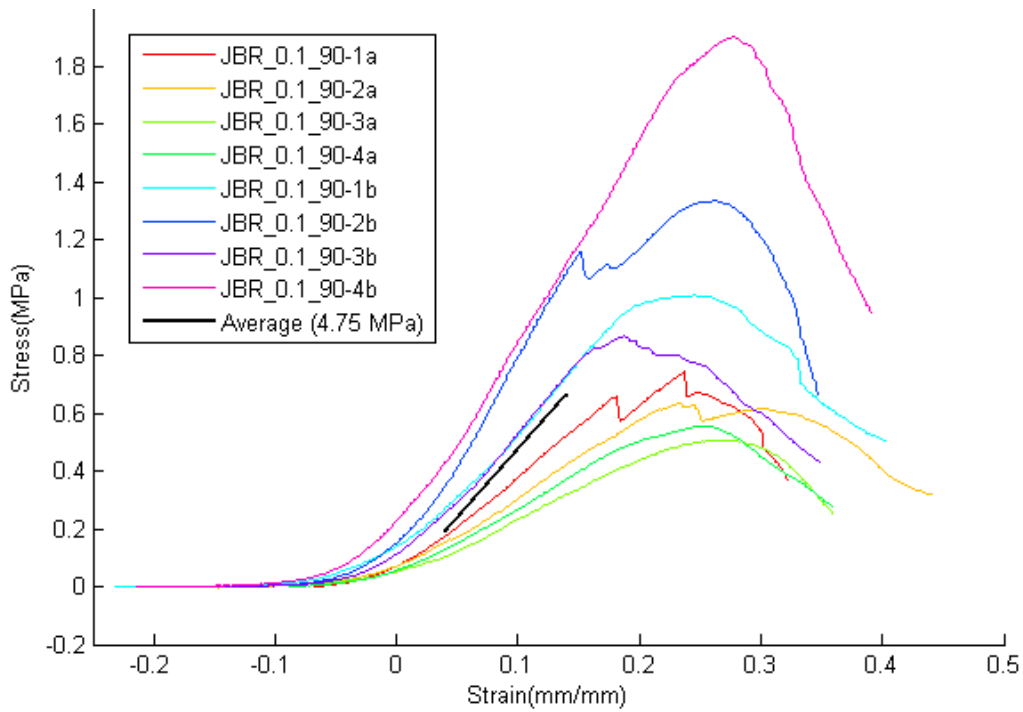


Figure C. 76. Juvenile Blubber Rectangular Samples (JBR) in in the 90 degree direction. Test performed at a crosshead speed of 0.1 mm/s

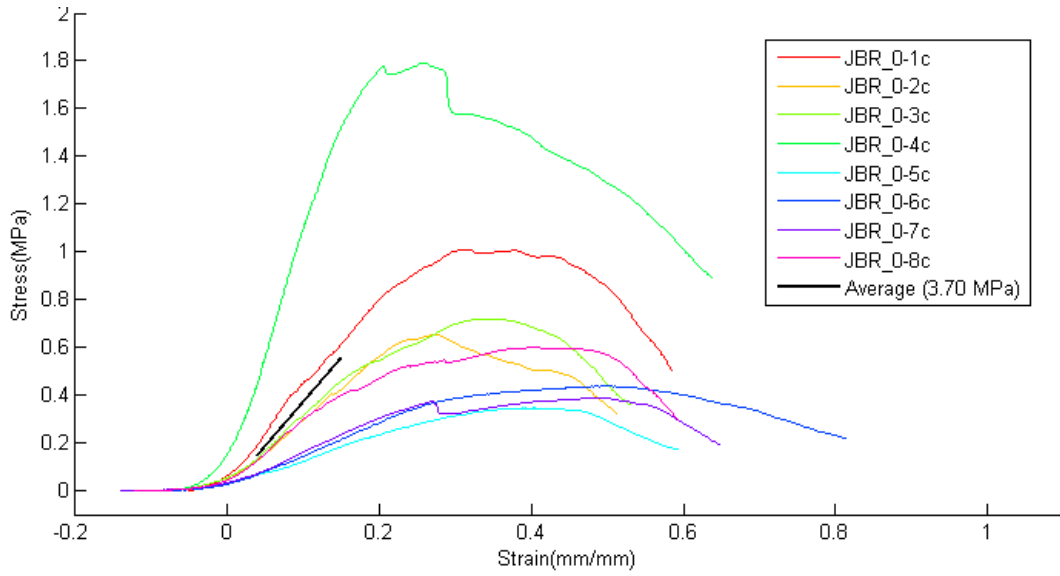


Figure C. 77. Juvenile Blubber Rectangular Samples (JBR) in in the 0 degree direction. Test performed at a crosshead speed of 1 mm/s.

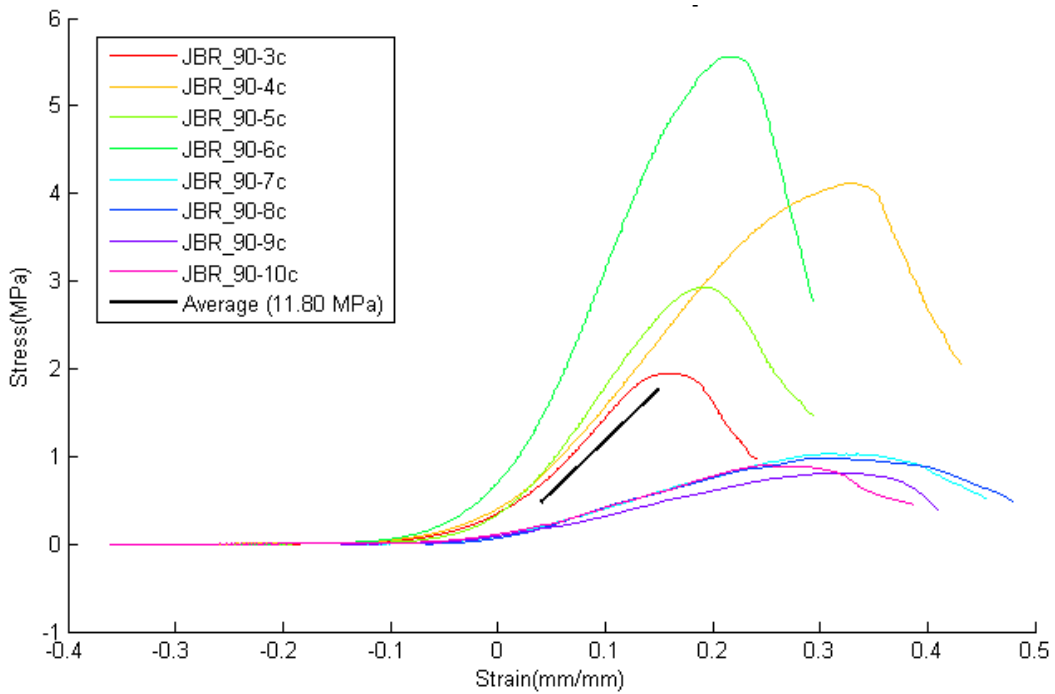


Figure C. 78. Juvenile Blubber Rectangular Samples (JBR) in in the 90 degree direction. Test performed at a crosshead speed of 1 mm/s.

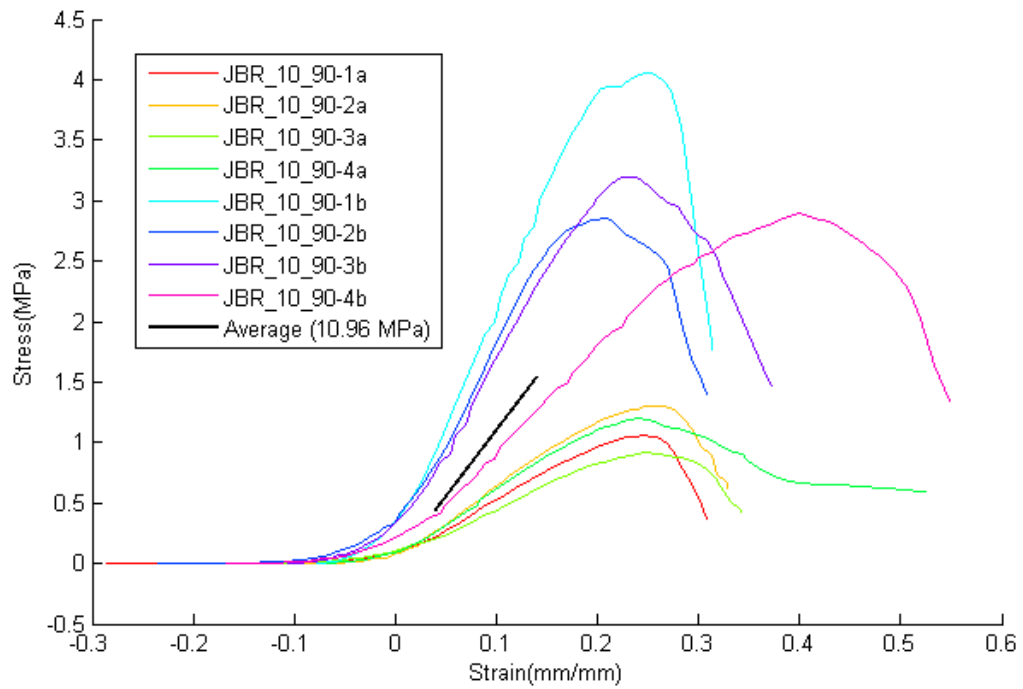


Figure C. 79. Juvenile Blubber Rectangular Samples (JBR) in in the 90 degree direction. Test performed at a crosshead speed of 10 mm/s.

Appendix D– Engineering Analysis

D.1 Material Properties for SRKW

Material properties for the SRKW were developed from the tissue testing performed by PNNL. The properties were developed by averaging each series of results, as well as comparing results to known biomechanical properties in the literature (Appendix B). As an isotropic constitutive model was used for the impact analyses, PNNL elected the 90° samples (more explanation of samples tested can be found in Appendix C) to be used in the finite element analysis. The rectangular samples were used to determine both the strain to failure and the elastic modulus.

PNNL provided averages for each series of testing, as well as the representative stress-strain curves shown in Figure D. 5.-Figure D. 7. The representative curves were chosen based on notes taken during the testing, so that each sample broke in the middle and appeared less deteriorated. All of the samples for each series are pictured in Figure D. 1-Figure D. 3

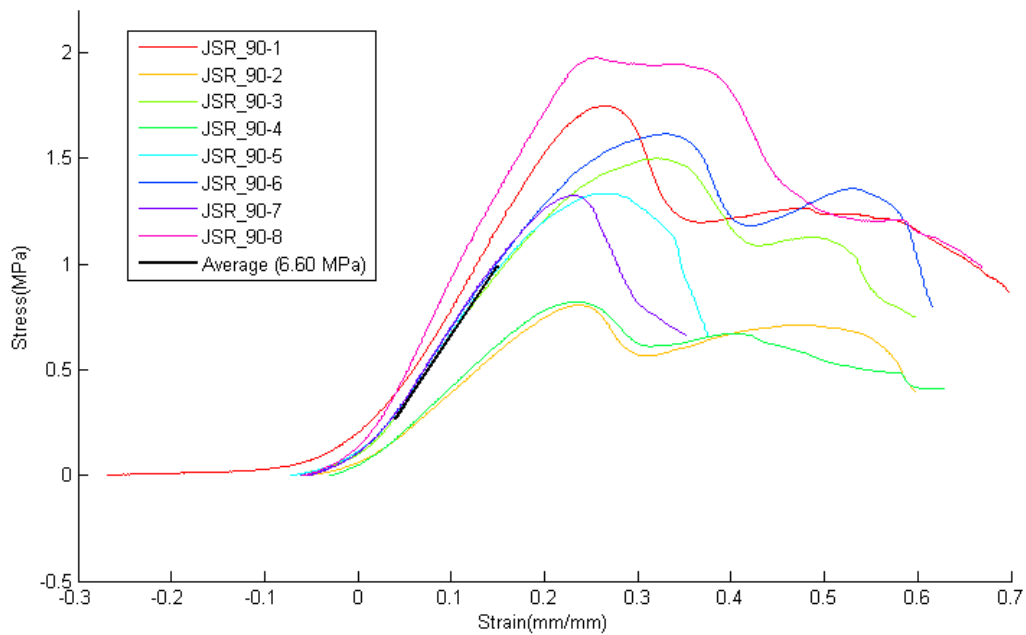


Figure D. 1. Juvenile Skin Rectangular Samples (JSR) in in the 90 degree direction. Test performed at a crosshead speed of 1 mm/s.

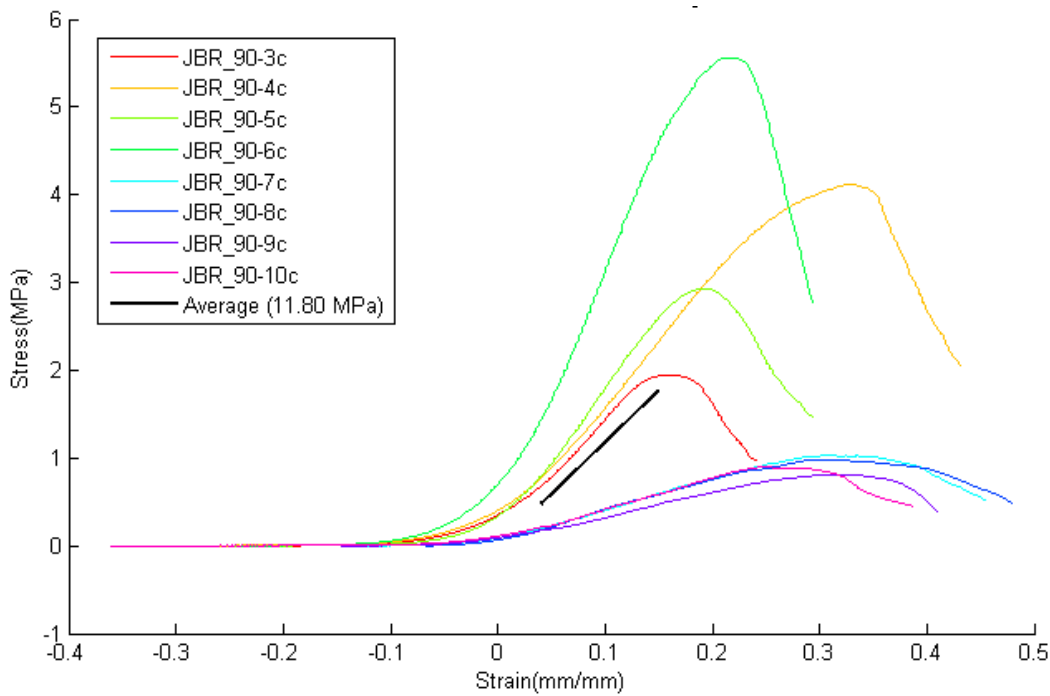


Figure D. 2. Juvenile Blubber Rectangular Samples (JBR) in the 90 degree direction. Test performed at a crosshead speed of 1 mm/s.

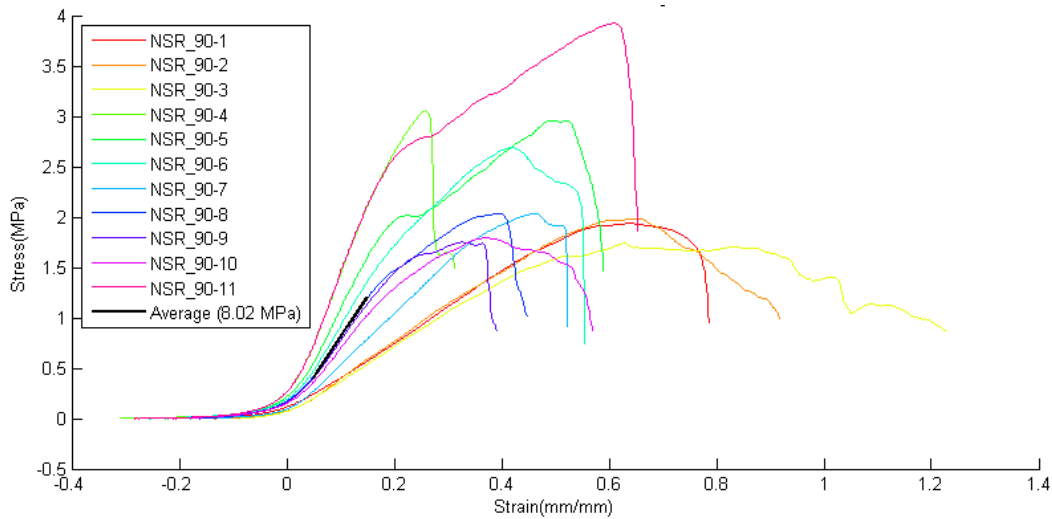


Figure D. 3. Neonatal Skin Rectangular Samples (NSR) in the 90 degree direction. Test performed at a crosshead speed of 1 mm/s.

Since the tissue samples were far from pristine, the estimated strains required to cause significant tissue damage and perhaps failure are based on tougher than average specimens. Figure D. 4 shows select anterior to posterior (90°) data from the straight stiffness specimens. Other tissue directions and specimen geometries were tested, but this data is believed to be the best choice for the blade strikes being

considered. Figure D. 5 - Figure D. 7 show how well a Neo-Hookean constitutive model represents the tissue response for a uniaxial tension test. The elastic moduli are the average values for each specimen type. The overall agreement between the test and analysis is pretty good for the neonatal skin and juvenile blubber. However, the relatively early drop in load that occurred in the juvenile skin specimen, which may be caused by tissue degradation, is not captured with this constitutive model. Table D. 1 lists the material properties used for this study. The Poisson's ratio for the biological materials were chosen to match the measured sound speeds, as well as verified by testing at Friday Harbor Laboratories

Table D. 1. Material Properties

Material	Elastic Modulus (MPa)	Density (kg/m ³)	Poisson's Ratio	Estimated Engineering Strain Thresholds for Tissue Failure
Juvenile Skin*	6.6	1000	0.4994	N/A
Juvenile Blubber*	11.8	1000	0.4990	0.5
Neonatal Skin*	8.02	1000	0.4993	0.6
Bone	300	1000	0.4745	N/A
Blade	7000	1200	0.3	N/A
Ballast	7000	2325100	0.3	N/A

* The Neo-Hookean constitutive model used for these materials is valid for large deformations.

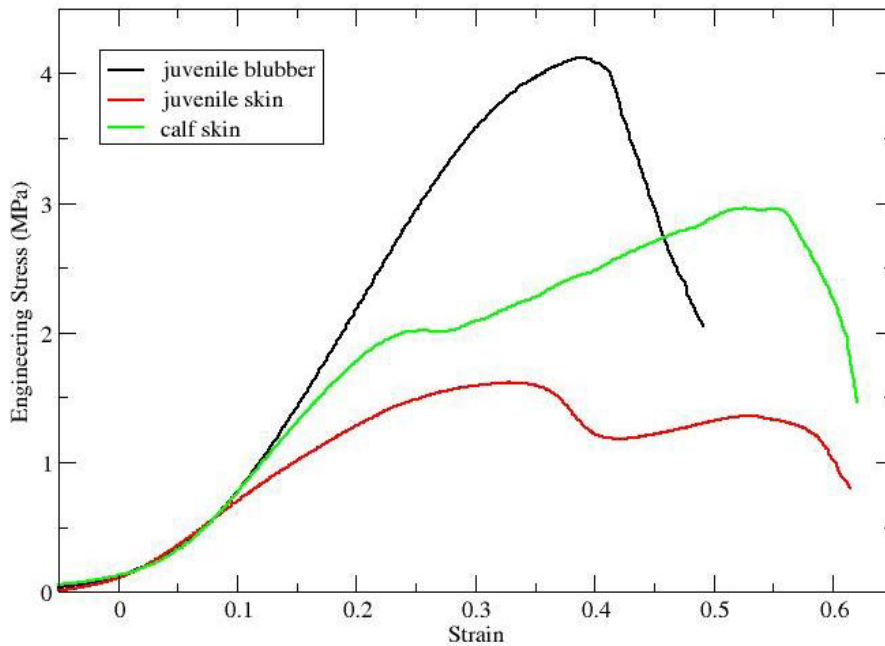


Figure D. 4. Anterior to Posterior (90°) Rectangular Sample Tissue Data. Each stress strain curve highlights a representative sample from that specified series of testing.

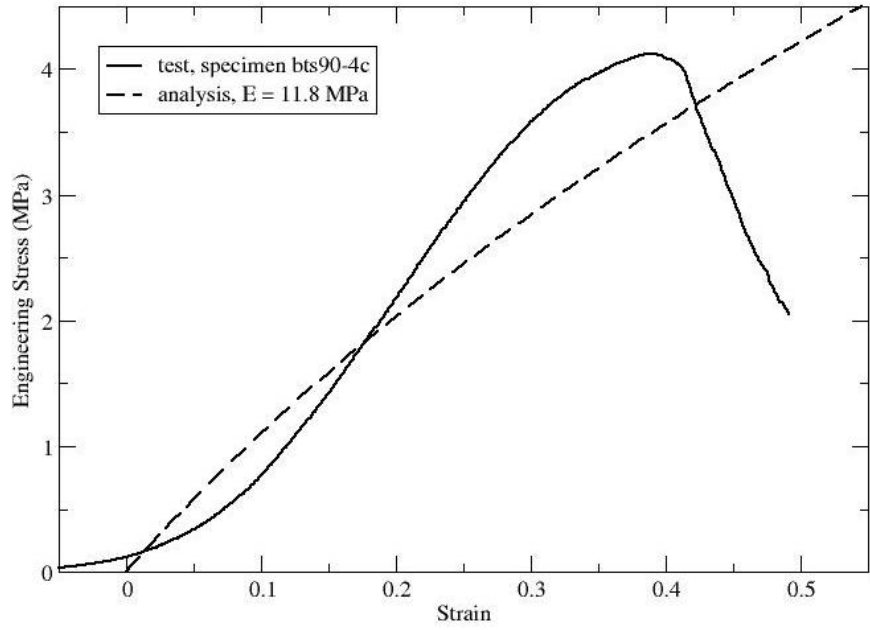


Figure D. 5. Dotted line represents the finite element analysis results for the juvenile blubber tests with rectangular 90° specimens.

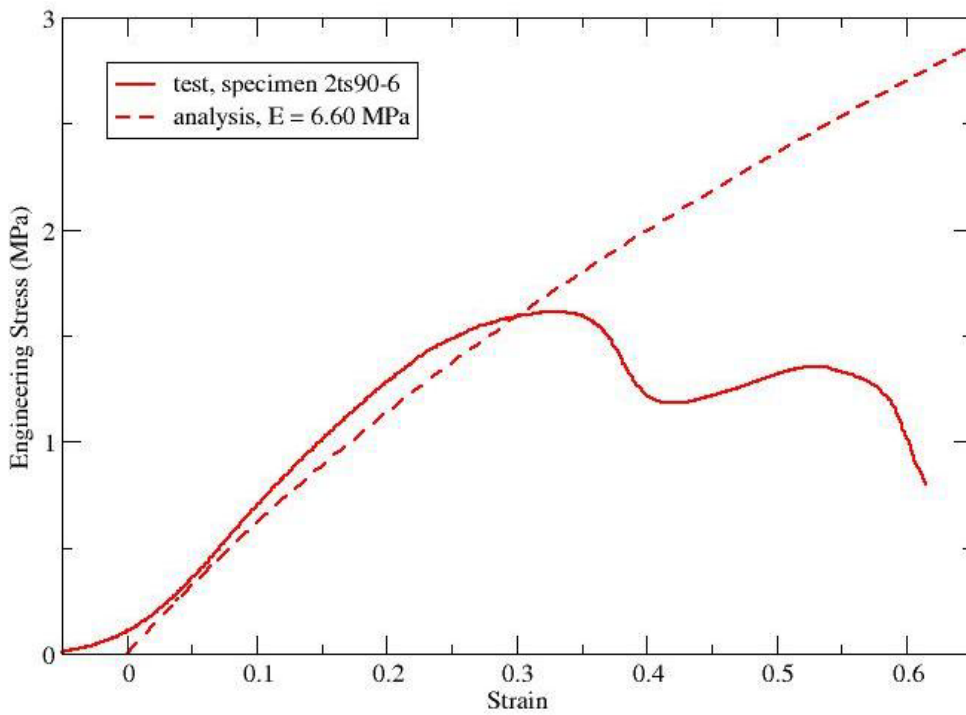


Figure D. 6. Dotted line represents the finite element analysis results for the juvenile skin tests with rectangular 90° specimens.

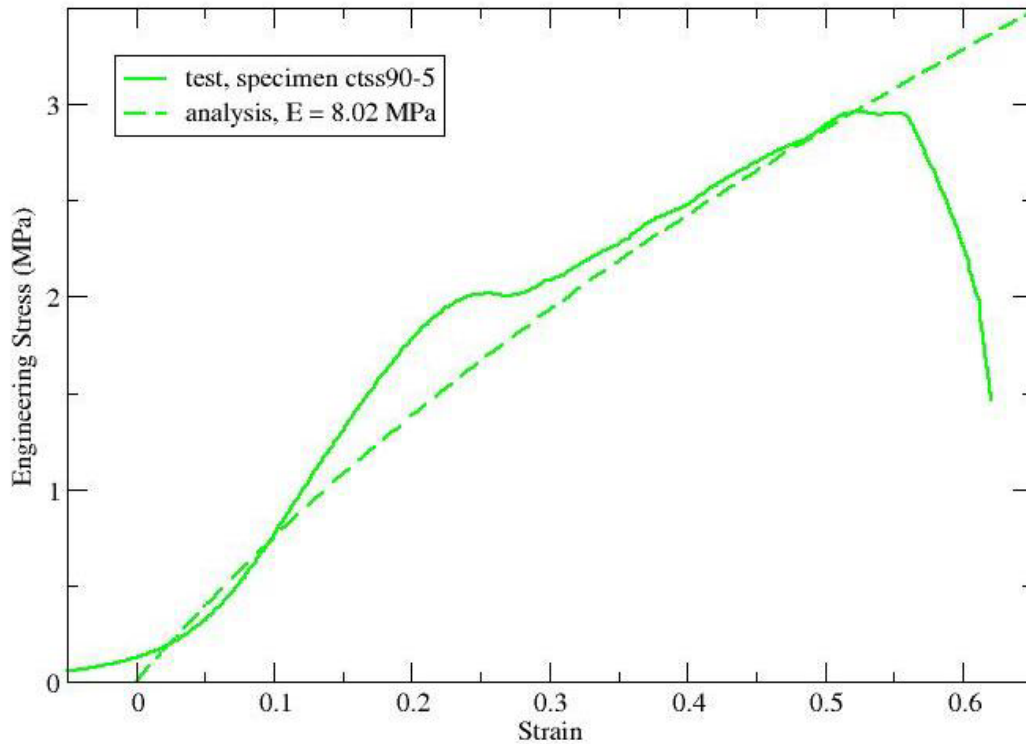


Figure D. 7. Dotted line represents the finite element analysis results for the neonatal skin tests with rectangular 90° specimens.

Structure of the head region and bone material properties were retained from FY12 analysis. Data provided by PNNL for the structure of the head region from McKenna (2005) provide sufficient detail to reconstruct the dimensions of bone matter in the head for use in the finite analysis model. The material properties of the bone matter can be extracted from Table 4.5 in Campbell-Malone (2007), which provides several values for elastic moduli of right whale (*Eubalaena glacialis*) mandible bone as a function of direction. The average value is approximately 300 MPa for both directional and bone type (trabecular or cortical); this value was used for the finite element model.

D.2 Impact Analysis Results

The transient dynamics code Presto was used to consider impact speeds of 1 to 5 m/s. This range is based on the shapes of the MHK device and a SRKW, as well as the expected range of the rotor’s angular speeds. In these simulations, the heavy blade is given an initial velocity, and its edges are allowed to translate but not rotate. The blade slows a small amount as it pushes the whale out of the way. Figure D. 8- Figure D. 9 show the maximum principal logarithmic strain in the blubber and skin, respectively, for an impact speed of 3 m/s. This baseline simulation uses blubber properties from the juvenile and skin properties from the neonate. This approach was taken because the juvenile skin sample was clearly degraded. Based on the estimated strain thresholds listed in Table D. 1, some significant tissue damage and perhaps tissue failure might occur. The simulations indicate that the tissue fails at the higher range of blade speeds (4 m/s & 5 m/s). The estimated lengths and depths of the damage are shown in Table D. 2.

The results of several analyses are summarized in Table D. 2. To facilitate comparison to the stress-strain curves shown Figure D. 8-Figure D. 9, the logarithmic strains have been converted to engineering strains based on a uniform strain assumption. It should be noted that the analyses do not simulate tissue damage or tearing. The tissue damage estimates listed in Table D. 2 are based on the number of elements that exceed estimated tissue failure strain thresholds. The loads would actually be redistributed if the tissue softens or tears. This redistribution could increase the amount of tissue that exceeds the strain thresholds. Additional analyses were performed using the juvenile skin properties to see if the lower elastic modulus (6.60 versus 8.02 MPa) would have a significant effect on the predicted strains. As shown in Table D. 3, using the neonate skin properties (instead of the juvenile skin properties) does not have a large effect on the predicted tissue strains.

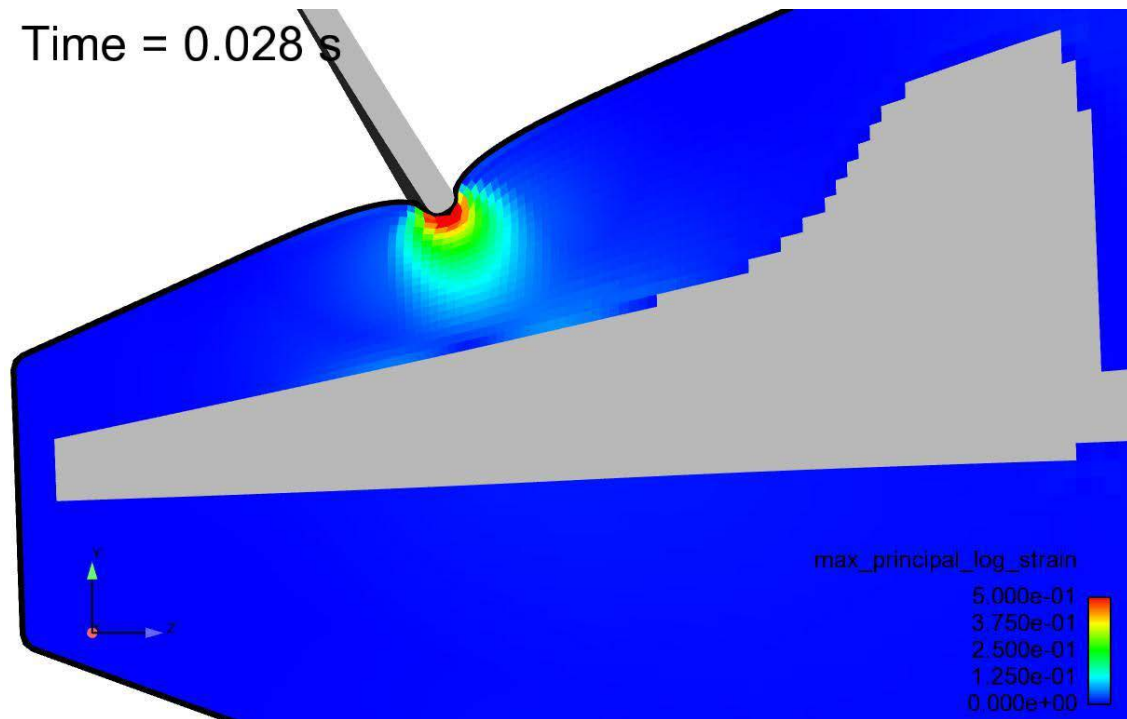


Figure D. 8. Blubber Strain, 3 m/s

Time = 0.028 s

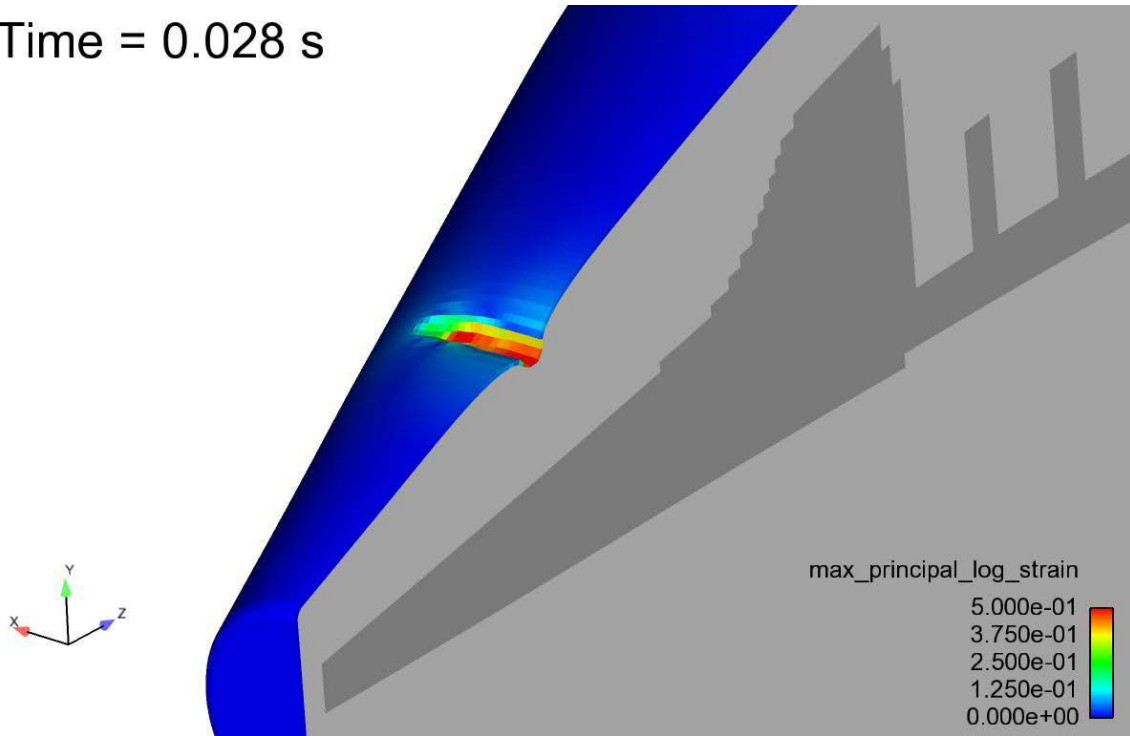


Figure D. 9. Skin Strain, 3 m/s

Table D. 2. Predicted Strains using Juvenile Blubber and Neonate Skin Properties

Blade Speed (m/s)	Tissue	Maximum Engineering Strain (Derived)	Estimated Depth of Blubber Damage (cm)	Estimated Skin Damage Length (cm)
1	Skin	0.27		0
	Blubber	0.39	0	
2	Skin	0.48		0
	Blubber	0.63	1.0	
3	Skin	0.67		14
	Blubber	0.85	2.5	
4	Skin	0.92		24
	Blubber	1.00	4.0	
5	Skin	1.25		26
	Blubber	1.23	4.7	

Table D. 3. Predicted Strains - Neonate Skin versus Juvenile Skin Properties

Blade Speed (m/s)	Tissue	Maximum Engineering Strain (Neonate Skin Properties)	Maximum Engineering Strain (Juvenile Skin Properties)
1	Skin	0.27	0.3
	Blubber	0.39	0.40
2	Skin	0.48	0.53
	Blubber	0.63	0.64
3	Skin	0.67	0.78
	Blubber	0.85	0.82
4	Skin	0.92	0.96
	Blubber	1.00	1.01
5	Skin	1.25	1.27
	Blubber	1.23	1.24

Appendix E – Blunt Force Trauma Literature Summary

E.1 Blunt Force Trauma Literature Summary

Initial literature searches were focused on marine mammal and whale head trauma, with most results describing consequences of collisions between ships and marine mammals and also for underwater detonations. However, few studies incorporate information on the forces that caused the trauma, which prevents direct comparison beyond the specific event or collision incident, and provides limited insight into the tidal blade strike scenario. One notable exception is the work by Tsukrov et al. (2009); this study developed a three-dimensional finite element mesh model to predict the mechanical behavior of a right whale's mandibular bone under strain, combined with the potential forces exerted by a whale-ship collision. This information provides insight into how a similar approach could be used to develop mechanical models of the SRKW skull and brain. If these biomechanical models were combined with biological models of brain trauma, the result might inform the potential effects of blade strike on the head of a SRKW.

By widening the scope of the literature search to other animal studies and studies related to traumatic brain injury and HIC development, it became apparent that the animal research community segregates head trauma into three main categories: clinical (research directly involving human subjects), large animal studies, and small animal studies. Literature focused on larger animals showed that porcine studies are most valuable, providing detailed descriptions of brain trauma in pigs after controlled, laboratory-induced head injury, from the sub-cellular to the whole brain level of biological organization. Literature on equine and canine head trauma is more limited; quantitative results on other livestock were not found.

The literature reflects a trend toward increasing reliance on small-animal models for head trauma research, which offer advantages associated with cost, animal welfare/ethical concerns, well-defined protocols for inducing head injury, and more sophisticated analytical tools. Most of the small-animal models are for rodents. The increasing use of rodent model systems for studying traumatic brain injury also coincides with the use of *in vitro* systems, including isolated brain tissue slices and axonal cell cultures, allowing for better characterization of the cellular mechanisms of injury. The results of the PNNL literature search include:

- [References on Animal Head Trauma](#)
- [References on Marine Mammal Ship Collisions](#)
- [References on Marine Mammal Neuroanatomy](#)
- [References on Porcine Head Trauma](#)
- [References on Dog Head Trauma](#)
- [References on Equine Head Trauma](#)
- [References on In Vitro TBI \(Traumatic Brain Injury\)](#)

Appendix F– Assessment of Harm to SRKWs, by Marine Veterinarians

F.1 Assessment of Harm to SRKW, by Marine Veterinarians

Investigations in strandings of marine mammals often do not yield clear cause of death. For example, a young SRKW (L112) was found dead off the coast of Washington State in February 2012. The necropsy outcome¹ reported that the animal

“...showed extensive bruising and swelling on both sides of the head and neck, more pronounced on the right, and continuing down the right side of the body. Although no skull fractures were seen during examination of the head, there was fragmentation of the brain and increased fluid in the right side of the skull. The grossly noted hemorrhage around the head and neck is consistent with physical trauma, which would have been sufficiently severe to account for the loss of this animal. The cause of this injury remains undetermined and investigations are ongoing...”.

The marine veterinarians were asked the questions listed below. However, as most of the veterinarians had little to no experience with orca injuries of the type hypothesized by a tidal turbine blade strike, most interviews became free form, with the marine veterinarians offering anecdotes about their experience examining stranded animals and/or caring for animals in captivity. In some cases, the marine veterinarians were able to suggest appropriate papers or reports that offer insight into the potential risk to collisions of marine mammals with other animals or with underwater objects. Their observations pertinent to our study are summarized in the following paragraphs.

- What would you estimate to be the likely outcome of a small whales (orca) swimming rostrum first into a tidal turbine blade, with the blade striking in the head region?
- Do you have any information on the compression biomechanics of orca tissue, particularly the skin?
- Have you experienced, treated, or handled cetaceans that have suffered from blunt force trauma? If so, what objects were responsible for the damage?
- If you have experience with a whale that has been struck, what was the outcome for the whale, particularly in terms of tissue damage (epidermis, dermis, bone, underlying hematoma, hemorrhaging, etc.)? How far did the damage spread laterally?
- How long did injuries take to heal?
- How frequently have you seen strike injuries to the rostrum region?
- If you have cared for animals (in captivity) that have struck, were there lasting effects of the strike injury? If so, what were the effects and how long did they persist?

When marine mammals are struck, it is not uncommon to see bruising in the underlying tissue, even if the skin is not broken. The veterinarians look at pink discoloration in the blubber layer as a focal point to investigate for underlying damage, including bone fracture.

Evidence on the effects of propeller strike on smaller marine mammals is most commonly studied in manatees. The dermal layers are thick in manatees as compared to most cetaceans. Mortality in manatees from boat strike is generally due to the combined effects of lacerations and blunt force trauma to the skeleton, including the skull. However, manatees have very powerful bone regenerative capabilities (Dr.

¹ Southern Resident Killer Whale L112 Stranding Progress Report, May 15, 2012.

W. McLellan, University of North Carolina–Wilmington, personal communication, September 2012). Key literature sources include Kipps and McLellan (2002), Lightsey et al. (2006), and Rommel et al. (2007).

Other marine mammal evidence of interest includes infanticide of harbor porpoise calves caused by attacks from bottlenose dolphins. Porpoise calves (as well as some bottlenose dolphin calves) have died from head trauma due to ramming by the adults. The injuries to the calves are not consistent with other forms of trauma such as boat strike, fisheries interactions, predation, or underwater blasts (Dr. W. McLellan, personal communication, September 2012). Key literature sources include Patterson et al. (1998) and Dunn et al. (2002).

Almost all the quantitative evidence pointing to severe or lethal outcomes for cetaceans arise from ship strikes, particularly strikes of North Atlantic right whales in the Atlantic. Modeling and laboratory efforts have helped to interpret necropsy findings that indicate that lethal encounters are generally the result of forces capable of breaking the whale's jawbone, often the result of multiple microfractures; these models have taken the speed and forces imparted by the ships, as well as the area and time of impact, into account. Controlled laboratory blunt force trauma experiments with pigs yield the closest analogue to marine mammals (Dr. R. Campbell-Malone, Johns Hopkins University, personal communication, month year). Key references include Knowlton and Kraus (2001) and Campbell-Malone et al. (2008).

Captive killer whales tend to avoid stationary objects underwater, so that curiosity is the only likely scenario in which an animal might encounter a turbine. The animals most likely to approach an underwater object are young; older animals are wary. The adults will examine an object but will seldom approach closely. Neonates will be protected by their mothers from harm. The young adolescent orcas, particularly those that do not have a parent nearby, might approach an object. However, the danger from turbines underwater is likely to be small, compared to the risk to these animals from ships moving at speed with high inertia and rotating propellers (Dr. J. McBain, Sea World, personal communication, September 2012).



U.S. DEPARTMENT OF
ENERGY

Prepared for the U.S. Department of Energy
under Contract DE-AC05-76RL01830

This report prepared in partnership with Sandia National Laboratories



Pacific Northwest
NATIONAL LABORATORY

*Proudly Operated by **Battelle** Since 1965*

902 Battelle Boulevard
P.O. Box 999
Richland, WA 99352
1-888-375-PNNL (7665)
www.pnnl.gov



Sandia
National
Laboratories